DEPARTMENT OF MATHEMATICAL PHYSICAL NATURAL SCIENCES

Università
Ca'Foscari
Venezia

MASTER'S DEGREE PROGRAMME in CHEMICAL SCIENCES for CONSERVATION and RESTORATION

Ca' Foscari University of Venice

Final Thesis

Ca' Foscari
Dorsoduro 3246
30123 Venezia

Characterization and quantification of modern painting materials by IR and Raman spectroscopies

Graduand: Pagnin Laura
Matriculation number: 843961

Advisors: Prof. Manfred Schreiner
Prof. Ligia Maria Moretto

Co-Advisors: Dr. Rita Wiesinger
Prof. Emilio Francesco Orsega

Academic Year
2016/2017

Art cannot be modern.
Art is primordially eternal.
-   Egon Schiele -

Table of contents

Abstract

This thesis has the aim to characterize and quantify different synthetic materials, which are widely used in modern and contemporary art. In these last years, the field of art is largely developed, beginning to employ synthetic materials such as acrylic, vinyl, alkyd, etc. Consequently, the study and analysis of their composition, properties and chemical-physical behavior is becoming more and more influential in the diagnostics of cultural heritage.

Initially the study focuses on the identification of modern materials used, i.e. polymeric binders such as acrylic (Plextol D498) and alkyd (Alkyd Medium 4) both pure and in mixture with three different inorganic pigments (artificial ultramarine blue, hydrated chromium oxide green and cadmium yellow). They were analyzed by various non-invasive spectroscopic techniques such as optical microscopy, spectrophotometry Vis-RS, IR and Raman spectroscopy. The results of this first evaluation allowed not only to characterize the main chemical functional groups of each component but also to investigate the different drying processes of the two polymeric binders.

The second part of the thesis has the objective to perform a quantitative analysis to evaluate the different pigment/binder ratio within each painting sample. Initially a mathematical-statistical model was developed, using calibration curves created with values of known sample concentration (P/BM ratios). The graphs were constructed choosing the ordinate to be the measured Area values (integrated IR and Raman bands) and the abscissa the values of their relative concentration. They were divided according to the technique used (IR and Raman). Once obtaining optimal calibration curves, in each of them, the values of the measured Area of unknown samples were added. From the interpolation of these values it was possible to determine the unknown value of their relative concentration. Subsequently, using the same experimental procedures employed for the previous graphs, it was possible to quantitatively determine a commercial painting sample. The results obtained from this research have confirmed that the quantitative model developed, is able to efficiently determine different pigment/binder relative concentrations within of samples, made in laboratory or commercially.

Riassunto

Questa tesi ha lo scopo di caratterizzare e quantificare diversi materiali moderni sintetici, ampiamente utilizzati nell'arte moderna e contemporanea. In questi ultimi anni, il settore dell'arte si è largamente sviluppato, iniziando ad impiegare materiali sintetici quali acrilici, vinilici, alchidici, ecc. Di conseguenza, lo studio e l'analisi della loro composizione, proprietà e comportamento chimico-fisico è diventando sempre più importante ed influente nella diagnostica dei beni culturali.

Inizialmente lo studio si è focalizzato sull'identificazione dei materiali moderni utilizzati, ossia i leganti polimerici come l'acrilico (Plextol D498) e l'alchidico (Alkyd Medium 4) sia puro che in miscela con tre diversi pigmenti inorganici (blu oltremare artificiale, ossido di cromo idrato verde e giallo di cadmio). Essi sono stati analizzati da diverse tecniche spettroscopiche non invasive, quali microscopio ottico, spettrofotometria di riflettanza Vis-RS, spettroscopia IR e Raman. I risultati di questa prima valutazione hanno consentito non solo di caratterizzare i principali gruppi funzionali di ogni componente ma anche di indagare sui diversi processi di essiccazione dei due leganti polimerici.

La seconda parte della tesi ha l'obiettivo di eseguire un'analisi quantitativa per valutare i diversi rapporti pigmento/legante all'interno di ciascun campione pittorico. Inizialmente è stato sviluppato un modello matematico-statistico, utilizzando diverse curve di calibrazione create con i valori di campioni a concentrazione nota. I grafici sono stati costruiti utilizzando sull'asse dell'ordinata i valori misurati dell'Area e in ascissa i valori della loro concentrazione relativa. Essi sono stati divisi secondo la tecnica utilizzata (IR e Raman). Una volta ottenute curve di calibrazione ottimali, in ciascuna di esse, sono stati aggiunti i valori dell'Area dei campioni incogniti. Dall'interpolazione di questi valori alla curva è stato possibile determinare il valore incognito della loro concentrazione relativa. Successivamente, utilizzando le stesse procedure sperimentali impiegate per i grafici precedenti, è stato possibile determinare quantitativamente un campione pittorico commerciale. I risultati ottenuti da questa ricerca hanno confermato che il modello quantitativo sviluppato è in grado di determinare in modo efficiente le diverse concentrazioni relative di pigmento e legante all'interno dei campioni, sia commerciali che eseguiti in laboratorio.

Abstrakt

Diese Arbeit hat zum Ziel, verschiedene synthetische Materialien zu analytisch zu charakterisieren und zu quantifizieren, die in der modernen und zeitgenössischen Kunst weit verbreitet sind. In den letzten Jahrzehnten hat sich in diesem Feld der Kunst viel weiterentwickelt und ein Fokus auf die Verwendung von synthetischen Materialien wie Ac5ryl, Alkyd usw. gelegt. Folglich wird die Untersuchung und Analyse ihrer Zusammensetzung, Eigenschaften und ihres chemisch-physikalischen Verhaltens immer wichtiger im Zusammenhang der Diagnostik und Erhaltung von kulturellem Erbe. Zunächst konzentriert sich die Arbeit auf die Identifizierung von modernen Materialien, dh polymere Bindemittel wie Acryl (Plextol D498) und Alkyd (Alkyd Medium 4) sowohl rein als auch in Mischung mit drei verschiedenen anorganischen Pigmenten (künstliches Ultramarinblau, hydratisiertes Chromoxidgrün und Cadmium Gelb). Sie wurden mittels verschiedener nicht-invasive spektroskopische Techniken wie optische Mikroskopie, Spektrophotometrie Vis-RS, IR und Raman Spektroskopie analysiert. Die Ergebnisse dieser ersten Auswertung erlaubten es nicht nur, die wichtigsten chemischen funktionellen Gruppen jeder Komponente zu charakterisieren, sondern auch die verschiedenen Trocknungsprozesse der beiden polymeren Bindemittel zu untersuchen. Der zweite Teil der Arbeit hat das Ziel, eine quantitative Analyse durchzuführen, um das unterschiedliche Pigment/Bindemittel-Verhältnis innerhalb jeder Probe zu bewerten. Zunächst wurde ein mathematisch-statistisches Modell entwickelt, wobei Kalibrationskurven mit Werten bekannter Konzentrations bzw. Mischverhältnissen erstellt wurden. Um diese Graphen zu erstellen wurden für die Ordinate die mittels IR and Raman gemessenen Bandenflächen und für die Abszisse die Werte ihrer relativen Konzentration verwendet. Sie wurden je nach verwendeter analytischer Methode (IR und Raman) unterteilt. Nach der Erstellung optimaler Kalibrationskurven wurden diese mittels Proben mit voererst unbekannten Mischungsverhältnissen getested. Aus der Interpolation dieser Werte konnte man den unbekannten Wert ihrer relativen Konzentration bestimmen. Anschließend wurde unter Verwendung der gleichen experimentellen Verfahren, die für die vorhergehenden Graphen verwendet wurden, eine quantitative Bestimmung einer kommerziellen Malprobe durchgeführt. Die aus dieser Forschung gewonnenen Ergebnisse haben bestätigt, dass sich das quantitative Modell eignet, verschiedene Pigment/Bindemittel-Relativkonzentrationen innerhalb von Proben, die im Labor oder im Handel hergestellt werden, effizient zu bestimmen.

Acknowledgements

It was possible to realize this thesis project thanks to all the people who helped, encouraged and supported me in all these months.

First of all, I would like to thank my advisor, Prof. Dr. Manfred Schreiner for giving me the opportunity to work with his working group. This experience taught me to believe in myself, be independent, but also learn how to work together as a true team. I also thank him for giving me the opportunity to develop my master thesis, allowing me to expand my knowledge more and more in this fascinating field of research.

I would like to thank my advisor Prof. Ligia Maria Moretto and my co-advisor Prof. Emilio Francesco Orsega who helped me throughout the thesis period. I thank them for having always dedicate me time, offering me wise advices and help to improve the thesis work and above all thank them for the patience they had with me. Without them I would not have reached this goal. Heartfelt thanks.

I would like to thank my co-advisor Dr. Rita Wiesinger for all the help she gave me, for the relaxing coffee breaks and the amusing conversation done together. I hope that, despite the distance, we will be able to remain not only colleagues but friends.

I thank my colleagues at the Institute, Valentina Pintus, Marta Anghelone, Carlotta Salvadori, Federica Cappa, Dubravka Jembrih-Simbuerger, Wilfried Vetter and Christine Jiru for making the work environment interesting, productive but also stimulating and funny.

I would like to thank my crazy roommate Cecilia Pesce who shared moments of fun, anxiety, fear, domestic life, feasts and above all many laughs. Thanks for the wonderful experience of living together.

I thank, from the deep of heart, Christian. I thank him for all the hours in video calling he spent encouraging me, for being always close to me, for motivating me every day to do my utmost to improve myself, for bearing my cries and my insecurities, but above all for having always appreciated and loved me during all these years. Thank you for how you are and how I grew up with you.

Last, but absolutely not least important, I would like to thank my big family, all the people and friends for all the support they gave me and for being always close to me. With their support, they made this great achievement of my life possible, and surely they will still be for the next future goals.

This project was a collaboration between the Institute of Natural Sciences and Technology in Art of the Academy of Fine Arts (Vienna) and the University of Ca' Foscari (Venice).

List of abbreviations

2-EHA/MMA: 2-ethylhexyl acrylate/methyl methacrylate

ATR: Attenuated Total Reflection

CIE: Commission International de l'Éclarage

CMF: Color Matching Function

DR: Diffuse Reflection

EA: Ethyl Acrylate

EM: Electromagnetic spectrum

FTIR: Fourier Transform Infrared

IR: Infrared

IRE: Internal Reflection Element

MMA: Methyl Methacrylate

Mid-IR: Medium infrared region

nBA: n-butyl acrylate

NIR: Near-infrared

OLS: Ordinary Least Squares

P/BM: Pigment/Binder Medium

p(EA/MMA): Poly ethyl acrylate methyl methacrylate

p(nBA/MMA): Poly n-butyl acrylate methyl methacrylate

PVA: Polyvinyl acetate

Tg: Transition temperature

UV: Ultraviolet

Vis-RS: Visible Reflectance

Chapter 1

Introduction

In the last few decades, the field of contemporary art conservation has become very important on international level, due to the importance to preserve artistic cultural heritage with suitable conservation practices based on knowledge of all the artistic material elements that constitute art objects [1]. With the development of synthetic organic chemistry at the beginning of the 20th century, a lot of different kind of organic materials have been used in the creation of artistic objects; among the most employed in the art field there are the alkydic and acrylic polymers. The first became the modern substitutes of traditional oil painting for their low-cost and easy availability. The fastest drying process of the polymeric layer and the possibility to employ it with more pigments, due to good optical properties, made it one of the most used polymeric binders in contemporary art industry. However, the most common and versatile polymer was the acrylic one. Initially it was used in the industry as a plastic material for structural applications; subsequently, through the possibility to add two or more acrylic monomers within the same polymer chain, it was possible to develop a more flexible and transparent polymer. Its stability, excellent optical and mechanical properties and rapid drying have made it the most used polymeric binder in the field of art materials [2]. For this reason, since World War II, art involved many professionals like restorers, conservators, art critics, art historians but above all the professional figure of scientist appeared, who best represented the innovation in the field of conservation of contemporary art. The conservation and restoration of cultural-historical materials and artifacts allowed to obtain information about their chemical-physical composition in order to understand the state of degradation with multi-elemental, universal and sensitive methods of analysis [3]. For this reason, in recent years, more complicated and specific analytical instruments increased. These diagnostic investigations for art can be divided into invasive, which require a small amount of material, and non-invasive, which do not require sampling. The latter can be differentiated into: destructive (i.e. that modify or destroy the sample) and non-destructive (i.e. that preserve the material unaltered). In order to maintain the best preservation of the investigated materials, it is necessary to intervene as little as possible, this is the reason why non-invasive techniques are the most commonly used, although sometimes they do not allow to obtain detailed information on the artefacts [4].

The first diagnostic analysis on contemporary materials had the aim to research the individual chemical components of the artworks. In this way, once identified, it was possible to understand the nature of degradation and to develop a specific conservation and restoration project for each artistic object under consideration.

This thesis project was divided into two parts: the first focused on the qualitative analysis of material used, i.e. acrylic and alkydic binders and inorganic pigments, by non-invasive analysis, such as IR and Raman spectroscopy, and Vis-RS spectrophotometry. The results allowed to identify the different functional groups constituting polymer binders (acrylic and alkydic) but also to study the two different drying processes involved. On the other hand, the second part was based on the development of a new quantitative model able to determine in detail the different pigment/binder ratios within a painting layer. This innovative type of analysis is useful not only to know more precisely the commercial paints used by modern contemporary artists, but also to develop more technologically advanced methods of conservation and restoration for these modern innovative materials.

Chapter 2

Materials and pigments

2.1 Binders

2.1.1 Acrylic resin

Numerous types of modern paints were developed and produced in the twentieth century. In the previous five hundred years, the most widely used binder was oil but with the development of new technologies in the field of art binders such as polyvinyl acetate (PVA) emulsion, vinyl acrylic emulsion, alkyd resin, water-miscible oil, etc. were included [5]. Among them the acrylic emulsion paints were the most successful, because of their fast drying, their environmentally friendly properties due to the presence of water instead of organic solvents. For this reason emulsion acrylic materials have been revolutionary in the paint and coating sector [6]. The acrylic emulsion paint, generally called "latex", is an acrylic copolymer, usually composed of methyl methacrylate (MMA) and either ethyl acrylate (EA) or *n*-butyl acrylate (*n*BA); fig. 1 shows the principal acrylic monomer [5]. In the early years, p(EA/MMA) was commonly used, but since the late 1980s paints with a p(nBA/MMA) binder, that promote the increase of toughness and hydrophobicity, have been preferred by many companies producing artists' acrylic emulsion paints. In recent years, 2-ethylhexyl acrylate/methyl methacrylate (2-EHA/MMA) has also been widely used [6].
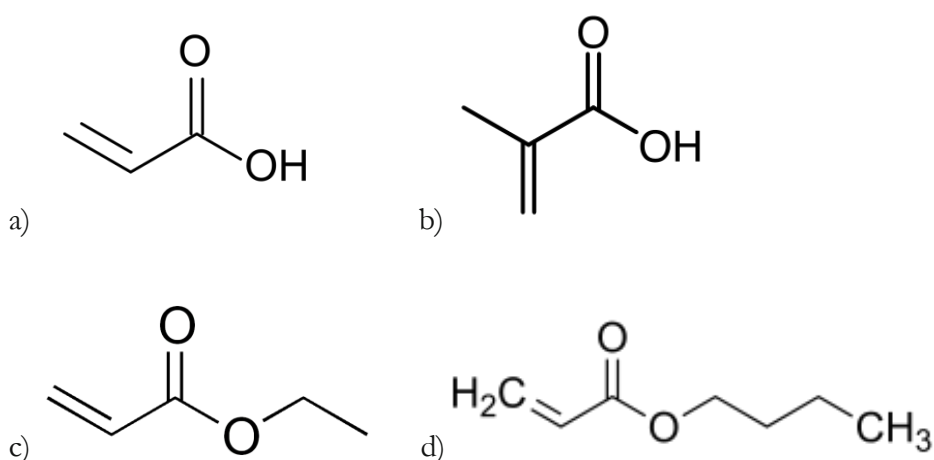

Fig. 1 – Chemical structure of acrylic monomers: a) acrylic acid, b) methacrylic acid, c) ethyl acrylate(EA), d) *n*-butyl methylacrylate (*n*BA)

The polymerization of acrylic monomers is an addition reaction between the carbon-carbon double bonds in the monomeric units and is normally catalyzed by an initiator. This is characterized by an highly exothermic reaction and, despite being an extremely rapid process, can be controlled to a high degree [7].

The acrylic resins exist in two categories: thermoplastic and thermosetting. The majority of the artists' acrylic products are thermoplastic, made up of polymers of acrylate and methacrylate monomers, even if sometimes a small amount of an acrylic acid monomer can be added to facilitate the adhesion of it to certain surfaces. The characteristic of this category is the tendency to have longer chain lengths whereby film formation occurs without any external chemical action, except for the evaporation of solvent or water. Whereas the thermosetting acrylics tend to have slightly shorter chain lengths and are usually manufactured for industrial applications [7]. The thermoplastic acrylics can be also divided in two distinct forms: acrylic solution and acrylic emulsion. The first type is the acrylic polymer dissolved in an organic solvent, generally with low aromatic content. Instead acrylic emulsions are two-phase systems in which the insoluble acrylic polymer is dispersed in an aqueous phase and stabilized with a surfactant, that are molecules with a hydrophobic part (their *tails*) and a hydrophilic part (their *heads*) able to interact physically with both the acrylic and water phases lowering the interfacial tension [7]. They are generally present in low concentration and they can be anionic (e.g., sodium lauryl sulfate or dodecylbenzene sulfonate), cationic (usually based on quaternary ammonium compounds), and nonionic (e.g., alkyl phenol ethoxylates) [8]. Through the time, the chemical and physical properties of the acrylic emulsions have been improved using several other additives. In fact, depending on their type, additives are able to modify color, to improve the performance, to increase resistance to light degradation and also to give resistance to heat degradation. An example are pigments, in fact they can influence the chemical stability of acrylics and decrease the durability, above all organic pigments [8].

The usefulness of acrylic resins as a paint binder is largely determined by its physical properties, such as the glass transition temperature (Tg), namely the point above which a polymer is flexible and rubbery. For acrylic emulsion paints, a copolymer is chosen with a Tg just below room temperature, more or less around 10-15 °C. In this way it is quite low to maintain the film flexible and avoid cracking, and high enough to prevent the dried film from becoming tacky. The Tg of acrylic solution paints is slightly higher, at around 20 °C [5].

All types of acrylic paints are extremely fast drying, but there are differences between the properties of solution and emulsion forms. While an emulsion is dispersed and thinned in water (therefore reduced toxicity), a solution dries purely by solvent evaporation, moreover can be redissolved in turpentine or aliphatic mineral spirits. For this reason it is difficult to apply subsequent layers

without disturbing an underlying layer, and once dried is very hard, often impossible, to redissolve completely even in strong organic solvents [7].

2.1.2   Film formation of emulsion paints

The drying process of a polymer is different depending on whether in solution or in emulsion. In the latter the size of the polymeric unit is larger, and they tend to be polymeric spheres rather than single molecules. Furthermore, in the emulsions, the diluent does not dissolve the polymer, and therefore can also be used with organic solvents.

The film formation process is based on two steps. The first is the evaporation of water, controlled by the vapor pressure diffusion of the water itself. Subsequently, the molecules of the dispersed phase, i.e. the polymer, begin to compress between them, also incorporating the pigment particles. This phenomenon is called coalescence. Finally the remaining water, between the polymer molecules, evaporates forming the final layer dried. When the polymer spheres start to coalesce, the process becomes irreversible [9]. Figure 2 shows the stages of the film formation.
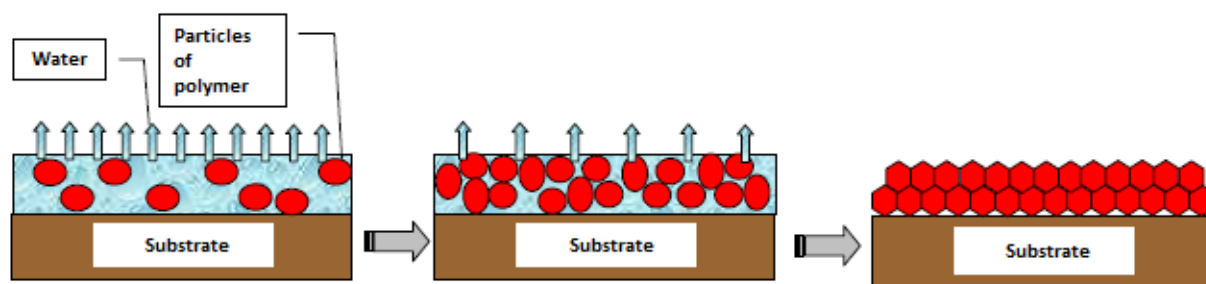

Fig. 2 – Ideal mechanisms for film formation in an emulsion system [10].

However, there are some factors which affect the film formation. First, the evaporation of the water must be complete, to avoid that some molecules remain trapped in the dried film. The time required to happen depends on several factors and it is related to the *open time* of the mixture. This term indicates the time within which a wet finishing layer can be "over painted" without defects appear as signs of stratification. Although this parameter does not coincide with the drying speed, it is closely linked. Also the glass transition temperature (Tg) of the polymers themselves is important. If it is higher than the drying temperature, it is not possible to obtain a thick film because of the non-plasticity of the resins, in this way they could not melt completely during the coalescence phase. This is a very critical parameter, and must be calibrated carefully. Polymers with low Tg at room temperature (which filming well) are soft and flexible, but generally do not possess the physical-chemical characteristics typical of polymers with high Tg (which, however, have difficulties in creating continuous film). For this purpose the so-called "coalescents", i.e. agents capable of lowering the Tg of the binder without affecting its technical characteristics are used. The coalescent

in fact acts "solvating" the polymer particles and making the surface quite sticky to promote the aggregation. Once it is evaporated, the water has been completely removed from the film. Coalescents are also called surfactants. They are substances capable of modifying the surface tension of liquids in which they are dissolved. To perform this action, their molecules must have at least two distinct and separate sections, one apolar and affine to fatty substances, and the other polar or containing ionic groups, similar to those polar (such as water). The classical distinction refers to the nature of the hydrophilic part: anionic, cationic, non-ionic [10].

2.1.3   Alkyd resin

Alkyd paints are oil-modified polyester paints, in which the introduction of oil is necessary to produce sufficient flexibility of the polyester formulation so that the resin is suitable for a paint film [7]. They were introduced in the late 1930s, although they didn't make a significant impact on the paint industry until the late 1950s. Since then, the vast majority of oil-based house paints have incorporated alkyd resins as their principal binder [5].

The term *alkyd* derives from the two main components, a polyhydric alcohol (or polyol) and a polybasic carboxylic acid. The majority of alkyd house paints use just three compounds: glycerol (polyol), pentaerythritol (polyol) and phthalic anhydride (polybasic acid) [5]. A typical alkyd resin is prepared by heating for example linseed oil, phthalic acid anhydride and glycerol to obtain a fatty-acid containing polyester [11]. In general, the polyester produced from these components is typically a hard, cross-linked thermosetting resin, but by incorporating a monobasic fatty acid, the degree of cross-linking is significantly reduced [7].

Specifically, the different components of an alkyd resin are (see figure 3):

-    **Polyol**: the two most widely used polyols in alkyd resin are glycerol and pentaerythritol. Glycerol was used before 1960, for short and medium oil alkyds, while pentaerythritol, earlier introduced, for long oil alkyd. Compared to long oil glycerin types, these alkyds are inclined to dry more quickly and to produce paint films more flexible and durable, increasing water resistance [7].

-    **Polybasic acid**: the most common polybasic acid is the dibasic acid phthalic anhydride, and generally all alkyd house paints use it. Also others dibasic acids are employed in the industrial alkyd paints, such as isophthalic, terephtalic, maleic, fumaric, adipic and sebacic acids [7].
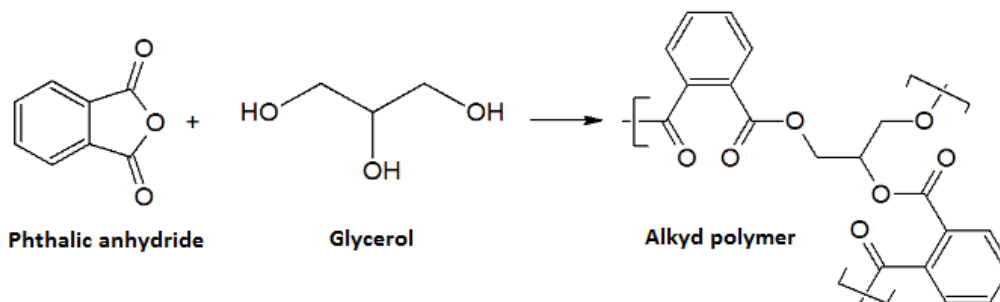
Fig. 3 – Principal reaction of the formation of an alkyd polymer

- **Drying oil:** alkyd differ from other polymer products made from the condensation of polybasic acids with polyhydric alcohols in that they also contain a source of monobasic fatty acids. The type of fatty acid used is important because it determines the drying characteristics of the final alkyd resin. As a matter of fact, to have the best drying properties, it is necessary adding an unsaturated fatty acid. Industrial alkyd paint formulations use a whole range of oils, but the principals are three: linseed oil, soy oil and safflower oil. The first is the most common but with a high yellowing tendency. For this reason it is used for dark colors in which a small amount of yellowing is not noticed; on the contrary for white colors the best choice is the soy oil. The latter also displays good resistance to yellowing but its use is limited due to the high cost [7].

As just mentioned, the importance of the oil component (and not the polyester) has the strongest influence on an alkyd's yellowing properties. In fact, the drying mechanism of alkyd is similar to oil, i.e. involving complex oxidative polymerization reactions, so a dried alkyd film becomes cross-linked and insoluble. However, once the polyester component is already cross-linked, far fewer oxidation reactions are needed for the paint film to dry completely, this alkyds dry more rapidly than oils [5]. Another important condition whereby alkyds are generally quicker drying than pure oil paints is the presence of driers, as naphthanates of cobalt, lead or cobalt and zirconium. These additives are metal soaps or coordination compounds which accelerate paint drying by increasing the rate of cross-link formation between the binder molecules, shortening the total drying time. Without the addition of driers, the drying time of alkyd paint would be over 24 h. Nowadays driers are supplied by solutions, usually in mineral spirits [11].

Another important classification of alkyd type is the proportion of oil to resin, called "oil length". This factor allows determining the working properties and solubility of the paint and it is divided in "short oil", "medium oil" and "long oil" alkyd. The latter can be applied by brush and diluted in

aliphatic mineral spirits; while the short oil alkyd needs aromatic hydrocarbons for thinning but dries faster. Because of their vastly reduced drying time and far superior durability and hardness, alkyd replaced the various combinations of drying oils, thickened oils and natural resins that had been used in the majority of decorative house paints. It remains one of the principal binders used in most industrial paints and by many modern artists, including Pablo Picasso and Jackson Pollock [7].

2.1.4 The drying of alkyd paints

As previously mentioned, the drying mechanism of alkyd is similar to that of oil, and it is developed in two different stages. The first process is the physical drying of the paint where the solvent evaporates and a closed film is formed. The second process is the chemical drying, called lipid autoxidation process [11]. The reaction proceeds by free-radical chain mechanism and can be divided in three step: initiation, propagation and termination (Fig. 4). The first can occur through the action of some unknown initiating species (Eq. (1)) on the substrate by thermal hydroperoxide decomposition (Eq. (2)) or by action of the metal drier. Subsequently propagation reactions involve mainly hydroperoxide formation (Eqs. (3) and (4)), but in this case the reaction is very rapid, except at very low partial pressures of dioxygen. At the end termination occurs via radical recombination to yield peroxy, ether and carbon-carbon cross-links (Eqs. (5-8)).

Initiation

$$RH + Initiator \rightarrow R^\bullet + Initiator\text{–}H \qquad Eq.(1)$$

$$ROOH \rightarrow RO^\bullet + {}^\bullet OH \qquad Eq.(2)$$

Propagation

$$R^\bullet + O_2 \rightarrow ROO^\bullet \qquad Eq.(3)$$

$$ROO^\bullet + RH \rightarrow ROOH + R^\bullet \qquad Eq.(4)$$

Termination

$$2\,RO^\bullet \rightarrow ROOR \qquad Eq.(5)$$

$$2\,ROO^\bullet \rightarrow ROOR + O_2 \qquad Eq.(6)$$

$$2\,R^\bullet \rightarrow R\text{-}R \qquad Eq.(7)$$

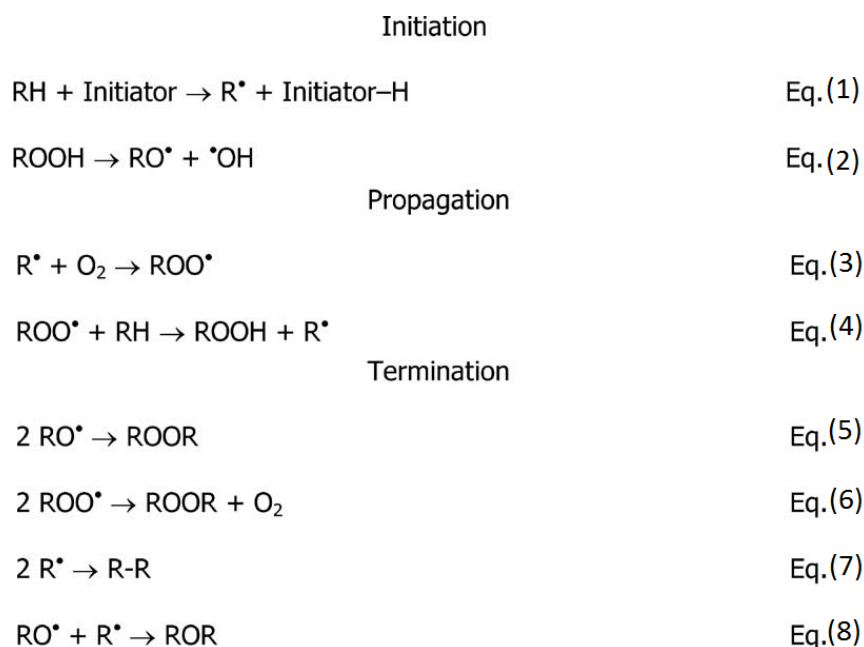$$RO^\bullet + R^\bullet \rightarrow ROR \qquad Eq.(8)$$

Fig. 4 – Radical reactions taking place in the autoxidation of an alkyd resin binder [11]

The autoxidation takes place at the fatty acid group of the alkyd resin. It is important to remember that the drying power of such oil depends on the chemical reactivity of the double bonds of the unsaturated acids, which permits to react with the oxygen of air and forms a polymeric film [12]. The first step of the autoxidation consists of the abstraction of one *bis*-allylic hydrogen atom from the unsaturated fatty acid. This process causes the formation of a radical species, which is stabilized by delocalization due to the local pentadienyl structure. The reaction of the molecular oxygen with this pentadienyl radical species is very rapid and forms a peroxy radical with conjugated double bonds. The peroxy radical can participate in several reactions but the principal is the abstraction of a hydrogen atom from another resin molecule to form a hydroperoxide and propagate the radical chain [12]. The next process is the hydroperoxide decomposition that can lead to the formation of cross-linked species non-volatile (Route I) or to numerous others products such as alcohols, ketones, aldehydes and carboxylic acids (Route II), see figure 5 [11].
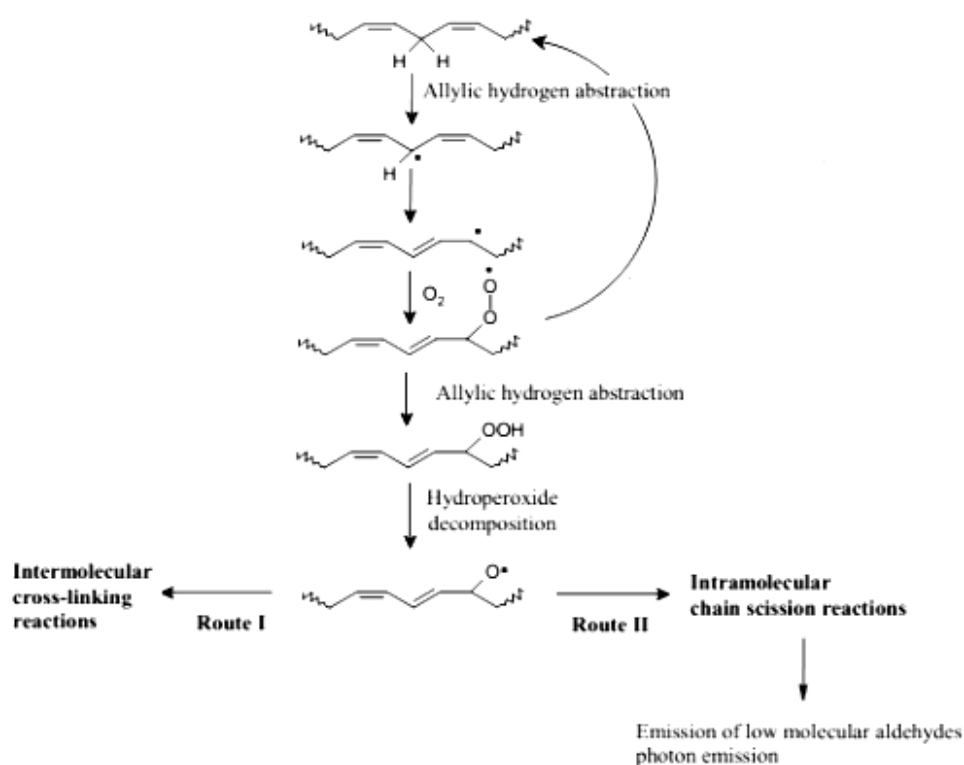

Fig. 5 – Hydroperoxide formation in the autoxidation of the fatty acid chain of an alkyd resin binder

However it is know that alkyd paints dry more rapidly than oils. It is due to different factors such as less presence of oxidation reactions, determined by the degree of unsaturation of its fatty acid chains, and the presence of driers. This innovative process of cross-linking represented a revolution in paint technology, in the household and in the industrial paint markets [7].
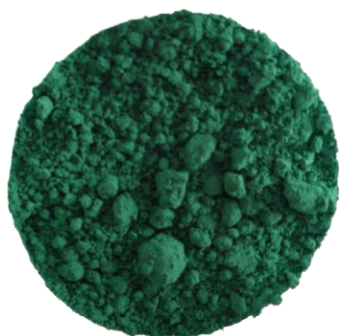
2.2 Pigments

2.2.1 Hydrate chromium oxide green

Fig. 6 – Powder of hydrate chromium oxide green

The hydrate chromium oxide green ($Cr_2O_3 \cdot 2H_2O$) has been introduced in the artistic field during the first half of the nineteenth century and, along with the chromium oxide (Cr_2O_3), is the most common chromium green pigment. Nevertheless the similar name, these two pigments show different shades; chromium oxide is dull and opaque, while hydrate chromium oxide has a color more intensive and transparent (Fig. 6). This pigment is also known as Viridian; apparently it was first applied in England in the 1860s and derives from the Latin name *viridi*(s), meaning green [13].

2.2.1.1 General pigment properties

This pigment has a bright hue, comparable with modern organic pigments such as phtalocyanine green. It is identified as $Cr_2O_3 \cdot 2H_2O$ or in the less common form $Cr_2O(OH)_4$. Based on the ideal formula, the pigment would consist of 55.4% chromium, 42.5% oxygen, and 2.1% hydrogen by weight [13].

2.2.1.2 History of use and preparation

The first attribution and production of this pigment was referred to Pannetier, a Parisian color maker, who prepared it about 1838. However, the expensive price and the secret production didn't allow to use it in the field of painting. Subsequently, with the development of the industrial color manufacture, this pigment took a new name from the French chemist who patented a different preparation method, namely Guignet's green. In this way it was available for a more affordable price and used by artists such as Turner [13]. However, this pigment was rarely found in modern samples of the postwar period. In the 1930 it appeared also in a Winsor and Newton catalogue that introduced the Viridian as a common color used also among English painters such as Penley [14].

The traditional preparation of Guignet's green involved calcining a mixture of two parts of boric acid and one part of potassium dichromate: the first step is an initial heating that produces $Cr_2(B_4O_7)_3$ that is then hydrolyzed in cold water to yield the hydrated oxide and boric acid. Calcining is carried out for about six hours at dull red heat at approximately 500 °C. An interesting information is that in contemporary pigment production literature of the early twentieth century the

Guignet's green is referred as a chromium oxide hydrate, pointing at boron-containing by-products; nevertheless there is no mention of the use of chromium borate as a distinct pigment. In fact, despite the widespread use of viridian, the borate component has not been characterized any further to date. The difficulty in characterizing it is probably due to the fact that most boron compounds are amorphous [14]. Another method of preparation consists in the reduction of a solution of alkali chromate or dichromates with sulfur or other agents to produce the hydrated oxide. The air drying of this intermediate form created another kind of pigment, called transparent chromium oxide [13].

2.2.2 Artificial ultramarine blue

This pigment is similar to the natural ultramarine but, depending on the different ratio used in the manufacture process and the conditions employed, its characteristic and properties could change. It is identified as $Na_{6-10}Al_6Si_6O_{24}S_{2-4}$, however the composition of the ultramarine pigment is very variable and never stoichiometric, due to the different manufacturing process and the nature and proportions of the raw materials [15].

Fig. 7 – Powder of artificial ultramarine blue

2.2.2.1 General pigment properties

The artificial pigment, compared to the natural one, has finer and more regular particle size (Fig. 7). As a matter of fact, under the microscope, the colored granules appear homogeneous even if generally consisting of aggregates of small particles, which can be detected at higher magnifications or if the pigment is dispersed in a medium such as glycerol [15]. Also the chemical properties are similar to the natural ultramarine, but there are some differences. The artificial pigment has a greater tendency to be attacked by dilute acids, even if the blue particles are coated with silica (industrially called "acid-resistant"), capable of withstanding acid effect. Another property is the capability of fading in the presence of excess calcium hydroxide, above all used in lime plaster. In the end artificial ultramarine is capable of ion exchange, for example by heating blue ultramarine in a closed tube with silver nitrate, Na^+ ions are replaced by Ag^+ giving so-called silver ultramarine, which has a yellow color [15].

2.2.2.2 History of use and preparation

The natural ultramarine derives from Lapis lazuli, a semi-precious stone that has been known from ancient times for its deep blue hue, lightened by the scattered presence of pyrite. In European countries, the stone itself was widely used as a pigment in its powdered form up to the thirteenth century. However, the natural pigment began to decline in popularity in the early decades of the nineteenth century due to the industrial production of the less expensive artificial ultramarine blue [16]. It was synthesized by Jean Baptiste Guimet, and subsequently adopted by European artists, in 1828. The artificial ultramarine is composed of sodium aluminium sulfosilicate and other additional materials used for its manufacturing such as anhydrous sodium sulfate and/or carbonate, china clay, silica and sulfur. While the natural ultramarine is just obtained by crushing, grinding and cleaning the raw material to separate the other minerals from lazurite [17], for the artificial pigment two different processes of preparation exist: the indirect and the direct. The first involves two separate stages of heating, on the contrary the latter considers only a single stage of heating giving the blue product. The final characteristics of the pigment such as the hue, depth of color, vulnerability to acids can be varied depending on the proportions, type of starting materials and the conditions of manufacture [15].

2.2.3   Cadmium yellow

Fig. 8 – Powder of cadmium yellow

This pigment is composed of cadmium sulfide, CdS, and exists in two principal types: the pure compound and the lithopone variety, consisting of coprecipitated cadmium sulfide and barium sulfate. The main natural cadmium sulfide minerals are greenockite and hawleyite, which frequently occur as a yellow coating on zinc sulfide (sphalerite). It is known that with chemical and physical modifications it is possible to produce shades ranging from very light lemon yellow to medium orange. This is due to the inclusion of an increasing amount of selenium inside the compound [18].

2.2.3.1   General pigment properties

As mentioned before, cadmium sulfide can be made in various shades ranging from very light yellow (Fig. 8) to deep orange, and this can also be achieved by introducing zinc sulfide in solid solution forming a series of pigments with decreasing redness [19]. Moreover, in the mineral form, cadmium sulfide exists in two crystalline and one amorphous phase. The hexagonal form (α-CdS) is found in nature as the mineral greenockite, the cubic form (β-CdS) as hawleyite, while the amorphous form is

only known as a chemically synthesized product [20]. An important property is that the pigment is a partially covalent compound with a stoichiometric composition of 77.8% Cd and 22.2% S. At normal temperature it is essentially inert to air, humidity, hydrogen sulfide and sulfur dioxide. It easily dissolves in concentrated hydrochloric acid and in diluted or concentrated nitric acids with the evolution of hydrogen sulfide, forming cadmium chloride or cadmium nitrate [18].

2.2.3.2 History of use and preparation

Cadmium yellow, also under the name of sulphuret of cadmium, was suggested for use as an artists' pigment by Stromeyer shortly after his discovery of the metal. Since 1840 cadmium became commercially available as a base material and manufacturers started to make intense use of this pigment [19]. This popularity was mainly due to the pigment's high tinting and covering power, bright yellow color, wide applicability, and suitability for mass production. In addition, CdS was employed in oil paint and watercolors due to its stability, instead of chrome yellow ($PbCrO_4$), the only bright yellow alternative available for painting at that time. By consequence, approximately from 19th to 20th century painters such as Claude Monet, Vincent Van Gogh and Pablo Picasso frequently employed CdS, as was documented by earlier analytical research [20].

The pigment cadmium sulfide was historically produced by means of either a dry or a wet process. For the first, either metallic cadmium, cadmium oxide, or cadmium carbonate was employed as starting material. It was mixed stoichiometrically or with an excess of sulfur and heated to 300-500 °C [18]. This is the reason why a release of gas often occurs in these industrial processes that, in small doses, can cause chronic poisoning to organisms [21]. On the contrary during the wet process (Fig. 9), CdS was obtained as a precipitate by adding a soluble sulfide to a soluble cadmium salt [20].
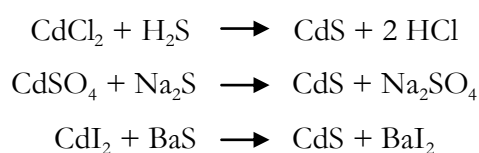
$$CdCl_2 + H_2S \longrightarrow CdS + 2\,HCl$$
$$CdSO_4 + Na_2S \longrightarrow CdS + Na_2SO_4$$
$$CdI_2 + BaS \longrightarrow CdS + BaI_2$$

Fig. 9 – Basic reactions of wet process of cadmium yellow preparation [18]

Chapter 3

Experimental methods and analytical techniques

3.1 Specific materials employed

3.1.1 Plextol® D498

This product (Kremer Pigmente, Germany) is an aqueous dispersion of a thermoplastic acrylic polymer based on methyl methacrylate and butyl acrylate. This emulsion has a nonionic character with pH values ranging from 9.0 ± 0.5. The average particle diameter is around ~0.15 μm; the minimum film-forming temperature is ~5°C. This binder, in addition to being used in paints, is also used in the building sector and for insulating varnishes.

3.1.2 Alkyd Medium 4

This product (Lukas, Germany) has a slightly reddish color, similar to oil. Compared to Plextol® D498, the Alkyd Medium 4 has longer drying-times, even if the final layer is more elastic and adhesive. This also increases the brilliance and translucency of the final color.

3.1.3 Pigments

All pigments used are products of Kremer Pigmente (Germany). The following information (Tab. 1) is obtained from the catalog offered by Kremer.

Pigment Name	Chemical composition	C.I. Name
Ultramarine blue	$Na_8Al_6Si_6O_{24}.S_x$ Sodium Aluminium Sulfo Silicate	PB29
Chrome green	$Cr_2O_3 \cdot 2H_2O$ Chromium Hydroxide, Hydrated Chrome Oxide	PG18
Cadmium yellow	CdS Cadmium sulfite	PY37

Tab. 1 – Principal information about pigments employed

3.2 Experimental method: samples preparation

Different mock-ups of pure Plextol® D498 (Kremer Pigmente, Germany) and Alkyd Medium 4 (Lukas, Germany) in combination with inorganic pigments. i.e. hydrated chromium oxide green, cadmium yellow and artificial ultramarine blue, were cast on glass slides. All pigments are products of Kremer (Kremer Pigmente Gmbh & Co. KG, Germany).The wet film thickness of these paint samples was 150 μm. The samples were prepared in different ratios of pigment to binder (P/BM), depending on the consistence of the paint achieved. In fact to some mixtures water was added to obtain a homogeneous layer. After having weighed the materials, they were put on a glass surface and mixed with a pounder for a few minutes. A detailed description of the mock-ups can be found in (Tab. 2). In total 18 samples were prepared, 9 with Plextol® D498 mixed with the three different colors in three ratios, and the same for Alkyd Medium 4.

Mock-ups	Name of samples	Chemical composition	Color Index: generic name	Ratio (P/BM)	Layer thickness	H_2O	Method of mix
Plextol® D498 + ultramarine blue	C1	$p(nBA/MMA) + Na_8Al_6Si_6O_{24}.Sx$	PB29	1.5g pigment 3g binder (1:2)	150 μm	/	Muller
Plextol® D498 + ultramarine blue	C2	$p(nBA/MMA) + Na_8Al_6Si_6O_{24}.Sx$	PB29	1g pigment 3g binder (1:3)	150 μm	/	Muller
Plextol® D498 + ultramarine blue	C3	$p(nBA/MMA) + Na_8Al_6Si_6O_{24}.Sx$	PB29	0.5g pigment 3g binder (1:6)	150 μm	/	Muller
Alkyd Medium 4 + ultramarine blue	NC4	Polymer oil modified polyester-resin based on orthophthalic acid and pentaerythritol + $Na_8Al_6Si_6O_{24}.Sx$	PB29	1.5g pigment 3g binder (1:2)	150 μm	/	Muller
Alkyd Medium 4 + ultramarine blue	NC5	Polymer oil modified polyester-resin based on orthophthalic acid and pentaerythritol + $Na_8Al_6Si_6O_{24}.Sx$	PB29	1g pigment 3g binder (1:3)	150 μm	/	Muller
Alkyd Medium 4 + ultramarine blue	NC6	Polymer oil modified polyester-resin based on orthophthalic acid and pentaerythritol + $Na_8Al_6Si_6O_{24}.Sx$	PB29	0.5g pigment 3g binder (1:6)	150 μm	/	Muller
Plextol® D498 + hydrate chromium oxide green	C7	$p(nBA/MMA) + Cr_2O_3 \cdot 2H_2O$	PG18	1.5g pigment 3g binder (1:2)	150 μm	0.5 ml	Muller
Plextol® D498 + hydrate chromium oxide green	C8	$p(nBA/MMA) + Cr_2O_3 \cdot 2H_2O$	PG18	1g pigment 3g binder (1:3)	150 μm	0.5 ml	Muller
Plextol® D498 + hydrate chromium oxide green	C9	$p(nBA/MMA) + Cr_2O_3 \cdot 2H_2O$	PG18	0.5g pigment 3g binder (1:6)	150 μm	0.5 ml	Muller

Alkyd Medium 4 + hydrate chromium oxide green	NC10	Polymer oil modified polyester-resin based on orthophthalic acid and pentaerythritol + $Cr_2O_3 \cdot 2H_2O$	PG18	1.5g pigment 3g binder (1:2)	150 µm	/	Muller
Alkyd Medium 4 + hydrate chromium oxide green	NC11	Polymer oil modified polyester-resin based on orthophthalic acid and pentaerythritol + $Cr_2O_3 \cdot 2H_2O$	PG18	1g pigment 3g binder (1:3)	150 µm	/	Muller
Alkyd Medium 4 + hydrate chromium oxide green	NC12	Polymer oil modified polyester-resin based on orthophthalic acid and pentaerythritol + $Cr_2O_3 \cdot 2H_2O$	PG18	0.5g pigment 3g binder (1:6)	150 µm	/	Muller
Plextol® D498 + cadmium yellow	C13	p(nBA/MMA) + CdS	PY37	1.5g pigment 3g binder (1:2)	150 µm	0.5ml	Muller
Plextol® D498 + cadmium yellow	C14	p(nBA/MMA) + CdS	PY37	1g pigment 3g binder (1:3)	150 µm	0.5ml	Muller
Plextol® D498 + cadmium yellow	C15	p(nBA/MMA) + CdS	PY37	0.5g pigment 3g binder (1:6)	150 µm	0.5ml	Muller
Alkyd Medium 4 + cadmium yellow	NC16	Polymer oil modified polyester-resin based on orthophthalic acid and pentaerythritol + CdS	PY37	1.5g pigment 3g binder (1:2)	150 µm	/	Muller
Alkyd Medium 4 + cadmium yellow	NC17	Polymer oil modified polyester-resin based on orthophthalic acid and pentaerythritol + CdS	PY37	1g pigment 3g binder (1:3)	150 µm	/	Muller
Alkyd Medium 4 + cadmium yellow	NC18	Polymer oil modified polyester-resin based on orthophthalic acid and pentaerythritol + CdS	PY37	0.5g pigment 3g binder (1:6)	150 µm	/	Muller

Tab. 2 – Summary of each sample prepared, with the relative name, composition, P/BM ratio chosen, layer thickness and mixing method

The mock-ups were prepared using the same procedure for each of them. Initially, the pigment and the binder were weighed, depending on each different proportion, with an analytical balance. The method of mixing was chosen after several tests carried out with different mixing instruments.
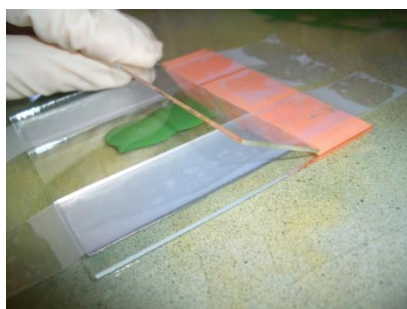

Fig. 10 – Manual mixing with a glass muller

Fig. 11 – Coating method of fresh paints

Initially, a glass container was used, inside of which, was placed a magnetic anchor, with the pigment and the binder. The elements were magnetically mixed for a couple of minutes, but the final result was not optimal because the components were not well blended together, forming lumps. At this point, the use

16

of a mortar has been considered. The first mixtures were fairly satisfactory, however, for yellow paints, this instrument did not allow a proper grinding of the pigment that was granular once applied on the slide. Therefore, for the final preparation of mock-ups, the manual mixing technique was chosen. The pigment powder, after weighed, was placed on a glass plate and subsequently also the binder, weighed too. The two elements were manually mixed with a glass muller (Fig. 10); to make sure to not lose grams of pigment or binder on the glass plate, after a first grinding, the mixture was collected with a small piece of glass in the center of the plate and mixed again. Once the correct texture was reached, a small amount of paint was placed and laid on a slide with another slide (Fig. 11). The chosen thickness for the layer is 150 µm. Once the coats have been completed, the samples have naturally dried (Fig. 12). Later, the samples were analyzed by IR, Micro-Raman and Vis-RS. The basic principles of these techniques are explained in the next chapter.
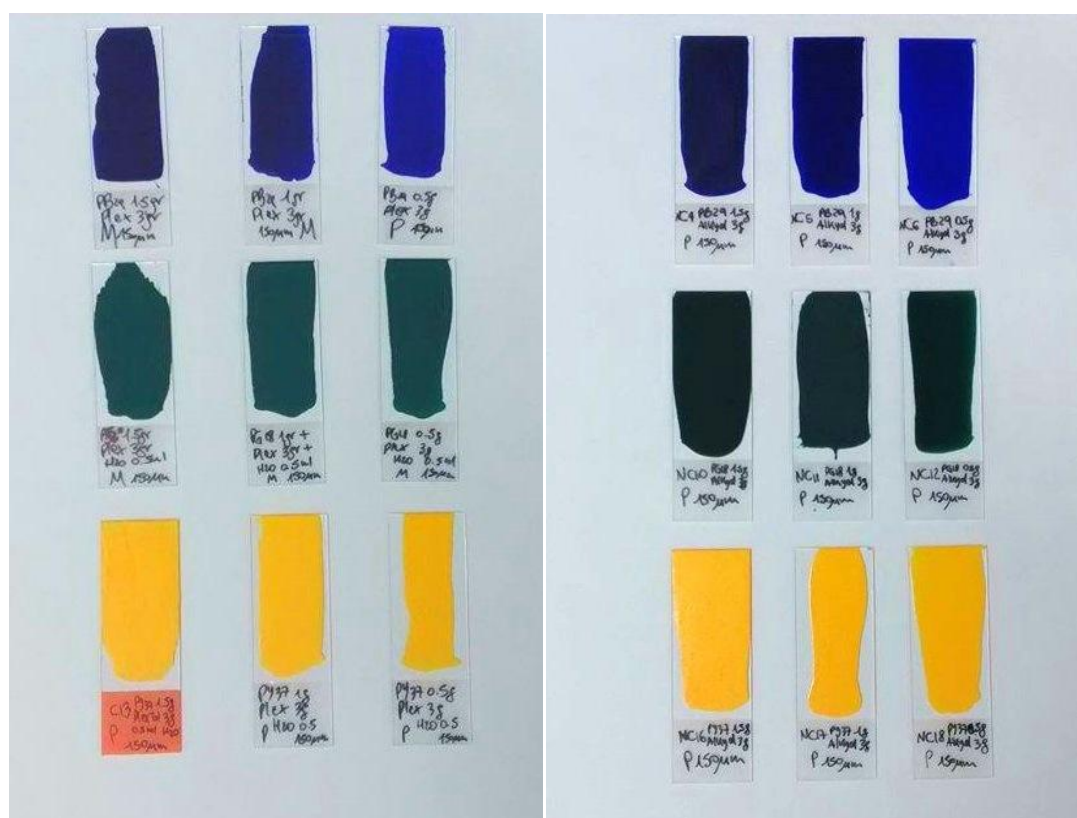
Fig. 12 – Image of self-made mock-ups: to the left, Plextol samples; to the right, Alkyd samples

3.2.1 Additional samples

The first aim of the project is to be able to mathematically quantify the P/BM ratio of an unknown sample by means of a calibration curve created not only with the previously mentioned samples, but also with those in table 3. Those in table 3 have been created by a second operator and used to develop the straight line and try to make the quantitative model more reliable and stable. In some cases some of these samples have been used as unknowns to test the effectiveness of the calibration line.

Mock-ups	Name of samples	Chemical composition	Color Index: generic name	Ratio (P/BM)	Layer thickness	H_2O	Method of mix
Plextol® D498 + ultramarine blue	BP1	p(nBA/MMA) + $Na_8Al_6Si_6O_{24}.S_x$	PB29	1:5	150 µm	/	Muller
Plextol® D498 + ultramarine blue	BP2	p(nBA/MMA) + $Na_8Al_6Si_6O_{24}.S_x$	PB29	1:2	150 µm	/	Muller
Plextol® D498 + ultramarine blue	BP3	p(nBA/MMA) + $Na_8Al_6Si_6O_{24}.S_x$	PB29	1:7	150 µm	/	Muller
Alkyd Medium 4 + ultramarine blue	BA1	Polymer oil modified polyester-resin based on orthophthalic acid and pentaerythritol + $Na_8Al_6Si_6O_{24}.S_x$	PB29	1:2	150 µm	/	Muller
Alkyd Medium 4 + ultramarine blue	BA2	Polymer oil modified polyester-resin based on orthophthalic acid and pentaerythritol + $Na_8Al_6Si_6O_{24}.S_x$	PB29	1:1	150 µm	/	Muller
Alkyd Medium 4 + ultramarine blue	BA3	Polymer oil modified polyester-resin based on orthophthalic acid and pentaerythritol + $Na_8Al_6Si_6O_{24}.S_x$	PB29	1:5	150 µm	/	Muller
Plextol® D498 + hydrate chromium oxide green	GP1	p(nBA/MMA) + $Cr_2O_3 \cdot 2H_2O$	PG18	1:15	150 µm	0.5 ml	Muller
Plextol® D498 + hydrate chromium oxide green	GP2	p(nBA/MMA) + $Cr_2O_3 \cdot 2H_2O$	PG18	1:6	150 µm	0.5 ml	Muller
Plextol® D498 + hydrate chromium oxide green	GP3	p(nBA/MMA) + $Cr_2O_3 \cdot 2H_2O$	PG18	1:1	150 µm	0.5 ml	Muller
Alkyd Medium 4 + hydrate chromium oxide green	GA1	Polymer oil modified polyester-resin based on orthophthalic acid and pentaerythritol + $Cr_2O_3 \cdot 2H_2O$	PG18	1:1	150 µm	/	Muller
Alkyd Medium 4 + hydrate chromium oxide green	GA2	Polymer oil modified polyester-resin based on orthophthalic acid and pentaerythritol + $Cr_2O_3 \cdot 2H_2O$	PG18	1:2	150 µm	/	Muller
Alkyd Medium 4 + hydrate chromium oxide green	GA3	Polymer oil modified polyester-resin based on orthophthalic acid and pentaerythritol + $Cr_2O_3 \cdot 2H_2O$	PG18	1:5	150 µm	/	Muller

Plextol® D498 + cadmium yellow	YP1	p(nBA/MMA) + CdS	PY37	1:1	150 µm	0.5ml	Muller
Plextol® D498 + cadmium yellow	YP2	p(nBA/MMA) + CdS	PY37	1:0.5	150 µm	0.5ml	Muller
Plextol® D498 + cadmium yellow	YP3	p(nBA/MMA) + CdS	PY37	1:10	150 µm	0.5ml	Muller
Alkyd Medium 4 + cadmium yellow	YA1	Polymer oil modified polyester-resin based on orthophthalic acid and pentaerythritol + CdS	PY37	1:2	150 µm	/	Muller
Alkyd Medium 4 + cadmium yellow	YA2	Polymer oil modified polyester-resin based on orthophthalic acid and pentaerythritol + CdS	PY37	1:1	150 µm	/	Muller
Alkyd Medium 4 + cadmium yellow	YA3	Polymer oil modified polyester-resin based on orthophthalic acid and pentaerythritol + CdS	PY37	1:0.5	150 µm	/	Muller

Tab. 3 – Summary table of samples prepared to create the calibration line

Instead, samples in Table 4 come from a project (WTZ, OeAD) that is still ongoing, in collaboration with Hungary, and were used as unknown samples for the evaluation of the P/BM ratio inside them.

Mock-ups	Name of samples	Chemical composition	Color Index: generic name	Ratio (P/BM)	Layer thickness
Plextol® D498 + ultramarine blue	B1	p(nBA/MMA) + $Na_8Al_6Si_6O_{24}.Sx$	PB29	1:3	150 µm
Alkyd Medium 4 + ultramarine blue	B2	Polymer oil modified polyester-resin based on orthophthalic acid and pentaerythritol + $Na_8Al_6Si_6O_{24}.Sx$	PB29	1:0.7	150 µm
Plextol® D498 + hydrate chromium oxide green	G1	p(nBA/MMA) + $Cr_2O_3 \cdot 2H_2O$	PG18	2:2.4	150 µm
Alkyd Medium 4 + hydrate chromium oxide green	G2	Polymer oil modified polyester-resin based on orthophthalic acid and pentaerythritol + $Cr_2O_3 \cdot 2H_2O$	PG18	1:1.5	150 µm
Plextol® D498 + cadmium yellow	Y1	p(nBA/MMA) + CdS	PY37	1:0.4	150 µm
Alkyd Medium 4 + cadmium yellow	Y2	Polymer oil modified polyester-resin based on orthophthalic acid and pentaerythritol + CdS	PY37	2:1.4	150 µm

Tab. 4 – Summary of Project samples used as unknowns for the quantitative analysis

3.3 Analytical techniques

In this thesis spectroscopic techniques were employed for the characterization of pigments and binders used, and for interpretation of different evaluations explained in the following chapters. These methods are based on the interaction of electromagnetic radiation that allows to obtain information about the molecular structure of inorganic and organic compounds and to analyze them in a non-invasive and non-destructive way. These are very important advantages, above all in these recent times where spectroscopic techniques represent one of the most powerful tools to investigate and study the structure of every kind of cultural heritage. The basic theory and the instrumental information of the analytical techniques employed are described in the following chapter.

3.3.1   Basic principles of electromagnetic radiation

Electromagnetic radiation is a form of energy that is produced by oscillating electric and magnetic disturbance, or by the movement of electrically charged particles traveling through a vacuum or matter. This energy has certain characteristics, such as amplitude (A), wavelength (λ) and frequency (ν). The first represents the distance from the maximum vertical displacement of the wave to the middle of the wave. It is basically the height of the wave. Larger amplitude means higher energy and lower amplitude means lower energy. The second is the distance of one full cycle of the oscillation. Shorter wavelength means higher frequency, and higher frequency means higher energy. This wavelength frequency relationship is characterized by:

$$c = \lambda \cdot \nu \qquad \text{(Eq. 9)}$$

Where c ($2{,}99 \cdot 10^8$ m/s) is the speed of light, λ is wavelength, and ν is frequency.
In the end, the latter represent the number of cycles per second, and it is expressed as $\sec^{-1}$ or Hertz (Hz). Frequency is directly proportional to energy and can be expressed as:

$$E = h \cdot \nu \qquad \text{(Eq. 10)}$$

Where E is energy, h ($6{,}626 \cdot 10^{-34}$ J·s) is Planck's constant, and ν is frequency.

The sequential disposition of all the possible ranges of these properties is represented in an electromagnetic spectrum (EM). The EM spectrum is generally divided into seven regions, in order of decreasing wavelength and increasing energy and frequency. The common designations are: radio waves, microwaves, infrared (IR), visible light, ultraviolet (UV), X-rays and gamma rays. Typically, lower-energy radiation, such as radio waves, is expressed as frequency; microwaves, infrared, visible and UV light are usually expressed as wavelength; and higher-energy radiation, such as X-rays and gamma rays, is expressed in terms of energy per photon (Fig. 13) [22].
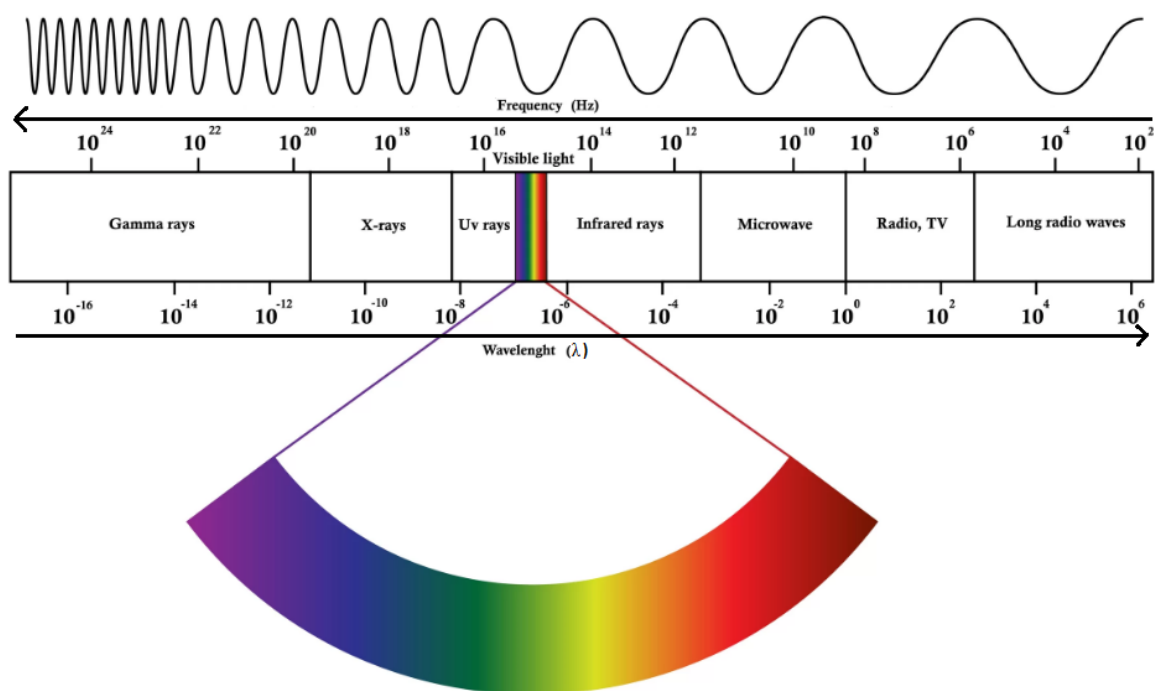
Fig. 13 – Electromagnetic spectrum and periodic wave characterized by wavelength (λ) and frequency (Hz)

As mentioned before, nowadays spectroscopic techniques are widely employed for the study of cultural heritage because they provide useful information about composition of the materials in a non-destructive way. For these reasons, in this project the following techniques were used::

- IR spectroscopy, based on absorption of IR radiation by the material;
- Raman spectroscopy, based on the Raman effect;
- Spectrophotometry (Vis-RS), based on the reflection of light, defined as the visible fraction of the electromagnetic radiation;
- Colorimetry, another photometric measurement based on the colors calibrated on the human eye sensitivity.

3.3.2 Infrared spectroscopy

Infrared (IR) spectroscopy is one of the most common and widely used spectroscopic techniques. It is employed for inorganic and organic compounds due to its usefulness in determining different chemical structures based on the absorption of the IR radiation of different functional groups [23]. A molecule can absorb radiation in three different processes and each of these routes involves an increase of energy that is proportional to the light absorbed. The first way occurs when absorption of radiation leads to a higher rotational energy level in a rotational transition. The second is a vibrational transition which occurs on absorption of quantized energy. The latter involves electrons of molecules being raised to a higher electron energy, which is the electronic transition (Fig. 14). The energy levels can be divided in electronic, vibrational or rotational. Each of these transitions differs by an order of magnitude. Rotational transitions occur at lower energies (longer wavelengths), while vibrational (near infrared) and electronic transitions (ultraviolet region of the electromagnetic spectrum) require higher energies [24].
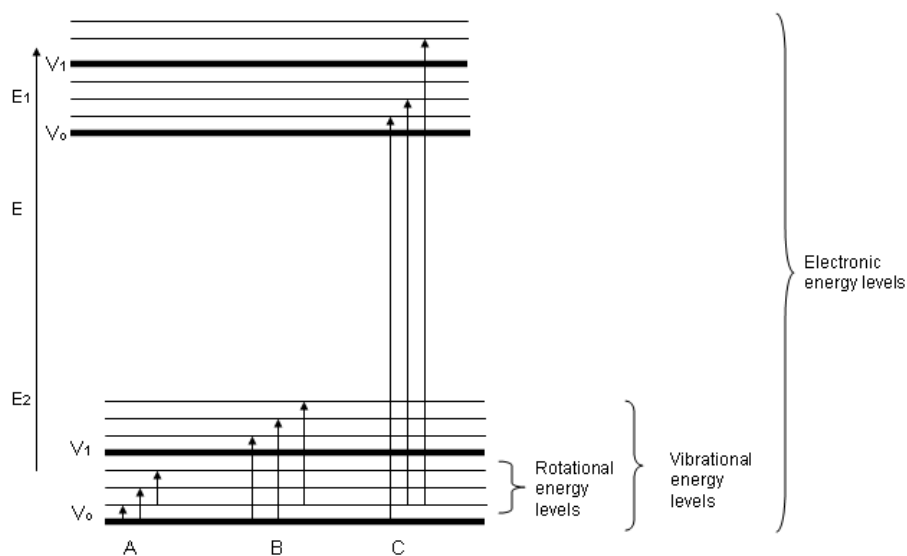
Fig. 14 – Absorption of IR radiation in a molecule: (A): pure rotational transitions, (B) rotational-vibrational transitions, (C) rotational-vibrational-electronic transitions

Infrared radiation can give rise to a vibrational transition when a change in the molecular electric dipole occurs as a result of the change in the position of the atoms. Hence, monoatomic molecules (such as N_2 or O_2) are not active in infrared, while non-polar molecules such as CO_2 can only resonate with radiation due to asymmetric vibrations that produce an instant dipole. It is also possible to observe so-called overtone bands due to the chemical bonding anharmony.

Considering a molecule formed by molecular bonds, moving with a orientation along the three Cartesian axes (x, y, z), the number of atoms present correspond to 3N, defined as *degrees of freedom*. For a non-linear molecule these modes are 3N-6 (3N degrees of freedom less 3 of translational and 3 of rotation), while for a linear molecule are 3N-5 (3N degrees of freedom less 3 of translational and 2 rotation).

The absorption of IR radiation by a molecule can be compared to two atoms attached to each other by a mass-less spring. So, considering a simple diatomic molecule, only one vibration is possible. The Hooke's law indeed relates the mass of the atoms in a molecule, the bond energy and the frequency of absorption (Eq. 11).

$$v = \frac{1}{2\pi C}\sqrt{\frac{k}{\mu}}$$ (Eq. 11)

k is the Hooke's constant, depending on the bond energy and length, and μ, defined as reduced mass, depends on the masses involved. The bond of a molecule experiences various types of vibrations and rotations [25]. The vibrational motions can be of two types: the stretching of the chemical bond and the deformation of the bonding angle (bending). Stretching consists of a periodic variation of the interatomic distance and can be: symmetric if the two atoms approach or move away at the same time, or asymmetric in the opposite case. Deformation can also be symmetrical or asymmetrical and can occur along the plane on which the bending is present or is out of the plane. The symmetrical deformation in the plane is called scissoring, while the asymmetric one is called rocking; the symmetrical deformation out of the plane is called twisting, while the asymmetric plane outside the plane is called wagging (Fig. 15) [22].
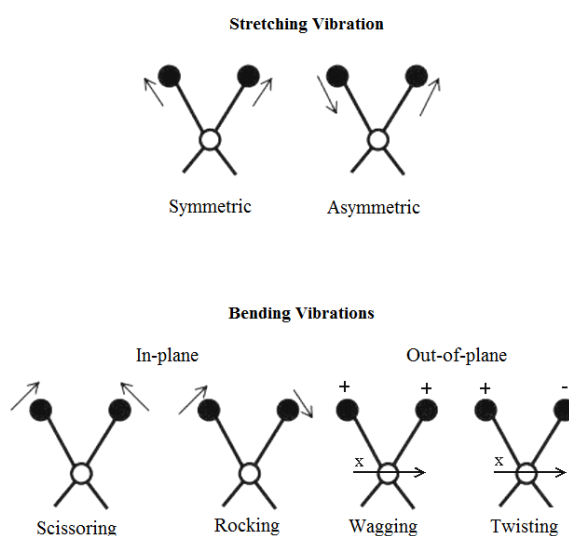
Fig. 15 – Different vibrations in a molecule after a IR absorption

As mentioned before, IR spectroscopy is a valid method for identification of compounds, especially for identification of functional groups. Therefore, it can also be applied in the field of quantitative analysis. The main theory of IR quantification is based on the Lambert Beer's law, which describes the relationship between the absorbed light and the concentration of the substance (Eq. 12):

$$log \frac{I_o}{I} = \varepsilon \cdot c \cdot d = A_\lambda \qquad \text{(Eq. 12)}$$

where A_λ is the absorbance of the sample, I is the intensity of transmitted light, I_0 is the intensity of incident light, d is the path length, ε is the molar absorptivity of the substance, and c is the concentration of the substance. However, the Beer's law is only valid at low concentrations (such as in diluted solutions) [22].

IR spectroscopic analysis can be divided in different techniques (transmission, reflection)that depend on the physical nature of the material and on the output required for the measurement. The analysis in transmission is useful for small samples or thin films where the IR radiation passes through the sample with a high energy, resulting in high sensitivity. In this way it is possible to obtain high resolution qualitative, quantitative or semi-quantitative information from samples. When the sample is not thin enough to allow transmission of IR radiation, reflection techniques are used. Reflection methods can be categorized as: diffuse reflection (DR), internal reflection and external reflection. These methods are based on the principle that, when incident radiation passes through two different media, it is split into reflected and transmitted beams in different proportions according to the ratio between the refractive indices characterizing the two materials [23].

In the internal reflection, called ATR (Attenuated Total Reflection), the sample is placed in intimate contact with the surface of a transparent material with a significantly higher refractive index (*n*) than the sample. This transparent material is called internal reflection element (IRE) and it is selected for its characteristic to be transparent to IR radiation and has a refractive index greater than the sample [26]. When the incident radiation passes through a material, forming a particular incidence angle it is called critical angle (θ). When this angle is greater than the critical one, an evanescent wave is formed on the surface of the higher refractive index material (IRE) and can penetrate the medium place in contact with it, resulting in attenuation.

The penetration depth of the evanescent wave (*dp*) not only depends on the refractive index of both the IRE and the analyzed material but it is also a function of wavelength (Eq. 13) [27].

$$dp = \frac{\lambda}{2\pi n_1 \sqrt{\sin^2 \theta - (n_2/n_1)^2}} \qquad \text{(Eq. 13)}$$

λ is the wavelength of the incident radiation, n_1 is the refractive index of the IRE, n_2 is the refractive index of the sample and θ is the incidence angle of the radiation on the interface. This is the reason why absorption bands at low wavenumber are increased while absorption bands at higher wavenumber are completely absent compared to the same spectrum acquired in transmission mode. For the external reflection, or specular reflection, the sample must be homogeneous, with a flat surface and be nonscattering. It means that it should be optically thick so that it is free from both reflection-absorption and interference fringe features. The light is reflected from a mirror-like sample to record its spectrum, so the incident and reflected angles of the IR radiation are equal. Compared to the internal reflection, the external one is a non-contact technique and for this reason it shows characteristics of both the absorption and refractive index spectra of the sample. This type of spectrum looks different from a transmission spectrum in many ways, e.g. bands may be shifted to higher wavenumbers, and usually has the appearance of the first derivative of an absorption spectrum [23]. Therefore, it is necessary to extract the more analytically useful absorption index spectrum by subjecting it to a Kramers-Kronig transformation (Fig. 16).
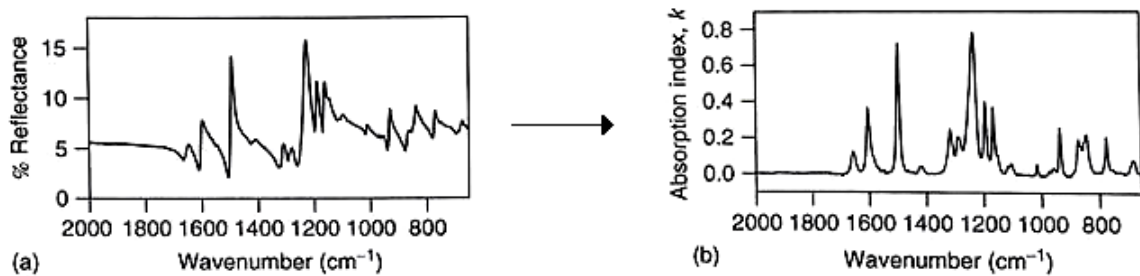
Fig 16 – Schematic representation of the Kramers-Kronig algorithm. (a) Reflectance index, (b) absorption index spectrum generated by applying the Kramers-Kronig algorithm to the specular reflection spectrum

The Kramers–Kronig transforms are based on the principle of causality and connect the real and imaginary parts of many complex quantities in physics. To understand this relation it is necessary to explain the basic principle interaction of an electromagnetic wave with a surface. When the electric field vector of the wave hits the surface, it can split in two parts: the first, called p-polarized, is parallel to the plane of incidence, while the second, called s-polarized, is perpendicular to the plane of incidence [25]. However, if the beam hits two media with different refractive indices, there will be not only reflection but also transmission.

For this reason it is important to consider the polarization direction: after reflection and transmission both p-polarized light and s-polarized light will be the same. This is described by the Fresnel equations. Thanks to them, it is possible to describe the part of the incident radiation which is reflected, defined ad reflectivity (Eq. 14).

$$R_\parallel = \left|r_\parallel\right|^2 \ and \ R_\perp = \ |r_\perp|^2 \tag{Eq. 14}$$

The reflectivity is dependent on the angle of incidence for s- and p-polarized light as shown in Fig. 17.
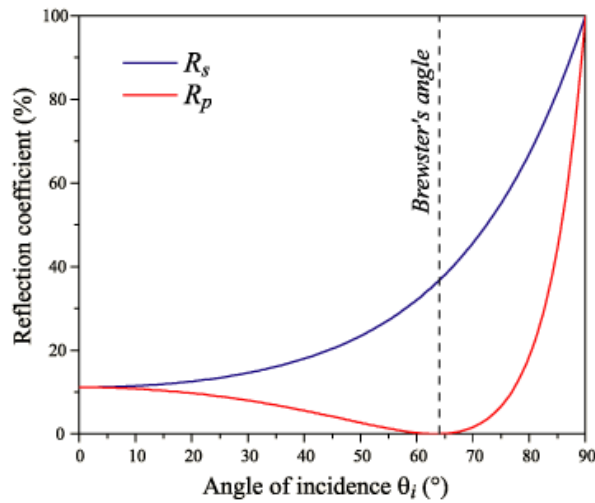
Fig. 17 - Reflectivity is dependent on the angle of incidence for s- and p-polarized light

The figure shows that, when the reflectance reaches the minimum, the s-polarized light is reflected while the p-polarized not. This angle is called Brewster angle or polarization angle and it is related to interfaces between two semi-infinite non absorbing materials. So, when a sample is analyzed, it can be characterized by its optical properties, i.e. the refractive index (n, the real part of the refractive index) and the absorptivity (k, the imaginary part) which are related to the absorption coefficient. These two elements describe the "complex refractive index" (Eq. 15).

$$\underline{n} = n + ik \tag{Eq. 15}$$

The relation between these two parts can be calculated by the Kramers-Kronig transformation [28]. Independently from the sampling technique employed, the IR instruments can use dispersive spectrometers (double beam) or, in most cases, Fourier Transform spectrometers (FTIR). FTIR uses an interferometer that allows to scan all the frequencies present in the IR radiation, generated by the

source. In this way it is possible to obtain an interferogram that shows the representation of the intensity in the time-domain. Subsequently, applying the mathematic operation of Fourier transform, a computer allows obtaining the infrared spectrum, converting the first representation of the intensity in frequency-domain. This provides higher performance than conventional infrared spectroscopy. In addition, the analysis times are substantially reduced [27].

3.3.2.1 Instrument used and experimental conditions

The IR instrumental system used for this project is a FTIR microscope with an integrated FTIR spectrometer, called Lumos (Bruker, Germany). This instrument is endowed with a motorized ATR-crystal that allows the system to switch from transmission or reflection to ATR mode without interaction of the operator. This IR instrument is composed of:

- A crystal, made of germanium with an internal controlled system of pressure for the measurement;
- An objective with a 8x resolution for automated measurements in transmission, reflection and ATR;
- Magnification can be increased to 32x by digital zooming;
- To focus the sample before the measurement in transmission and reflection, the instrument has an independent white light LED illumination;
- It has a incorporated microscope that allows to obtain images of the sample by highly resolving digital CCD camera;
- For the background of the reflection analysis a gold coated mirror for highest efficiency is used.

3.3.3 The Raman spectroscopy

Nowadays, the Raman spectroscopy is the most important contact-free and non-destructive technique used to obtain information on chemical and physical structures, to be able to identify different substances from the characteristic spectral patterns and to determine quantitatively and semi-quantitatively the amount of the substance in a sample. In the past the Raman spectroscopy showed some problems (as sample degradation/decomposition and the fluorescence), but the recent technological development has reduced these disadvantages. For this reason the use of Raman spectroscopy for material analysis in art is grown rapidly [29].

3.3.3.1 Basic theory and principles

In the past this technique used a system of optical filters to create the scattered radiation with a different frequency from the incident light, now the principle is the same but more elaborate. As a matter of fact when a material interacts with monochromatic light most of the incident radiation collide with the molecules in the sample and they can be absorbed, scattered, or transmitted. [30]. The scattered interaction between material and source represents a collision between a vibrating molecule and an incident proton. This collision is divided in:

- Elastic scattering of proton: generally it is called *Rayleigh scattering* and in this effect the energy of the molecule and the proton remains the same.
- Inelastic scattering of proton: it is called *Raman effect* and in this case the energy of proton changes upon the interaction with the molecule, so the energy gap is represented by the difference between two energy levels of a molecular vibration. Even if this effect happens with lower probability, it is the basis of Raman spectroscopy [31].

Interacting with the electrons of the molecules, the electromagnetic radiation induces on them an electric dipole responsible for the diffusion process of the incident radiation. Analyzing the scattered radiation, three components with different energies can be distinguished:

1) The *Rayleigh scattering* represents the most intense component of the scattered radiation. It comes from an elastic scattering process that does not involve exchange of energy with the system and has the same energy of the incident radiation.

2) On the contrary the *Raman scattering* takes place when a photon interacts with a molecule and involves an inelastic scattering, characterized by a loss of energy. This process leads from the ground vibrational state to absorption of energy by the molecule and promotes the shift to a higher excited vibrational state. This component is known as Stokes scattering, and presents lower energies ($v < v_0$). However some molecules may be present in an excited state, for

this reason the transfer of energy to the scattered proton, from these states to a virtual one and finally to the ground state, involves higher energies than the incident radiation ($v > v_0$); this component is called anti-Stokes scattering (Figure 18) [31].
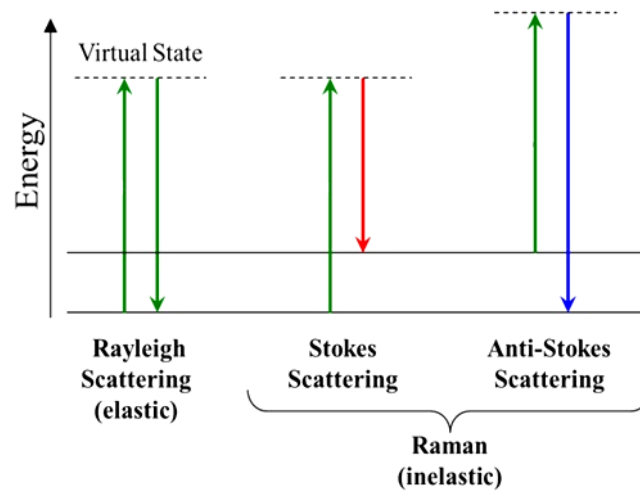

Fig. 18 – Diagram of the Rayleigh and Raman scattering processes

3) The Raman effect can be also considered as a particular case of *fluorescence*, that happens when the incident light-radiation does not match with the absorption bands of atoms or molecules. It corresponds to the gap between two different atomic or molecular energetic levels when they absorb light at a particular wavelength. Considering that fluorescence is much more intense than Raman scattering, very low amount of fluorescence species can cover Raman scatter of a material [32]. Hence, to avoid the fluorescence contribution, it is necessary:

- Selecting an excitation wavelength far away from any electronic transition, e.g. NIR laser;

- It is possible to obtain useful information from the anti-Stokes shift, if fluorescence covers the Stokes lines, even if the intensity is lower;

- Where the fluorescent species represent impurities, a process of photo-bleaching can be employed. It consists on irradiating the sample with Raman laser with the aim of decomposing fluorescent components. Nevertheless also the matrix of the sample can cause fluorescence: therefore it is necessary to close the confocal hole of the Raman microscope in order to reduce the collection volume and the fluorescence, too.

3.3.3.2 The molecular theory

Exactly as in IR spectroscopy, also for Raman analysis the energy of a molecule can be divided into a number of different parts or "*degrees of freedom*". So, if the number of atoms present corresponds to 3N, for a non-linear molecule these modes are 3N-6, while for a linear molecule they are 3N-5. This means that a diatomic molecule will have only one vibration and a triatomic molecule will have three modes of vibration. These vibrations are called *normal modes of vibration* of the molecule and each of them is characterized by its symmetry, intensity and frequency [22]. The vibrational motions can be characterized as (Fig. 15):

- Stretching vibration: between two bonded atoms;
- Bending vibration: between three atoms connected by two bonds;
- Out-of-plane deformation modes: that changes the planar structure into a non-planar one.

However a molecule with a three-dimensional structure exists with a pattern of varying electron density, covering the whole molecule. If either the molecule vibrates, the electron cloud will alter as the positive nuclei change position and depending on the nature of the charge, this can cause a charge of dipole moment or polarization. In these triatomic molecules, the symmetrical stretch cause large polarization charges and hence strong Raman scattering with weak or no infrared absorption. Instead the deformation mode causes a dipole change but little polarization charge and hence strong infrared absorption and weak or non-existent Raman scattering [30].

The change is described by the polarizability derivative (Eq. 16), that determines the section rules for a Raman-active vibration.

$$\frac{d\,\alpha}{d\,Q} \neq 0 \qquad \text{(Eq. 16)}$$

The scattering intensity is proportional to the square of the induced dipole moment and so to the square of the polarizability derivative. If a vibration does not greatly change the polarizability, then the value of the derivative will be near zero and the intensity of the Raman band will be low. It is for this reason that the vibrations of molecules with high polar moiety, e.g. the O-H bond, are usually weak [33].

3.3.3.3 Instrument used and experimental conditions [34]

The instrumental system used in this project is an integrated confocal micro-Raman system (LabRAM Aramis, Horiba Jobin Yvon). This instrument is divided in four principal parts:

- <u>Lasers</u>: in the instrument are present three internal lasers as excitation wavelength sources: the Nd-YAG laser, that is a frequency-doubled laser and a diode pumped solid state laser. It emits green light with a wavelength of 532 nm in the visible spectrum. It has a nominal output power (P_0) of 150 mW, even if the real output power (P) should be 148 mW. The HeNe laser operates at a wavelength of 632.8 nm in the red part of the visible spectrum, with a P_0 of 20 mW (P = 12,5 mW); and the AlGaAs laser, that is a diode laser with a wavelength of 785 nm in the near-infrared spectrum, with a P_0 of 100 mW (P = 92 mW).
- <u>Filters</u>: in order to reduce the laser power at the sample, for filtering out the backscattered excitation line (Rayleigh scattering), there is a density filter wheel driven by the LabSpec software with six neutral filters of different optical densities (Tab. 5).

Density filter	Transmission (VIS-laser)	Output power (P)
No filter [---]	100%	P_0
D 0,3	50%	$P_0/2$
D 0,6	25%	$P_0/4$
D1	10%	$P_0/10$
D2	1%	$P_0/100$
D3	0.1%	$P_0/1000$
D4	0.01%	$P_0/10000$

Tab. 5 – Optical density filters and respective output power

- <u>Microscope</u>: the confocal microscope set up on LabRAM Aramis spectrograph is a BX41 of Olympus with three objective of increasing magnifications (Tab. 6).

Objective magnification	Numeral aperture	Working distance (mm)
10x	0.25	10,60
50x	0.75	0,37
100x	0.90	0,21

Tab. 6 – Microscope objective details

- Spectrometer: the spectrograph disperses the multichromatic Raman signal onto two front illuminated CCDs multichannel detectors, both cooled at -70°C.

Before starting every measurement it is fundamental to calibrate the instrument. It is necessary to fix the zero-position corresponding to laser frequency and Rayleigh scattering, to evaluate the accuracy of Raman wave-number axis and to avoid unexpected wave-number shifts during analysis. To do this, a standard material in this case a crystal silicon (Si^{14}) is used, due to its simple and well-known spectrum which shows a band around 520.7 cm^{-1}.

3.3.4   Short comparison between Raman and IR spectroscopy

Raman spectroscopy is very similar to the frequently mentioned infrared spectroscopy, considering that in both techniques information on molecular vibrations is provided. However, the basic processes to obtain the same vibrational modes are mechanically different. As a matter of fact vibrations which are strong in the Raman spectrum are usually weak in an infrared spectrum and vice versa. It is due to the tendency of polar bonds in antisymmetric vibrational modes and in general in the functional group (such as O-H, N-H, C=O) to be more visible in infrared bands, while Raman tends to emphasise vibrations involving more symmetrical bonds (such as C=C, C-C, S-S), (Fig. 19). Molecules with a center of symmetry have no fundamental lines in common in the IR and Raman spectra [32].
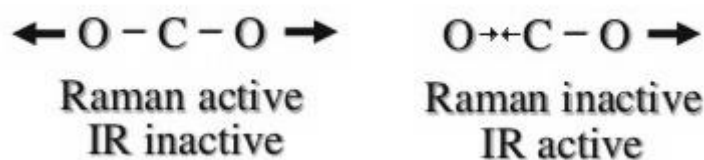
Fig. 19 – IR and Raman active vibrations

The important difference is that in IR absorption the vibrational mode of the molecule requires a change in dipole or change distribution associated with it, and only in this way radiation of the same frequency can interact with the molecule and promote it to an excited vibrational state. On the contrary, scattering involves a momentary distortion of the electrons distributed around a bond in a molecule, followed by re-emission of the radiation as the bond returns to its ground state. In its distorted form, the molecule is temporarily polarized and it develops momentarily an induced dipole, which disappears upon relaxation and re-emission [33].

Another important advantage of Raman spectra is the possibility to obtain them from an aqueous solution because the vibrational modes of O-H bond do not greatly change the polarizability and the Raman band will be low. In addition, also glass or quartz can be employed, thus avoiding working with atmospherically unstable elements, such as KBr. Nevertheless Raman spectroscopy is subject to interferences due to fluorescence, caused by the material of the sample or by impurities [22].

3.3.5   Spectrophotometry and Colorimetry

The basic principles of Spectrophotometric techniques are based on the molecular electronic transitions that take place when the incident beam (i.e. visible radiation) hits the surface of the material and electromagnetic radiation of various wavelengths will be absorbed. This corresponds to a electronic transition, in which electrons in a molecule are promoted from one energy level (ground state) to a higher one (excited state). The energy change associated with this transition provides information on the structure of a molecule and determines many molecular properties, such as color. The parts of the molecule, which are sensitive to electronic transitions, are known as chromophore groups. Generally, all unsaturated groups can be defined as chromophores, such as polyenic systems, aromatic rings, etc. The transitions responsible of this phenomenon are divided in the following types (Fig. 20):

- $\pi \rightarrow \pi *$: from π bonding orbitals to π anti-bonding orbitals (π^*)

- $n \rightarrow \sigma *$: from non-bonding orbitals to σ anti-bonding orbitals (σ^*)

- $n \rightarrow \pi *$: from non-bonding orbitals to π anti-bonding orbitals (π^*)
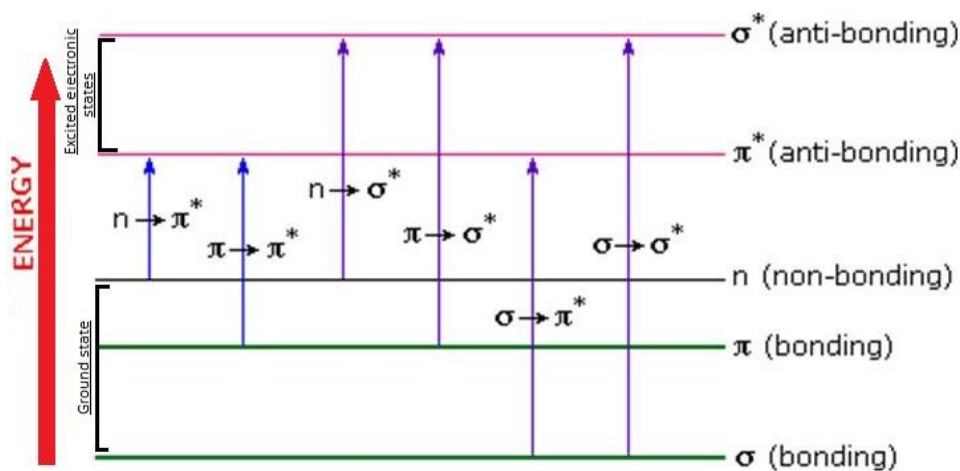
Fig. 20 – Electronic transitions from ground state to excited states

The characteristic associated with the various chromophore groups, involving in the electronic transition and the frequency of radiation, is the absorption wavelength which can be calculated by Planck's law (Eq. 17):

$$\lambda = \frac{hc}{\Delta E}$$

(Eq. 17)

Where h ($6,626 \cdot 10^{-34}$ J·s) is the Planck's constant, c is the light speed and ΔE is the variation of energy related to the transition [35].

The absorption can be measured in transmittance or in reflection. In the latter case, for the analysis of diffuse reflection spectra, obtained from samples with weak absorption, the Kubelka-Munk theory is generally used. It provides a correlation between reflectivity and concentration; therefore it is possible to determine the concentration of the absorbent species using the following equation (Eq. 18):

$$R = \frac{k}{s} = \frac{(1-R)^2}{2R}$$ (Eq. 18)

On the other hand, Colorimetry is the qualitative and quantitative study of the reflected portion of light that stimulates the human eye, defining the color of the material itself. So, the wavelengths of the visible light correspond to associated color (reflected radiation) and complementary color (absorbed radiation); (Tab. 7).

Color	Wavelength (nm)	Complementary color
Violet	400-435	Greenish-yellow
Blue	435-480	Yellow
Light blue	480-490	Orange
Green	500-560	Violet
Yellow	580-595	Blue
Orange	595-605	Light blue
Red	605-750	Bluish-green

Tab. 7 – Principal wavelengths in a electromagnetic spectrum associated to each color
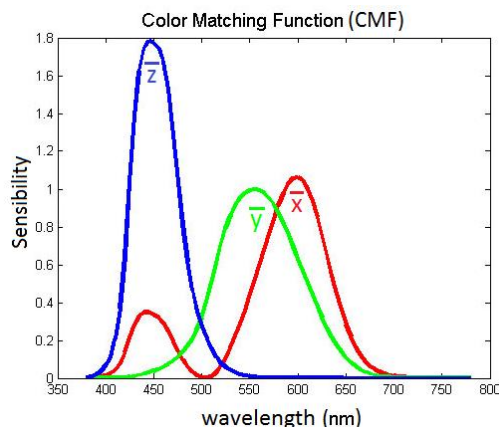
According to the additive theory of colors of light, the white light is given by the sum of three main components: Red (R), Green (G) and Blue (B). If different proportions of these elements are mixed the whole colors spectrum will be covered. Therefore, the human eye has a different sensitivity to R, G and B components and this is described by the Color Matching Function; Fig. 21 (CMF).

Fig. 21 – Color Matching Function for the three components

The real perception of the color of an object depends on three factors: the spectral distribution of the illuminant (S(λ)), the reflection spectrum of the sample, absorbing at wavelengths corresponding to electronic transitions (R(λ)), and the CMF, i.e. the sensibility of the human eye to the visible light (intends as sum of RGB components). To obtain the color matching function it is necessary to calculate the tristimulus values, of which sums, give the chromaticity coordinates x, y, z (Eq. 19-20-21).

$$x = \frac{x}{x + y + z} \qquad \text{(Eq. 19)}$$

$$y = \frac{y}{x + y + z} \qquad \text{(Eq. 20)}$$

$$z = \frac{z}{x + y + z} = 1 - x - y \qquad \text{(Eq. 21)}$$

The color can be characterized by three values: hue, given by the chromaticity coordinates, chroma, i.e. saturation or quantity of grey, and brightness, i.e. the amount of reflected light. The relation between one of this elements and another is described with the color spaces[1]. The color spaces are used to define and quantify the color properties of an object, depending on the object itself, the illuminant and the human eye perception [36].

Trying to establish uniform colorimetric specifications, at the beginning of the twentieth century the International Commission on Illumination (CIE, Commission International de l'Éclarage) was founded. This commission represents an international authority on light, illumination and color and, in order to describe them and color change uniformly, developed several color spaces for standardized illuminants and observers. The first idea, called CIE (1931) was to define a two-dimensional color space chromaticity diagram, based on the chromaticity coordinates, i.e. the hue and the chroma, and adding a Y value to quantify the brightness attribute of the color. However, this diagram is not uniform and cannot quantify the color differences uniformly to the human perception. For this reason, to achieve perceptual uniformity, a new attempt has been developed, known as CIELAB (1974), based on the representation of a three-dimensional spherical space where the chromaticity coordinates are described as a* and b*, while the brightness is L* [37].

---

[1] It represents an algebraic structure with precise mathematical properties that allows to represent a space (that is, the three-dimensional world or the space that contains all the colors) through the use of particular mathematical objects, the vectors. They serve to build the space and determine which properties it owns. The distance between two points, and hence even between two colors, can be calculated using the same formula, but the set of visible colors will appear in a different shape.

These values can be calculated as (Eq. 22-23-24):

$$L^* = 166 \left(\frac{Y}{Yn}\right)^{1/3} - 16 \tag{Eq. 22}$$

$$a^* = 500 \left[\left(\frac{X}{Xn}\right)^{1/3} - \left(\frac{Y}{Yn}\right)^{1/3}\right] \tag{Eq. 23}$$

$$b^* = 200 \left[\left(\frac{X}{Xn}\right)^{1/3} - \left(\frac{Z}{Zn}\right)^{1/3}\right] \tag{Eq. 24}$$
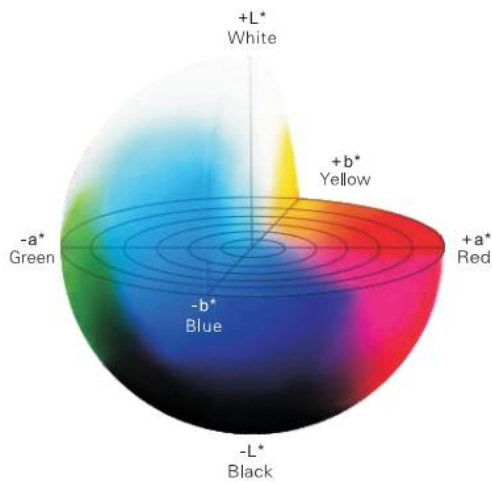
Fig. 22 – CIELAB spherical space

In particular, the L* represents the brightness, and it can assume values from 0 (minimum brightness - black) to 100 (maximum brightness - white), a* expresses the red part when it is positive and the green one when it is negative, lastly the b* expresses the yellow when it is positive and the blue when it is negative (Fig. 22). Both can have values ranging from infinite to less infinite. With this system, as well as having more uniformity, it is possible calculate the difference between two colors, defined as ΔE (Eq. 25) [38].

$$\Delta E = \sqrt{(\Delta L^*)^2 + (\Delta a^*)^2 + (\Delta b^*)^2} \tag{Eq. 25}$$

This parameter is important in the field of cultural heritage because, after a certain age or consolidation treatment in a material, it provides useful information about color change, studying the reflection spectra. It is also possible to check the trend of the chromatic alteration as an effect of interaction of the environment of location-conservation with the art work and, then to determine the causes, i.e. the environmental operating-factors. The measurements of the chromatic parameters are also allowed to establish if the modifications, caused by an inappropriate environment, must be linked to irreversible or reversible effects and, then, with the possibility of being removed.

3.3.5.1 Instrument used and experimental conditions

The instrumental system used in this project is an X-Rite Spectro Eye (Switzerland), employed to acquire reflection spectra of the samples. The principal parameters used are:

- Optical observation system with integrating sphere, having reading angle of 10° (Standard Observer);
- Standard illuminant D65 (6500 °K);
- Measurement range 380-730 nm;
- Diameter opening Ø 3mm;
- Geometry 45°/0°.

After calibrating the system with a reference material, five spots were measured on the mock-ups and the average was calculated using Microsoft Excel software.

Chapter 4

Results and discussion

4.1 Introduction

The results obtained, with the different analytical techniques previously explained, provide useful information for the characterization of various painting materials and the mathematical quantification of different P/BM ratios used for realization of the mock-up.

In paragraphs 4.1.1 and 4.1.2 preliminary results, by optical microscopy and spectrophotometry Vis-RS, are reported. The methods allow to acquire optical and aesthetic information from the paint layers. Instead, paragraphs 4.1.3 and 4.1.4 show IR and Raman results for the identification of the pigments and the binders studied, with an important comparison between the two techniques used.
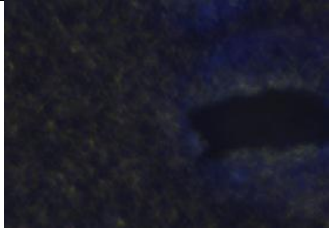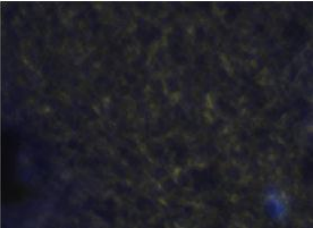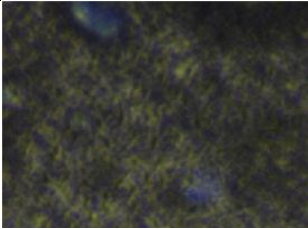
In paragraph 4.2, the graphs of the mathematical evaluation are reported and used to quantify the different P/BM ratios in the mock-ups. In particular, information on the evaluation of unknown and commercial samples, inserted in the calibration curve obtained, is described.

In the end, in paragraph 4.3, results of time-resolved in-situ analysis (IR and Raman) of drying of different P/BM mixtures is presented.
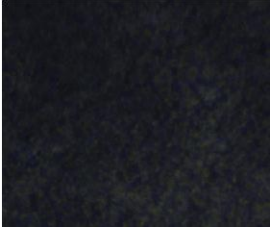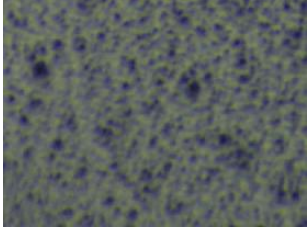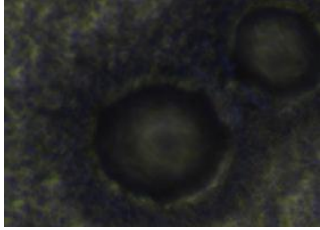
4.2 Characterization of materials

4.2.1 Microscopic and morphological analysis
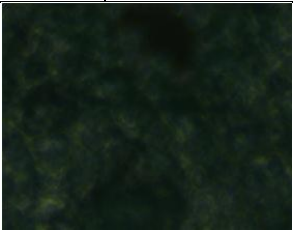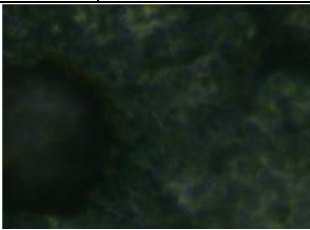
The images in the following tables show the different textures obtained in the mock-ups, made with different binders (acrylic and alkyd) and pigments (artificial ultramarine blue, hydrated oxide green and cadmium yellow). Depending on the different P/BM ratios, it is possible to observe morphological and microscopic differences. The images have a magnification of 32x approximately and were obtained by the FT-IR microscope, called Lumos (Bruker, Germany).

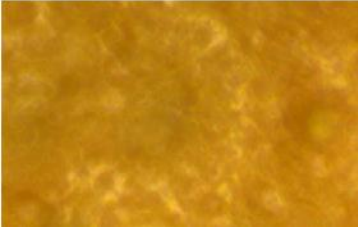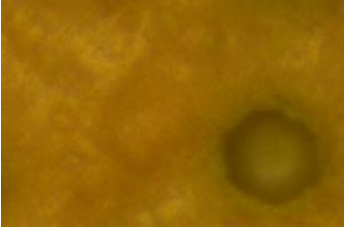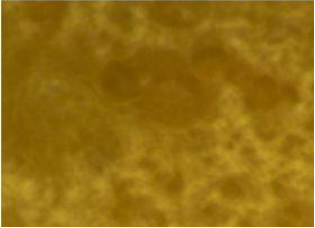| PB29 + Plextol D498					
Name of sample	Ratio (P/BM)	Name of sample	Ratio (P/BM)	Name of sample	Ratio (P/BM)
C1	1.5g pigment + 3g binder (1:2)	C2	1g pigment + 3g binder (1:3)	C3	0.5g pigment + 3g binder (1:6)
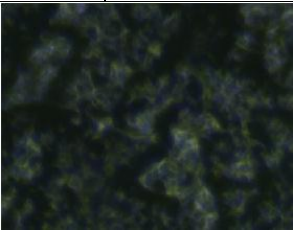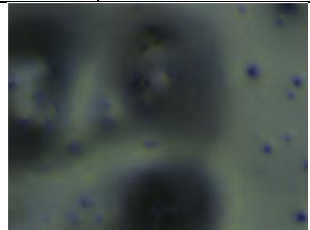
Tab. 8 – Microscopic images of artificial ultramarine blue and Plextol D498 with corresponding sample information

PB29 + Alkyd Medium 4					
Name of sample	Ratio (P/BM)	Name of sample	Ratio (P/BM)	Name of sample	Ratio (P/BM)
NC4	1.5g pigment + 3g binder (1:2)	NC5	1g pigment + 3g binder (1:3)	NC6	0.5g pigment + 3g binder (1:6)

Tab. 9 - Microscopic images of artificial ultramarine blue and Alkyd Medium 4 with corresponding sample information

PG18 + Plextol D498					
Name of sample	Ratio (P/BM)	Name of sample	Ratio (P/BM)	Name of sample	Ratio (P/BM)
C7	1.5g pigment + 3g binder (1:2)	C8	1g pigment + 3g binder (1:3)	C9	0.5g pigment + 3g binder (1:6)

Tab. 10 - Microscopic images of hydrated chromium oxide green and Plextol D498 with corresponding sample information

PG18 + Alkyd Medium 4					
Name of sample	Ratio (P/BM)	Name of sample	Ratio (P/BM)	Name of sample	Ratio (P/BM)
NC10	1.5g pigment + 3g binder (1:2)	NC11	1g pigment + 3g binder (1:3)	NC12	0.5g pigment + 3g binder (1:6)

Tab. 11 - Microscopic images of hydrated chromium oxide green and Alkyd Medium 4 with corresponding sample information

PY37 + Plextol D498					
Name of sample	Ratio (P/BM)	Name of sample	Ratio (P/BM)	Name of sample	Ratio (P/BM)
C13	1.5g pigment + 3g binder (1:2)	C14	1g pigment + 3g binder (1:3)	C15	0.5g pigment + 3g binder (1:6)

Tab. 12 - Microscopic images of cadmium yellow and Plextol D498 with corresponding sample information

PY37 + Alkyd Medium 4					
Name of sample	Ratio (P/BM)	Name of sample	Ratio (P/BM)	Name of sample	Ratio (P/BM)
NC16	1.5g pigment + 3g binder (1:2)	NC17	1g pigment + 3g binder (1:3)	NC18	0.5g pigment + 3g binder (1:6)

Tab. 13 - Microscopic images of cadmium yellow and Alkyd Medium 4 with corresponding sample information

In the tables below it is possible to observe the morphological variation of the sample surface, depending on different P/BM ratios. Sample C1 (Tab. 8) shows a compact and homogeneous surface with a slight crack due to the water evaporation of the binder. In C2 and C3, it is possible observe that as the pigment portion decreases, the surface is more brilliant and granular. The same phenomenon is noticed in the alkydic blue samples (NC4, NC5, NC6). Only in the last sample (NC6) there are craters on almost the entire surface, due to the low content of pigment and the drying of the binder (Tab 9).

In the green coats (Tab 10-11), depending on the different binder used, different surface in the mixtures structures are observed. In the samples with Plextol (C7, C8, C9) the surface appears almost unchanged, except in the latter one where there are some cracks due to the low amount of pigment. This homogeneity is probably due to the small portion of water added during the preparation to make the painting more workable. In the alkyd samples it is observed that in the coats with most pigmented formulations, the surface is more cross-linked and rough while in the latter it is more smooth, homogeneous and with small holes.

The yellow coats (Tab. 12-13) are the most compact and uniform. There are no large differences in both acrylic and alkyd samples. In the first, the surfaces have more cross-links, while the latter is more regular and shiny.

The different morphological effects observed are due to several factors. First, the chosen thickness (150 µm) is very thin, so the results of the drying observed on the surfaces could have been affected. Also the type of pigment used is important in the final yield of the coats. Pigments such as artificial ultramarine blue and hydrated chromium oxide green have larger and more compact grains, while in cadmium yellow they are finer and lighter. Therefore, mixed with the various binders, this has allowed getting greater homogeneity than the previous ones. Finally, depending on the two binding media, different surface textures are observed.

In the case of acrylic samples, the coats are more dry and cross-linked, due to the evaporation of water inside. Instead, in the alkyd samples, more glossy and apparently more homogeneous surfaces were noticed. Probably this is due to a slower drying of the binder, before being superficially dried by the evaporation of the solvent (physical drying) and after more internally by the lipid autoxidation process (chemical drying), see chapter 2.1.4. The final result shows a more regular and polymerized surface.

4.2.2   Spectrophotometric measurements

An additional characterization of the examined pigments is carried out by reflectance spectrophotometry (Vis-RS). As explained in chapter 3.3.5, it is a noninvasive technique in which the analyzed surface is irradiated with light and the spectral response of the surface is recorded.

It represents the ratio of light intensity affecting the surface and what it reflects, and it is called percentage reflectance (R [%]). This, calculated for each wavelength in the visible, defines the spectral behavior of the surface under consideration. For this reason, for different materials, a characteristic and identifying spectral behavior is observed; therefore this technique is useful for qualitative investigation. The resulting spectra from the analyzed samples are compared. The study allows to characterize the pigments used, by the FORS database, but also to observe probable spectral changes between a P/BM ratio and another.
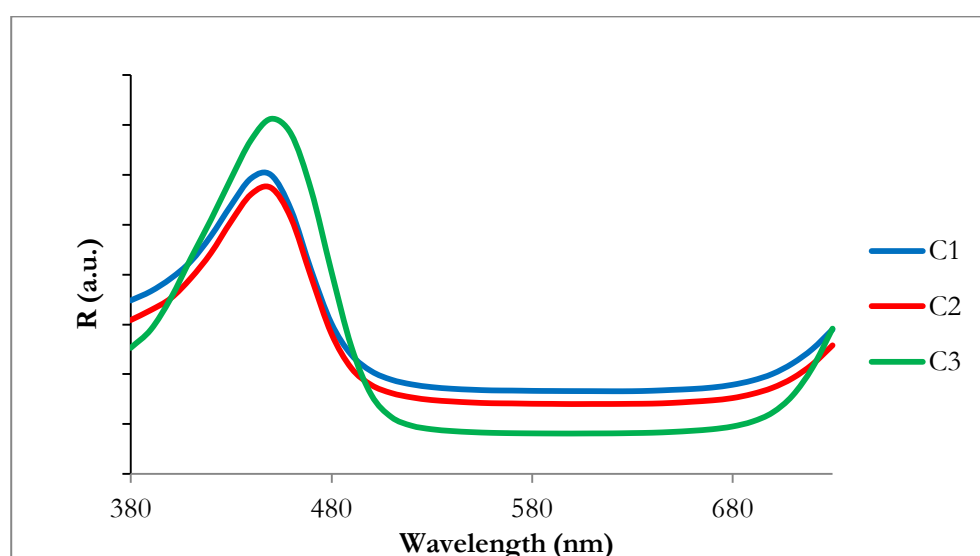
Fig. 23 - Comparison of Vis-RS spectra of samples C1, C2, C3
(Artificial ultramarine blue pigment + acrylic binder)

The Vis-RS spectra, shown in figure 23, present similar characteristics to the Vis-RS spectrum of the artificial ultramarine blue. Compared to the reference in FORS database, they show the same reflectance band around 450-460 nm, the same reflectance minimum (absorption band) around 530 nm and the same reflectance in the red (680-730 nm). However, it is possible to observe that the absorption bands of three spectra present different values of reflectance. As a matter of fact, sample C1 shows higher R value compared to sample C3. This shift is probably due to the different shade and intensity of the color, depending on the P/BM ratio employed in the samples [39]. For this reason spectrum C1, composed of 1.5 g of pigment, presents a high absorption band, while in spectrum C3 (0.5 g of pigment) it is lower.
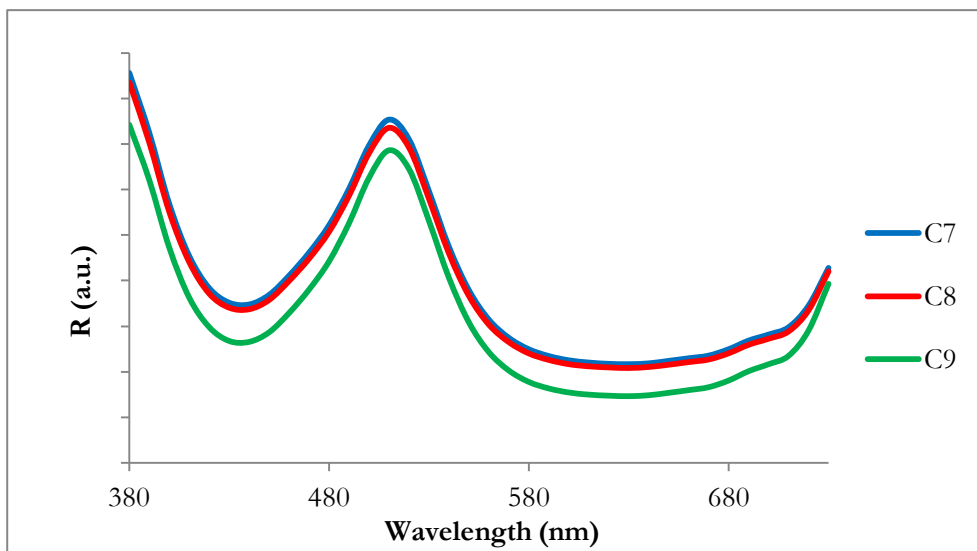
Fig. 24 - Comparison of Vis-RS spectra of samples C7, C8, C9
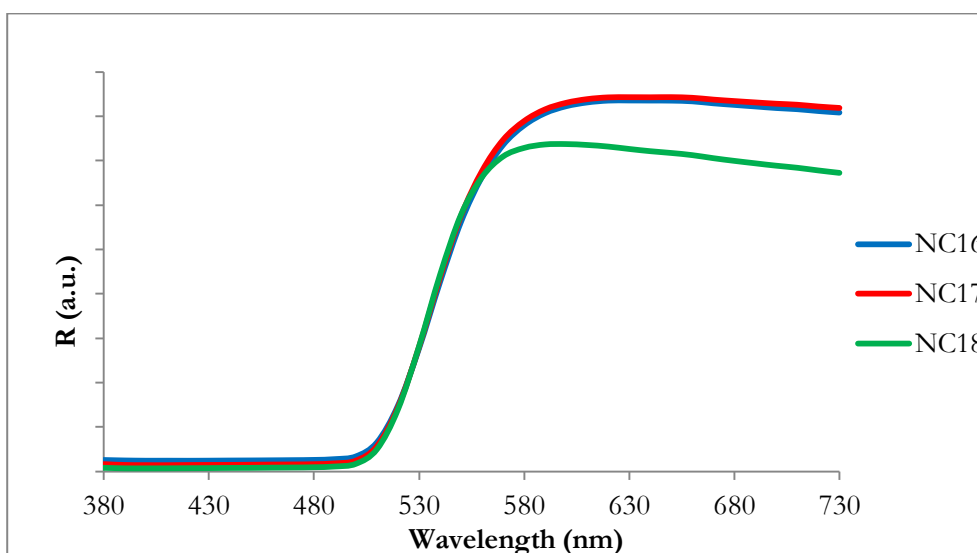
(Hydrated oxide green pigment + acrylic binder)

Fig. 25 - Comparison of Vis-RS spectra of samples NC16, NC17, NC18

(Cadmium yellow pigment + alkydic binder)

Figure 24 depicts the spectrophotometric spectrum of hydrated oxide green. It presents the significant reflectance band around 510 nm and a small band around 690 nm. Around 430 nm and 575 nm the reflectance minima are observed. These spectral signals are characteristic of this pigment. In figure 25 the spectrum shows an absorption maximum around 540 nm; this reflectance value is typical for cadmium yellow pigment. Also in these two spectra the spectral shift due to the different P/BM ratios of the samples is observed. This study confirms the possibility to obtain, with this technique, information not only about the characterization of colored compounds but also to distinguish different reflectance values depending on the P/BM ratios in the samples.

4.2.3 IR and Raman characterization

This chapter represents the first step of the project, i.e. the identification and characterization of the materials used for the realization of mock-ups. It was necessary to have a detailed knowledge of the exact chemical nature of pigments and binders obtained by IR and Raman, in order to decide how to evaluate the spectra for the quantitative analysis and for the study of drying process with the time-resolved mode. It is well known that coating materials such as paints are mixed with several components, such as binding media, pigments, solvents and fillers. In this case the mock-ups are only composed of two components. In fact binding media are not simple mixtures but rather complex polymers, so their characterization is more complicated. To investigate each sample, FTIR and Raman spectroscopy have been used.

These techniques are non-invasive and non-destructive. Raman spectroscopy allows, for example, to distinguish between pigments of the same color, to determine the differences between samples identifying a possible process of preparation and/or identifying the raw materials used and their possible origin, while infrared spectroscopy is useful for the identification and characterization of a wide range of materials whose chemical components and molecular structures are identified through their characteristic absorption bands.

For these reason it is possible to say that these two techniques are complementary. Vibrations which are strong in the Raman spectrum are usually weak in an infrared spectrum and vice versa. Therefore, antisymmetric vibrational bonds, in general in the functional group, are be more visible in infrared bands, while symmetrical vibrational bonds are more empathize in Raman spectra.

According to the type of technique used, the following results are divided. According to literature it was possible to assign each band to a certain chemical group.
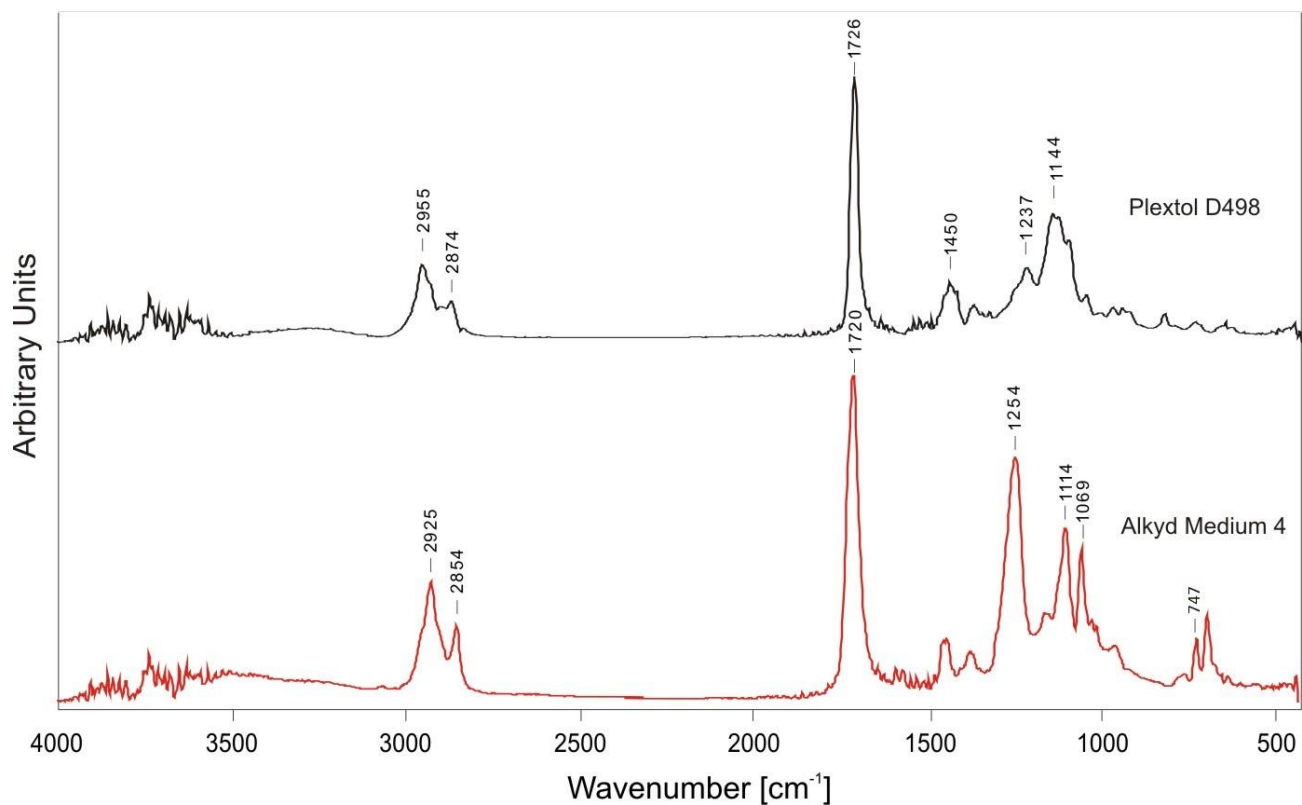
4.2.3.1 Characterization of IR spectra

Fig. 26 – Comparison between pure Plextol and pure Alkyd infrared spectra

	Wavenumber (cm^{-1})		Wavenumber (cm^{-1})	Assignment
Plextol D498	2955-2874		2925-2854	**C-H stretching (symm. - asymm.)**
	1726		1720 (oil and phthalate)	**C=O stretching**
	1450		/	**C-H bending**
	1237-1144	**Alkyd Medium 4**	1250 (phthalate)	**C-O-C stretching (asymm.)**
	/		1114 (phthalate)	**C-O-C stretching (symm.)**
	/		1069 (phthalate)	**C=C unsaturated in-plane deformation**
	/		747 (phthalate)	**Aromatic out-of-plane bending**

Tab. 14 – Relative assignment of each band [40; 7, 41; 29]
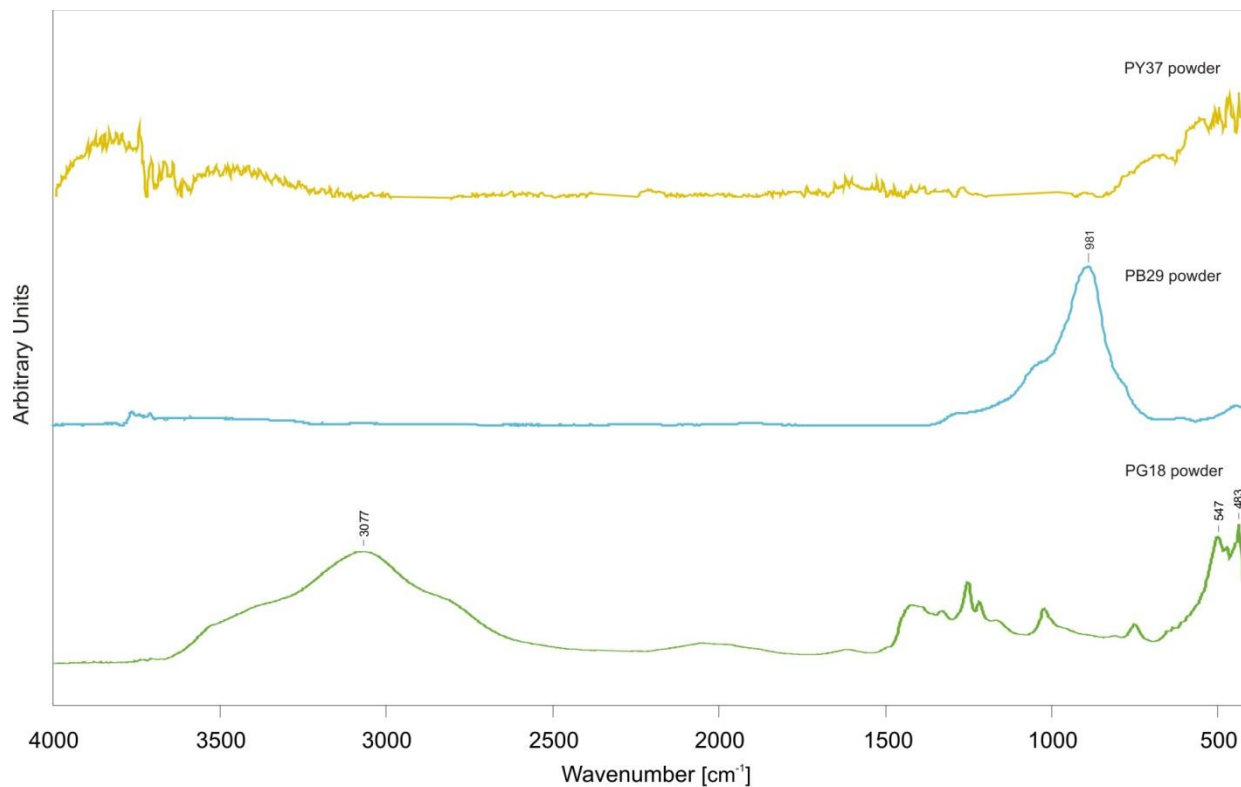
Fig. 27 – Comparison between colored powder infrared spectra of each pigment

	Wavenumber (cm⁻¹)	Assignment
PY37	/	Completely transparent to IR
PB29	981	Si-O bond vibrations
PG18	3077	O-H bond vibrations
	547-483	Oxide bond vibrations

Tab. 15 – Relative assignment of each band [7; 42; 43; 44; 45]

4.2.3.2　　　Characterization of Raman spectra
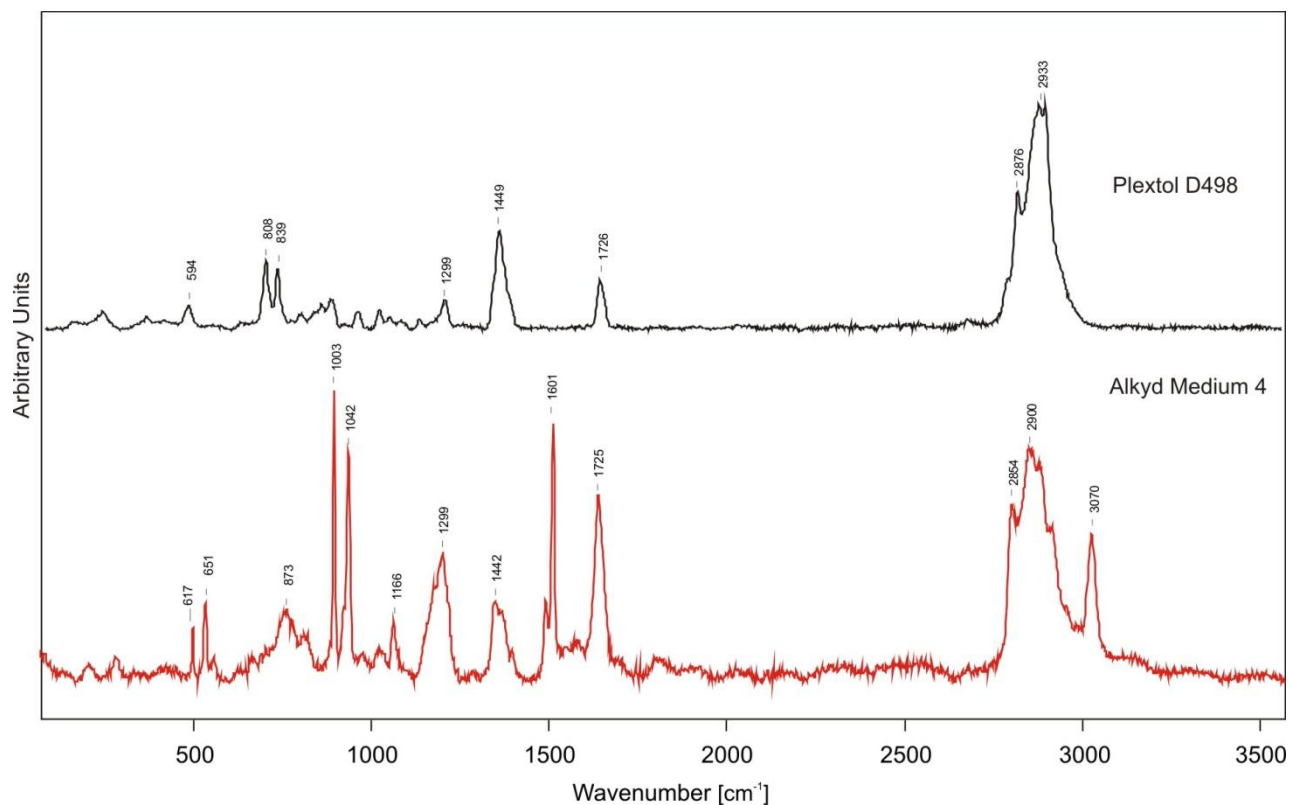
Fig. 28 – Comparison between pure Plextol and pure Alkyd Raman spectra

	Wavenumber (cm⁻¹)		Wavenumber (cm⁻¹)	Assignment
	594		/	C=O bending
	/		651	C=O wag
	808-839		/	C-H rock
	/		873	C-O-C stretching, symm. (aliphatic ether)
	/		1003-1042	Ring breathing (*o*-phthalate)
Plextol D498	/	**Alkyd Medium 4**	1166	C-O stretching (alcohol)
	1299		1299	CH₂ twist/rock
	1449		1442	CH₂ bending
	/		1601	C=C stretching (aromatic)
	1726		1725	C=O stretching
	/		2854	C-H stretching (-CH₂- symm.)
	2876		/	C-H stretching (-CH₃)

	2933		2900	**C-H stretching (-CH$_2$- asymm.)**
	/		3070	**C-H stretching (aromatic)**

Tab. 16 – Relative assignment of each band [46; 29]
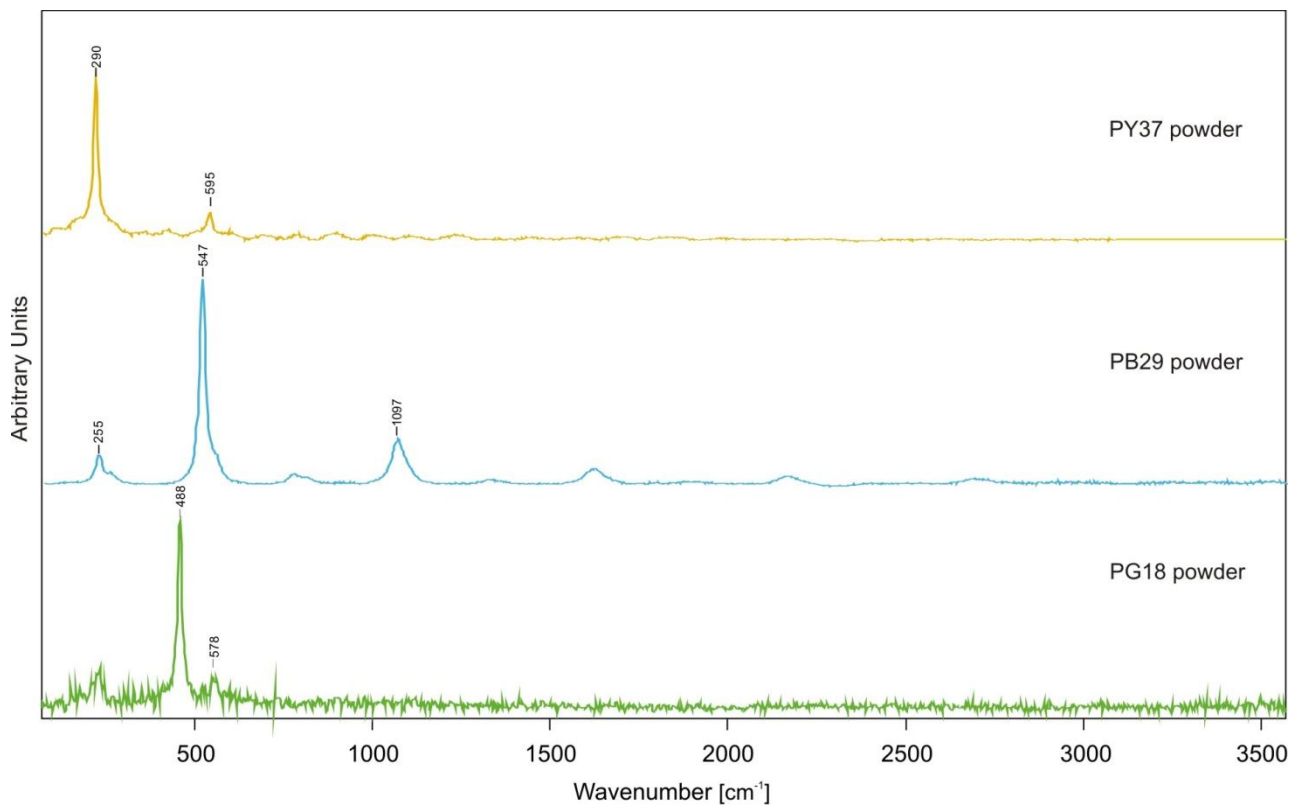
Fig. 29 – Comparison between colored powder Raman spectra of each pigment

	Wavenumber (cm^{-1})	Assignment
PY37	290	Optical Longitudinal Mode
	595	2° Optical Longitudinal Mode
PB29	255	Lazurite δ (S$_3^-$)
	547	Lazurite ν (S$_3^-$)
	1097	Lazurite ν (S$_3^-$)
PG18	488	Attributed to the hydrated oxide
	578	Attributed to the hydrated oxide
	271	Attributed to the hydrated oxide

Tab. 17 – Relative assignment of each band or Raman shift [17; 47; 48]

4.2.4 Comparative discussion about IR and Raman results

When IR and Raman spectra are used, it is necessary to consider the potential and limits of both techniques. Energy differences between incident radiation, the Rayleigh radiation, and the Raman radiation correspond to wavelengths in the medium infrared region (Mid-IR), i.e. in the range of 2.5 to 50 µm (expressed in wavenumbers from 4000 to 200 cm^{-1}). For this reason, in some cases the Raman and the infrared spectrum of a material may be similar as both results from quantized vibrational changes.

However, the two techniques are more complementary than competitive. First of all, the basic theory of these techniques is different. In IR, the selective radiation absorption causes energy transitions, while Raman spectroscopy is based on the anelastic diffusion of light. In addition, the so-called selection rules that determine which vibration modes are active and which are not, are different: in the IR are absorbed energies that cause changes at the dipole moment of a molecule, while Raman is required to change its polarizability, property related to the possibility of distortion of the electronic cloud. As a result, some vibration modes are active in the IR and not in Raman and vice versa [49]. The advantage of IR technique is that spectra are usually richer in signals and therefore the technique is used for more general application. On the contrary, the advantage of Raman technique is that water and glass do not cause interference and that the Raman spectrum lines are generally narrower and therefore easier to identify. [50].

In the present case the differences of the two techniques mentioned before are observed depending on the type of binder and pigment. In the IR analysis the two binders are distinguished by the presence of the phthalic component in the alkyd medium (1254-1069-747 cm^{-1}), while in the Raman analysis this distinction is clearer and more detailed, such as the different polarizability of the two binders molecules leads to the characterization of the more specific functional groups, less visible with the IR. Regarding pigments, in powder form, differences in the use of one technique or another have also been observed in this case.

In the case of IR, artificial ultramarine blue is only identified by vibration of the Si-O bond, while in Raman it is possible to identify more accurately the various distortions of the molecule. Using this technique it is also possible to distinguish the artificial blue from the natural one [Osticioli I.]. In the case of the hydrated chromium oxide green, the identification is simpler with the use of IR that characterizes both the hydrated part of the molecule (3077 cm^{-1}) and the vibration of the oxide bond (547-483 cm^{-1}). With Raman, however, this attribution is not yet completely clear and generally the two resulting bands are attributed to the hydrated oxide part [47].

Finally, the cadmium sulfide yellow pigment can only be distinguished by Raman spectroscopy; analyzed with IR this pigment has no absorption band in the Mid-IR region [51].

4.3 Study of drying process in time-resolved mode

In this part of the project, the study developed by IR analysis for determination of spectral changes in alkyd resin and acrylic emulsion is presented. In particular, pure binders (Alkyd Medium 4 and Plextol D498) mixed with pigments, used and described previously (PB29, PG18 and PY37), are studied. The aim is to characterize the possible increase and/or decrease of significant absorption bands depending on the drying stages of two different polymers, and the different pigments used. Samples are prepared on glass slides; to monitor the various continuous changes IR measurements are performed every 60 min for 12 hours. The results are presented below. Additionally, these changes are also investigated by Raman spectroscopy, but some limitations (shown in chapter 4.3.3) are observed, which do not allow to effectively evaluating the drying processes.

4.3.1 Parameters used for time-resolved measurements

In order to obtain the best results for the evaluation of the drying process of binders, specific parameters are selected for each mock-up. The number of analyzed samples are 8, and for each one the same binding/pigment ratio (see table 18) is used. In this way, it is easier to compare the drying changes for each sample.

Mock-ups	Name of samples	Chemical composition	Color Index: generic name	Ratio (P/BM)	Layer thickness	Method of mix
Pure Plextol® D498	S1	p(nBA/MMA)	/	/	150 μm	/
Plextol® D498 + ultramarine blue	S2	p(nBA/MMA) + $Na_8Al_6Si_6O_{24}.Sx$	PB29	1g pigment 3g binder (1:3)	150 μm	Muller
Plextol® D498 + hydrate chromium oxide green	S3	p(nBA/MMA) + $Cr_2O_3 \cdot 2H_2O$	PG18	1g pigment 3g binder (1:3)	150 μm	Muller
Plextol® D498 + cadmium yellow	S4	p(nBA/MMA) + CdS	PY37	1g pigment 3g binder (1:3)	150 μm	Muller

Pure Alkyd Medium 4	S5	Polymer oil modified polyester-resin based on orthophthalic acid and pentaerythritol	/	/	150 µm	/
Alkyd Medium 4 + ultramarine blue	S6	Polymer oil modified polyester-resin based on orthophthalic acid and pentaerythritol + $Na_8Al_6Si_6O_{24}.Sx$	PB29	1g pigment 3g binder (1:3)	150 µm	Muller
Alkyd Medium 4 + hydrate chromium oxide green	S7	Polymer oil modified polyester-resin based on orthophthalic acid and pentaerythritol + $Cr_2O_3 \cdot 2H_2O$	PG18	1g pigment 3g binder (1:3)	150 µm	Muller
Alkyd Medium 4 + cadmium yellow	S8	Polymer oil modified polyester-resin based on orthophthalic acid and pentaerythritol + CdS	PY37	1g pigment 3g binder (1:3)	150 µm	Muller

Tab. 18 - Summary of each sample prepared for drying study, with the relative name, composition, P/BM ratio chosen, layer thickness and mixing method

Once the mixture is placed on the glass slide, it is analyzed with IR spectroscopy in reflection mode. The analysis lasted 12 hours and, every hour, one spectrum is obtained. This results in a total of 12 spectra for each sample. As explained in chapter 3.3.2, the reflection mode is used when the sample is not thin enough to allow transmission of IR radiation. It is a non-contact technique (useful in this case because initially the sample is fresh) and can show characteristics of the absorption and refractive index spectra. The result is a spectrum different from a transmission one, therefore, as already mentioned, to extract the more analytically useful information it is necessary to perform the Kramers-Kronig transformation.

Once having re-elaborated the reflection spectra, they are compared observing chemical changes in time zero (first measurement), in 6 hours (360 minutes), and 12 hours (720 minutes).

To understand the role of pigments on the drying cross-linking process, it is necessary to analyze individually the two pure polymers too. In this way it is possible to examine the significant changes of the functional groups during the time, compare them with the samples in the mixture with pigments and observe if these changes increase or decrease depending on the type of pigment and/or binder.

4.3.2 Results of time-resolved analysis

The results, reported below, show the different spectral signals obtained during time-resolved analysis by IR spectroscopy. Initially, the results obtained by the response of pure alkyd binder and in mixture with the pigments are shown, and successively those of the acrylic binder, also in pure form and in mixture. The different spectral changes due to the drying phenomenon and/or the binder/pigment interaction are explained below.

Alkyd binders were introduced in the 1930s as art material, thanks to their compatibility with other polymers, stability and the suitable formulation for ageing. As mentioned in chapter 2.1.3, alkyd resins are polyesters modified with fatty acid polyesters. The drying process is divided into two steps: the solvent evaporation (physical drying) and the autooxidative drying (chemical drying), these different stages are observed in the analysis of IR spectra, at different exposure time [52].

As shown in figure 30, with the drying process it is possible to observe an increase in the bands in the region of 1730-1680 cm^{-1} due to carbonyl stretching. The reason of this increase may represent the oxidation reactions that take place during natural ageing and that lead to the formation of alcohols and carbonyl species. A small increase of the shoulder at 1635 cm^{-1} is observed, probably due to the stretching vibration of C=O groups in diketones and their enol form. This band is a representative parameter of oxidation and can monitor the ageing process [53].
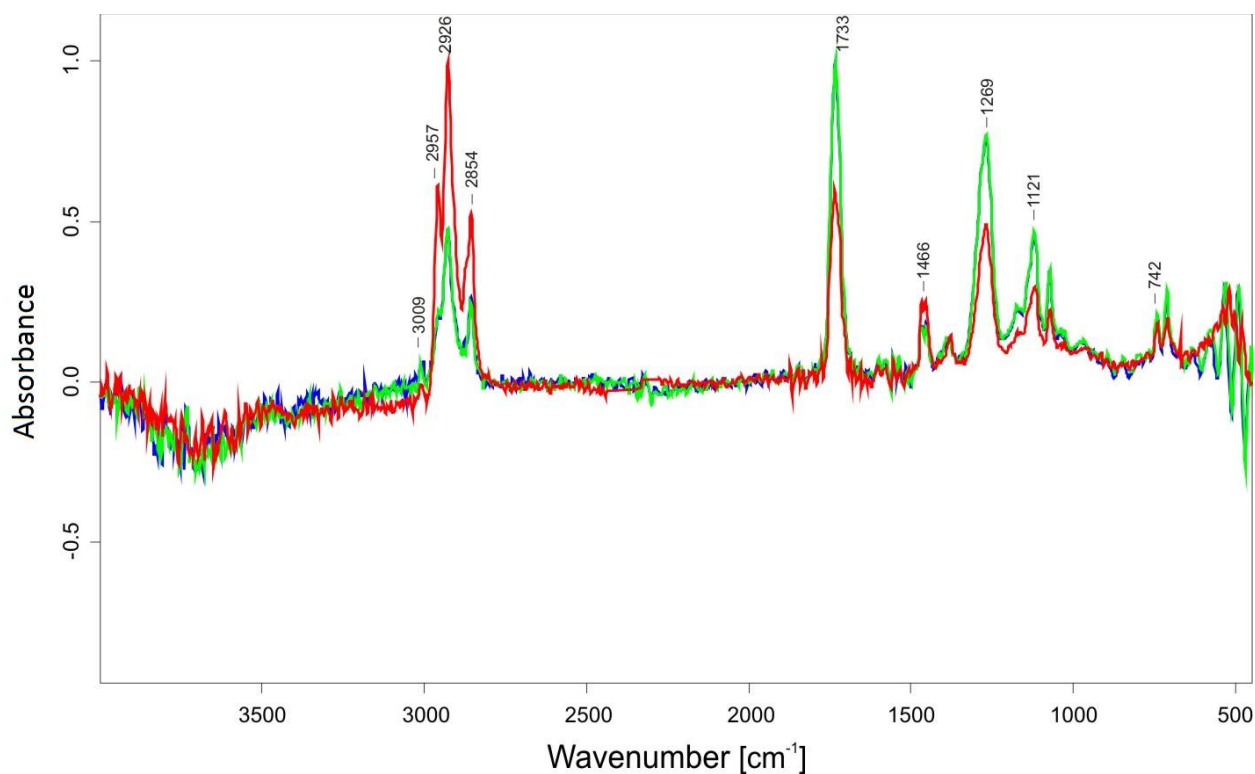
Fig. 30 – Sample S5, pure Alkyd. Red spectrum 0min, green spectrum 360min, blue spectrum 720min

In the region of 2930-2855 cm^{-1} a decrease of methylene C-H absorptions is shown, due to the oxidation of double bonds. In the absorption band at 3009 cm^{-1} a progressive reduction is indicated, that corresponds to the mono/bisallylic H-C=CH antisymmetric stretching vibration [54].

Also in the spectra with pigments it is possible to observe a decrease in the aliphatic C-H group absorptions (2920-2850 cm^{-1}), probably due to a partial depolymerization and hydrolysis of the resin with the loss of organic volatile species; and a increase in the C=O stretching absorption (1730 cm^{-1}), that could be due to the formation of mono- or di-carboxylic acids [52]. The negative band at 3600 cm^{-1} represents the gas phase water signal.
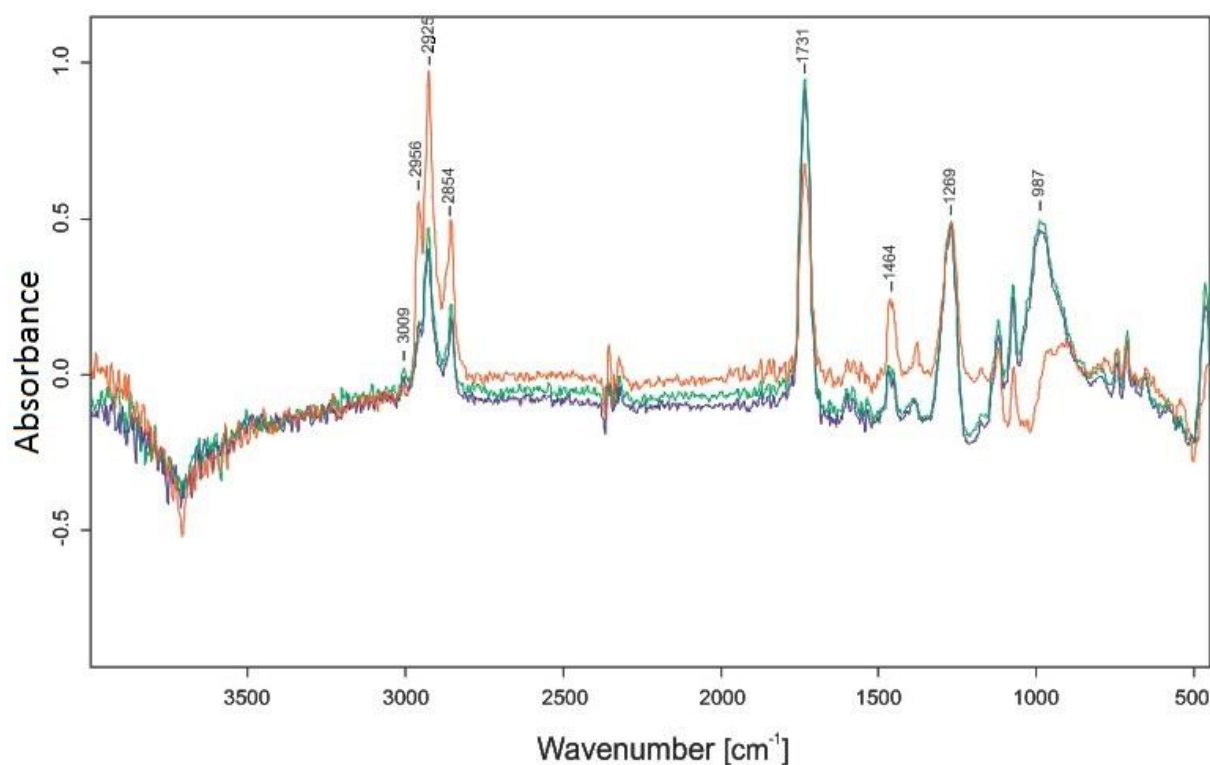
Fig. 31 – Sample S6, PB29 + Alkyd. Red spectrum 0min, green spectrum 360min, blue spectrum 720min

In these spectra several particular spectral features, due to the different chemical composition of the pigments, are observed. In figure 31 the general trend of the spectrum is similar to that of pure alkyd. Only the increase of the bands at 987 cm^{-1} can be noticed, that represents the Si-O bond vibrations of artificial ultramarine blue, more visible after the physical drying of the binder.

In figure 32, the trend of alkyd binder mixed with the hydrate chromium oxide green is shown. Generally the drying trend is the same as of other spectra, and an increase of the oxide bond vibrations at 567 cm^{-1} is observed. However, compared to the previous two spectra, more spectral interference at 3600 cm^{-1} and at 1720-1490 cm^{-1} is present. This signal appears after 200 min ($\sim$ 3 h) of IR analysis, and increases over time.
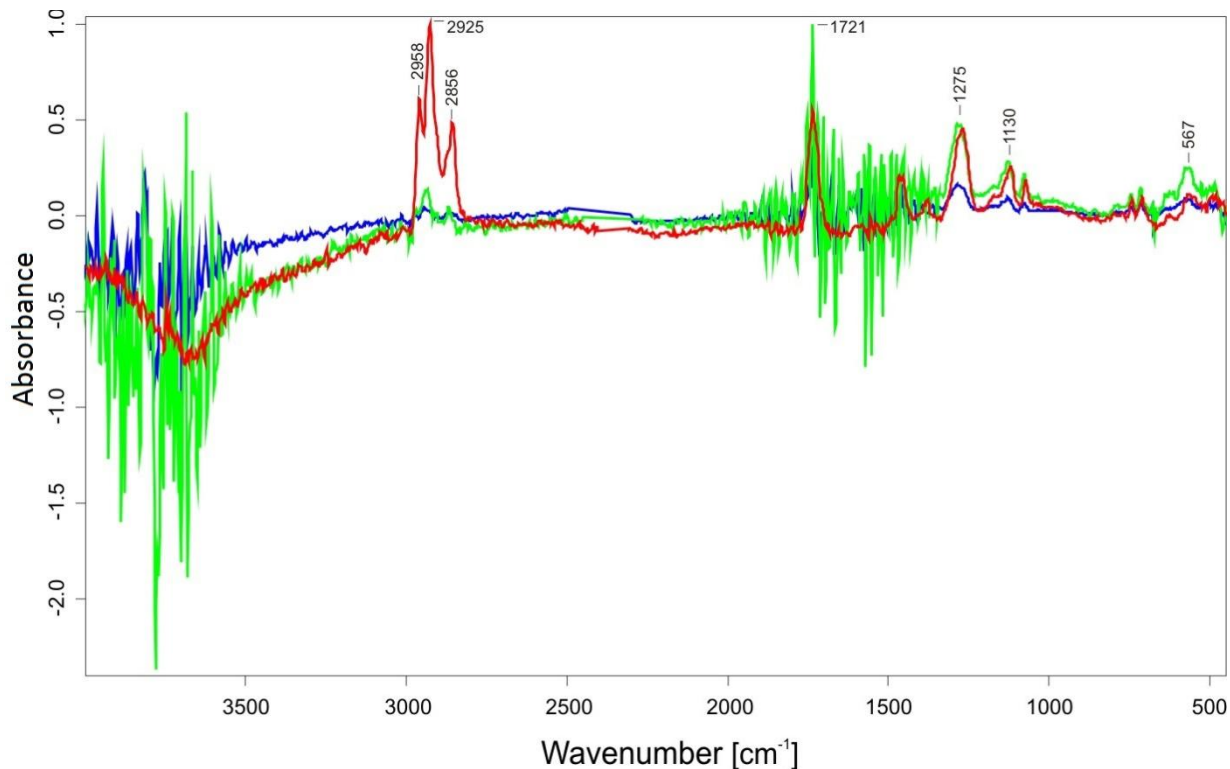
Fig. 32 – Sample S7, PG18 + Alkyd. Red spectrum 0min, green spectrum 360min, blue spectrum 720min

After a hypothetic evaluation of the interaction that this pigment can have with the alkyd binder, it is decided to examine the same mixture but with green chromium oxide, i.e. without the hydrated component. Comparing the two resulting spectra (Fig. 33), it is possible to confirm that the cause of spectral interference is due to the presence of the hydrated component within the chemical structure of the pigment. Probably the hydrated pigment contributed more to the formation of this spectral noise in relation to the drying of the alkyd binder [55]. However, the chemical and physical causes that have led to this result have to be investigated further.
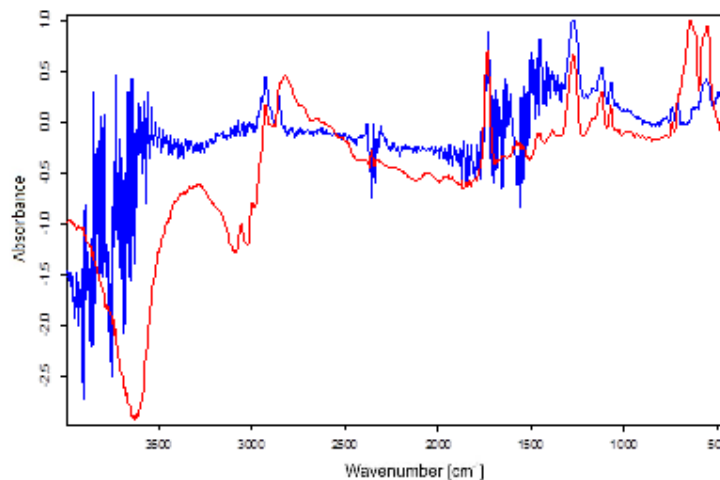
Fig. 33 – Spectrum of PG18 (hydrated) with Alkyd blue, spectrum PG18 (anhydrite) with Alkyd red. After 200min

56
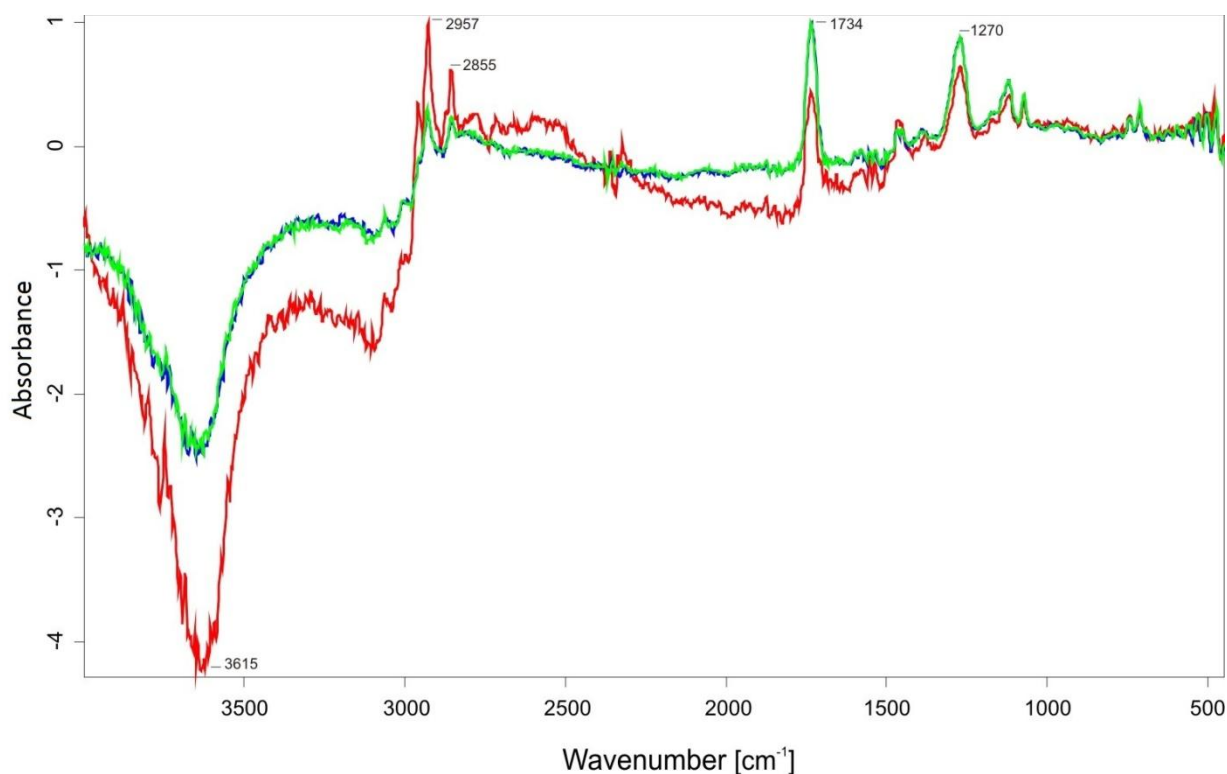
Fig. 34 – Sample S8, PY37 + Alkyd. Red spectrum 0min, green spectrum 360min, blue spectrum 720min

In the end, the spectrum of sample S8 (PY37 and alkyd binder) is shown. Also in this case, the significant bands of the binder drying are observed; the component of the pigment is not visible in the spectrum because it is invisible to IR. However, compared to the previous spectra, a large negative band at 3615 cm^{-1} is present. According to Socrates [29], this particular spectral frequency is due to the aliphatic sulphide compound CH$_3$S-, which is created by the pigment/binder interaction. The band intensity is reduced during the time, probably due to evaporation of the solvent in the polymer. It is also possible that this band is more evident and shifted with high wavenumber due to the transformation of the reflection spectrum into the transmission one.

As mentioned in chapter 2.1.1, acrylic/methacrylic polymers derive from the polymerisation of esters of acrylic and methacrylic acid, and form materials adapted for many fields. Their formulation allows having suitable mechanical properties, adhesion and chemical stability useful for paints and surface coatings. Compared to drying alkyd binder, where first the solvent evaporates and after the autoxidation process occurs, the drying process of acrylic binder is different. In fact the first step is the evaporation of water, and subsequently the phenomenon of coalescence, where molecules of the polymer begin to compress between them, incorporating the pigment particles [56].
It is possible to observe these stages in the analysis of IR spectra.
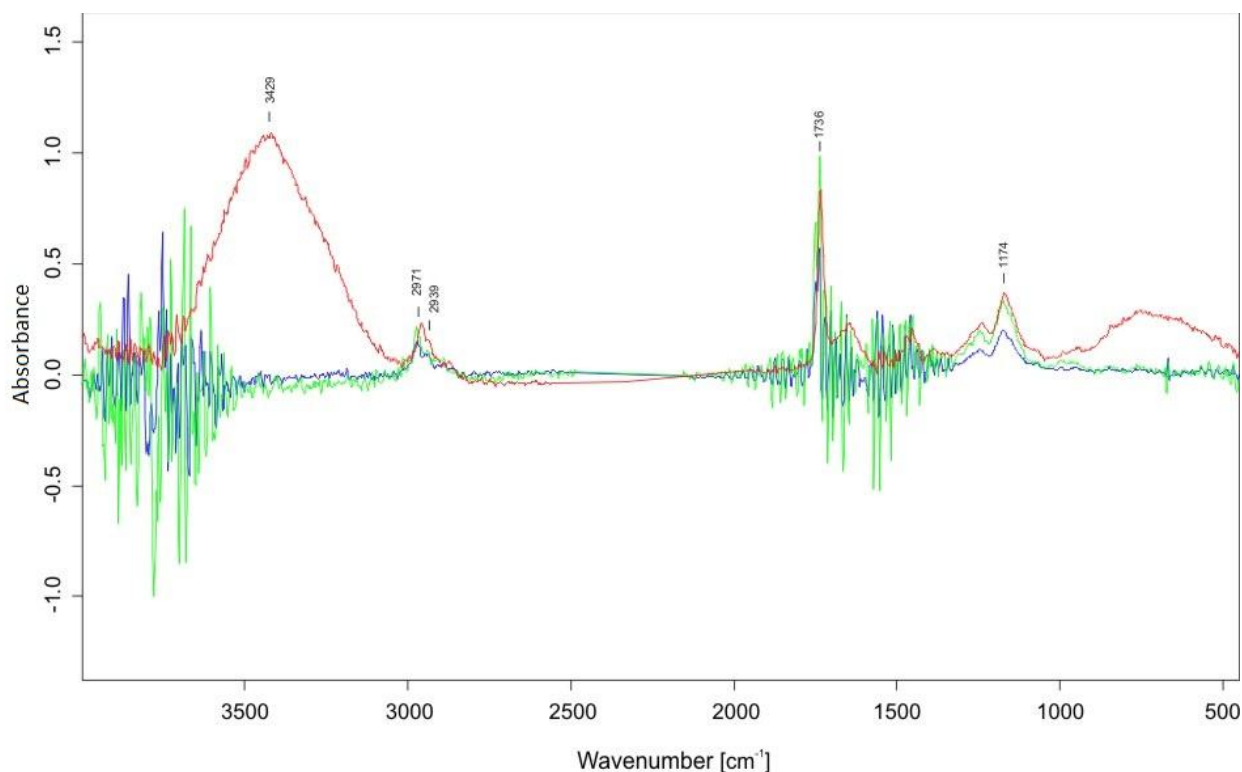
Fig. 35 – Sample S1, pure Plextol. Red spectrum 0min, green spectrum 360min, blue spectrum 720min

The specific binder employed is Plextol® D498, i.e. an aqueous dispersion of a thermoplastic acrylic polymer based on methyl methacrylate and butyl acrylate. For this reason the two monomers are responsible for different spectral changes [57]. As shown in figure 35, the general and progressive decreases of the principal bands represent the evaporation of small molecules; in particular at 3429 cm^{-1} the decrease of hydroxyl groups is observed, due to the evaporation of water. Another change involves the C-H stretching (2971-2939 cm^{-1}), this suggests that monomer molecules are formed as a result of the chain scissions. The most important signal of oxidation is the increase in the carbonyl region at 1736 cm^{-1}. In general the acrylic and alkyd drying stages are similar and present the same spectroscopic changes, except in acrylic one where the O-H band is observed [56]. Therefore, the drying process of acrylic binder is characterized by:

- The graduate decrease of principal absorption that indicate loss of low molecular weight molecules produced by degradation (as the C-H stretching at 2971-2939 cm^{-1}, and the C-O-C groups at 1242, 1177 and 1153 cm^{-1}) and water evaporation (as the hydroxyl region between 3600 and 3000 cm^{-1});
- The increase of carbonyl absorption at 1736 cm^{-1}, representing the polymer oxidation.

Specific spectral changes are not observed in the spectra of binder mixed with pigments, except for the reduction of carbonyl absorption at 1735 cm^{-1}, due to the loss of the butyl ester group. In figure 36 and 37, the increase of Si-O bond vibrations of artificial ultramarine blue (at 1003 cm^{-1}) and oxide bond vibrations of hydrated chrome oxide green (at 564 cm^{-1}) are present. Cadmium yellow is not visible to IR analysis (figure 38), however, as in the alkyd sample, the negative band at 3434 cm^{-1} is observed. As before, this phenomenon is probably due to aliphatic sulphide compound CH$_3$S.
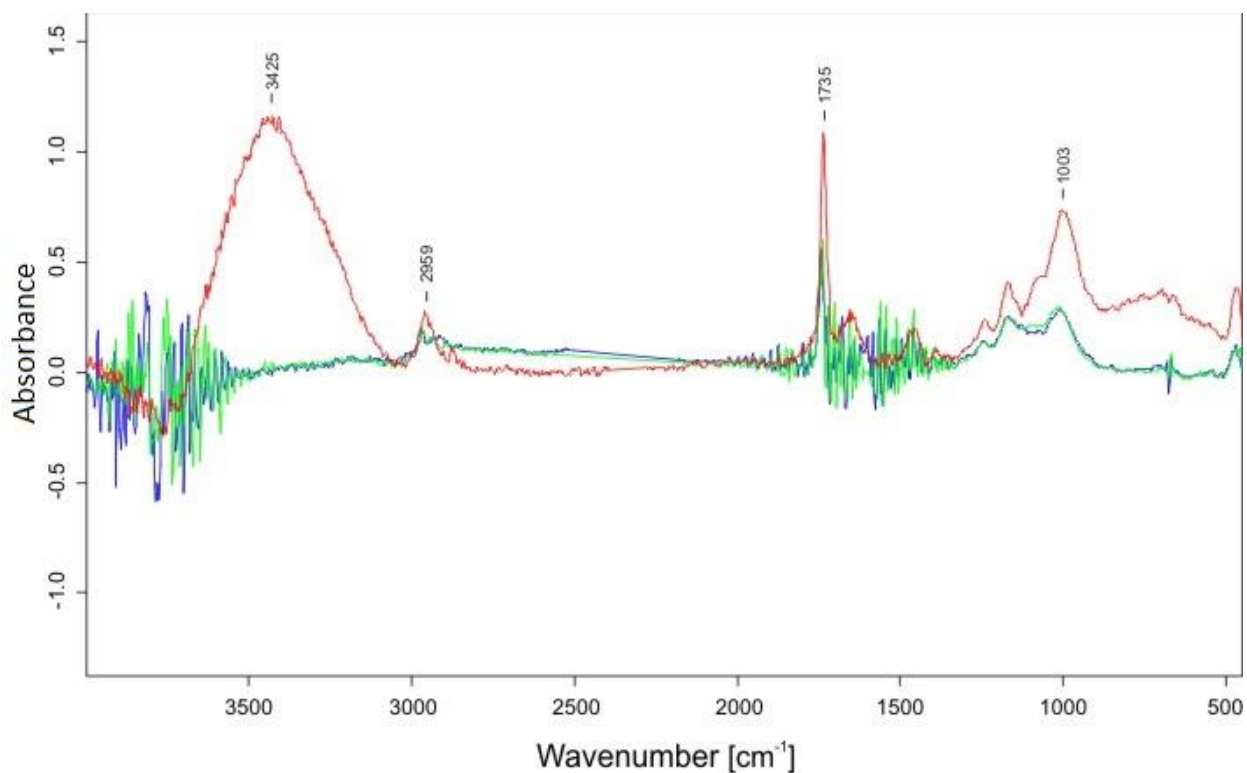
Fig. 36 – Sample S2, PB29 + Plextol. Red spectrum 0min, green spectrum 360min, blue spectrum 720min
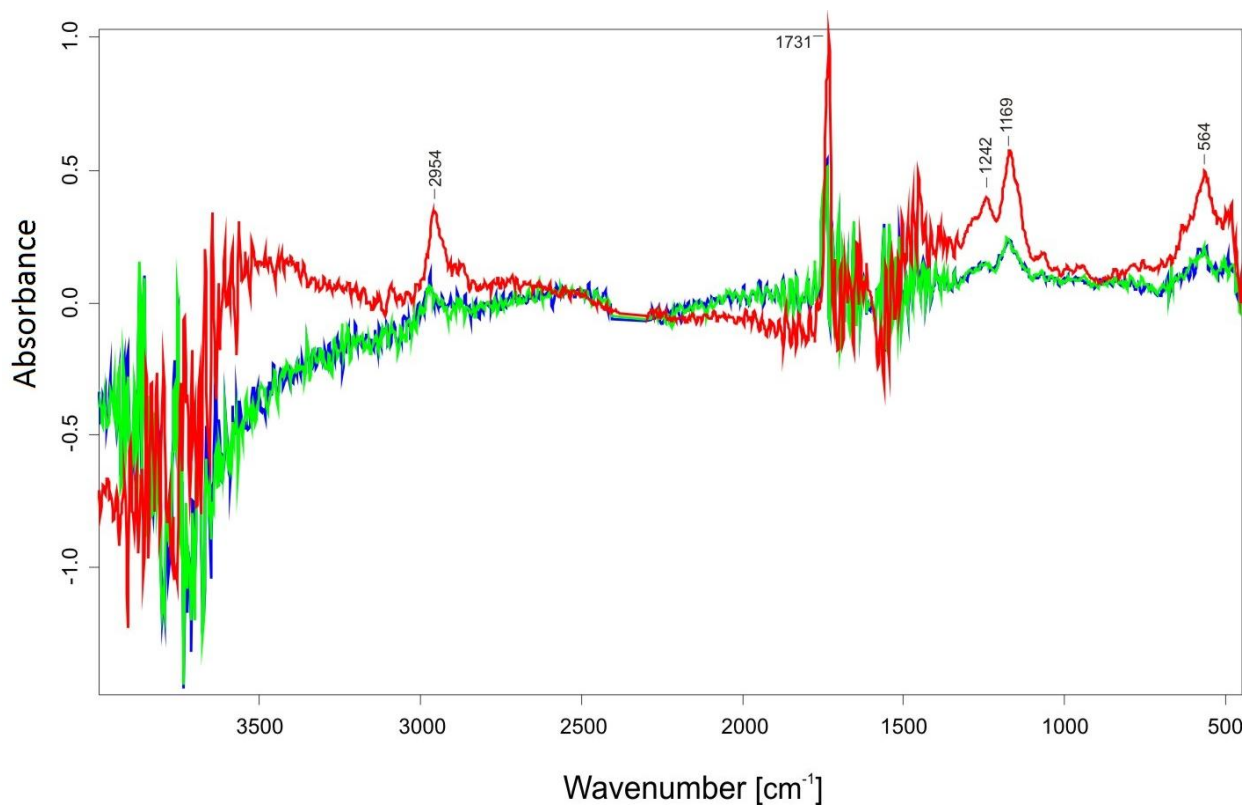
Fig. 37 – Sample S3, PG18 + Plextol. Red spectrum 0min, green spectrum 360min, blue spectrum 540min
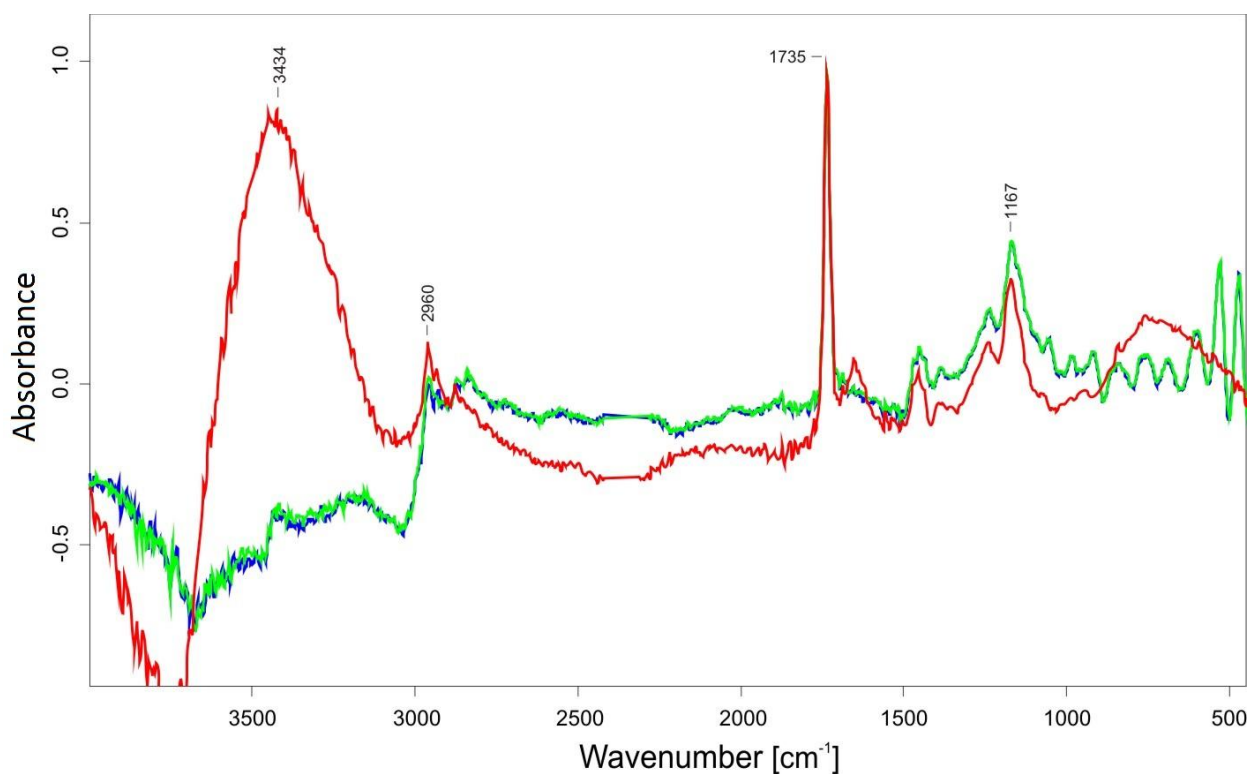
Fig. 38 – Sample S4, PY37 + Plextol. Red spectrum 0min, green spectrum 360min, blue spectrum 540min

4.3.3 Limitation of Raman spectroscopy for the study of drying process

As previously reported, the study of the drying processes of the various binders could not be investigated by Raman analysis. Raman spectroscopy is a non-invasive and non-destructive technique based on the interaction between radiation and matter. A laser beam emits a radiation that interacts with the vibrational motions of the molecules, causing re-emission of light at different wavelengths than the incident one. The Raman spectrum that is obtained allows identification of the molecule under examination. For this reason, it is used for the study of pigments and, in this project, also binders. In fact, each material has different reticular vibrations and, irradiated with an appropriate wavelength, allows to obtaining different Raman spectra, in this way it is possible to distinguish one material from the other. However, both Raman instrumentation used and the spectroscopic technique, have limitations that have not allowed analyzing the various cross-linking processes of the binders. The main problems are due to the signals obtained depending on the different characteristics of the spectroscopic instrument used:

- Before the analysis it is necessary to focus the sample. But, during the first minutes of the drying process, the surface layer of the sample begins to decrease (due to evaporation of solvent/water), so the focus, initially set, is not longer suitable. This limit is accentuated by the different measuring area of the instrument, while with IR the spot size/area is around 0,5 mm, in Raman it is a few microns. This has allowed obtaining appropriate IR spectra for the analysis while in Raman ones there are spectral interferences.

- As explained in chapter 3.3.3.1, some materials, especially those of organic origin, cause fluorescence, which occurs when the incident light-radiation does not match with the absorption bands of atoms or molecules. For this reason, fluorescence signals can cover Raman scatter of a material. Therefore these interferences not only cover the signal of the principal functional groups of binders, but do not allow evaluating if any spectral changes have occurred. Already during the qualitative analysis of the binders by Raman analysis these spectral problems are present, but they are resolved by resetting the measuring parameters of the instrument. This solution is also evaluated for time-resolved analysis, but it is difficult to achieve it because a continuous set of instrumental parameters that can modify the final result of the analysis is necessary.

- In the end, it also has to be considered that a contribution of the long-term laser exposure can cause effects in the examined sample. In fact the high wavelengths employed can damage the molecules, leading to the decomposition of the binder.

4.4 Quantification analysis of different P/BM ratio by IR and Raman spectroscopy

After having characterized, the materials used to make mock-up, by IR and Raman techniques, the quantitative analysis was carried out. It allows evaluating the pigment/binder (P/BM) ratio within each painting sample. Before employing the mathematical-statistical model that will enable one to evaluate and quantify the different composition of unknown samples, it is necessary to calibrate the model with values of known P/BM ratios (Tab. 2, chap. 3.2), selected with appropriate parameters, different for each mock-up. Calibration is important not only to mathematically confirm the P/BM ratio itself, but also to ensure that the chosen samples, inserted to create the calibration curve, are efficient to quantifying unknown samples.

4.4.1 Statistical foreword

In order to explain and evaluate the developed models to quantitatively determine each sample in question, it is necessary to understand the main statistical processing and evaluation systems in order to determine whether the quality of experimental measurements is acceptable.

In each analysis a relationship exists that connects the amount of analyte to the experimental measurements and, ideally, the analyte concentration should be linearly correlated with the result of the measurements. The straight lines are defined algebraically as:

$$Y_i = mX_i + b \qquad\qquad (Eq.\ 26)$$

where m is the slope of the straight line, Xi is the concentration of the corresponding Yi, and b is the intercept of Yi (see figure 39).

In order to carry out this statistical analysis, it is necessary to assume that the values of Xi are known with higher precision than those of Yi. The second hypothesis is that values of measurement Yi are independent of each other. The parameter for finding the best straight line equation is to evaluate the distance between each experimental point and the interpolating line [58]. For each Xi value, the value of this difference, called residual, is given by:
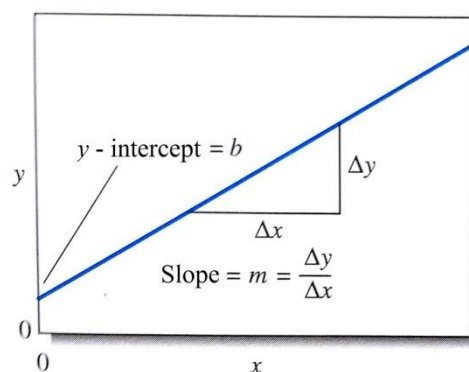
Fig. 39 – Slope and intercept of a straight line [59]

$$[Y_i - Y_{straight\ line}] \hspace{4cm} \text{(Eq. 27)}$$

The value of the residuals depends on the equation of the line and, in order to find the best line, the residual sum of the squares is evaluated. In particular, the optimal line is the one that minimizes the value of this summation, from which the name of Ordinary Least Squares (OLS) derives. Another term used for this operation is linear regression. This method represents an optimization technique (or regression) that allows finding a function, represented by an optimum curve (or regression curve) that approaches as much as possible to a set of data (typically plan points). In particular, the found function must be the one that minimizes the sum of the squares of the distances between the observed data and those of the curve representing the function itself [59].

A statistical parameter to evaluate the interpolation quality performed is the correlation coefficient, indicated as R. It indicates how much, a variation in the independent variable X, is reflected on the dependent variable Y, and it is represented as:

$$R = \frac{cov\ (X,Y)}{\sigma_A \cdot \sigma_B} \hspace{4cm} \text{(Eq. 28)}$$

Where $cov(X,Y)$ indicates the covariance of X and Y and represent, respectively, the standard deviation of X and Y. The values of the various correlation indices vary between -1 and +1; both extreme values represent perfect relationships between the variables. If $R > 0$, the data series X and Y are directly correlated, or correlated positively. More the value approaches 1 and the stronger is the positive correlation. If $R = 0$ the data series X and Y are not correlated, that is, represent the absence of relationship. In the end, if $R < 0$, the data series X and Y are inversely correlated, or negatively correlated, and more the value R approaches -1, stronger is the negative correlation. A positive relationship means that samples that obtain high values in a variable tend to get high values on the second variable. For this reason, the more the value of R approaches 1, the more the values, representing each sample, are correlated [60].

To evaluate the precision of the measurement, it is necessary to carry out an error analysis of slope and intercept. Since m (slope) and b (intercept) errors are related to measurement errors in each value of Yi, first of all it is necessary calculate the standard deviation that describes the population of Y values. It measures the tendency of data to gather around the average, the smaller the standard deviation, the more data tend to cluster around the average. It is expressed as the square root of variance, see equation 29 [61].

$$\sigma = \sqrt{\frac{\sum_{i=1}^{N}(x_i - \mu)^2}{N}}$$

In most analytic cases, the true value of the average μ cannot be determined, since it would require a huge number of measurements. However, it is possible to set an interval, around an experimental average x, which is expected to find with a certain probability the population average μ. This interval is known as confidence interval (CI) (equation 30) and the boundary lines are called confidence limit. The latter represents the probability that the true average value is within a certain range. If a single measure x is carried out, that comes from a known distribution of σ, it is possible to assume that the true average should be in the range x ± z σ with a probability that depends on z, i.e. the deviation of a data from the average expressed with the standard deviation unit (see figure 40) [59]. Therefore, for a value of z = 1.96, this probability is equal to 95%.

$$(C\ I)\ per\ \mu = x \pm \frac{z\sigma}{\sqrt{N}}$$

Ideally, it would be always necessary to have a small confidence interval for a determinate experimental value. In fact, a small confidence interval makes easier to decide if two experimental values are statistically equivalent or less. It is possible to obtain a closer confidence interval for a certain average value by increasing the number of data used to calculate this value. Additionally, a greater number of data also improves the total standard deviation estimate for the whole observation group. The only way to get a smaller confidence interval for a certain population of results is

Fig. 40 – Underlying area in a Gaussian curve for z = ±1.96 value [59]

to improve the measurement method to obtain more accurate results. The choice of the confidence level can have a significant impact on the range of results that represent the confidence interval. For example, a confidence level of 90% will always give a lower confidence interval than a confidence level of 99%. This occurs because when the confidence level is increased, a result that will fall within a certain confidence interval is obtained, which also involves the extension of the range of values that are used to define that interval. For this reason generally a confidence level of 95% is used, it allows to have a relatively small but still wide confidence interval to ensure a good probability of include the true value of a measurement [62]. On the other hand, the prediction interval relates to a

future observation in the same way that a confidence interval relies on an undetectable parameter of the population. Prediction intervals predict the distribution of individual points that cannot be compared to the average (refer to new points included in the linear model), while the confidence intervals estimate the true average of the population or other quality of interest that cannot be observed.

4.4.2   Experimental procedures

In order to obtain the best results for the quantitative analysis of unknown samples, specific parameters for each mock-up are selected. Five measurements are performed on each sample. The resulting five spectra are compared using the program Opus 11 (Bruker, Germany), and matched with the same baseline. Subsequently vector normalization[2] is applied to the spectra, i.e. the process of dividing all the terms of an expression for the same factor, so that the resulting expression has a standard of 1, or unitary. Vector normalization is performed only on IR spectra and not on Raman spectra. At this point, depending on the different technique, the ranges for band integration are chosen. The choice of selecting specific spectral bands, different for binder and pigment, is made to avoid errors in the formation of the calibration curve. The chosen bands are the most characteristic of each material and present a greater change depending on different P/BM ratios. In the figures 41-42 it an example of the range chosen for the integration step is shown.

From the integration of these bands, numeric values are generated, expressed as Area (A).

Therefore for each sample, the area values of every spectral band are added. The binder and pigment values are divided in different graphs, also depending on the spectroscopic technique used, in order to quantify individually every component.

| Plextol	PG18	Assignment
3100-2800		C-H stretching
1800-1700		C=O stretching
1500-1400		C-H deformation (bending)
1200-1000		C-O stretching
	656-458	Oxide
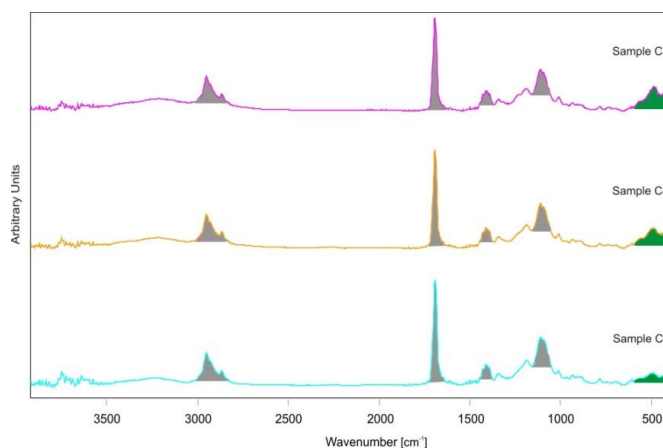
Fig. 41 – Example of integration method: each range corresponds to a spectral IR band. The grey bands represent the binder, the green ones the PG18 pigment

[2] This method calculates the average y-value of the spectrum. The average value is subtracted from the spectrum decreasing the mid-spectrum to y = 0. The sum of the square of all y-values is calculated and the spectrum is divided by the square root of this sum. The vector norm of the result spectrum is 1.

Plextol	PG18	Assignment
3039-2811		C-H stretching
	526-452	Oxide
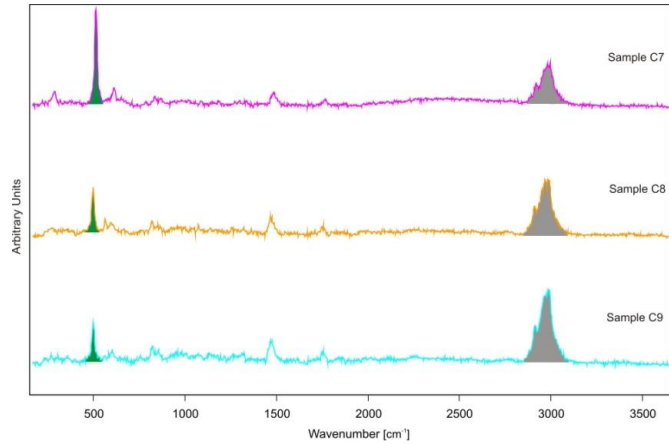
Fig. 42 – Example of integration method: each range corresponds to a spectral Raman band. The grey bands represent the binder, the green ones the PG18 pigment

4.4.3   Calibration curves for quantitative evaluation of unknown P/BM ratios

The following graphs represent the calibration curves obtained by the procedures previously mentioned; some graphs mentioned below are in the appendix.. These models are constructed using 5 samples, with known concentrations (Tab. 2-3), in order to find a mathematical system more stable, logical, representative and reproducible. The graphs are divided according to the technique used (IR and Raman) and depending on the different binder and pigment used in the samples. They are arranged in the graph depending on their Area value (IR and Raman bands) and the value of their relative concentration (Tab. 19).

The relative concentration values were obtained using the P/BM ratios of each sample and replace to these mathematic equations:

$$Relative\ concentration\ binder\ (sample\ C1) = \frac{BM\ value}{total\ \frac{P}{BM}\ value} = \frac{2}{3} = 0.67 \qquad (Eq.\ 31)$$

$$Relative\ concentration\ pigment\ (sample\ C1) = \frac{P\ value}{total\ \frac{P}{BM}\ value} = \frac{1}{3} = 0.34 \qquad (Eq.\ 32)$$

Graph 1 shows the calibration curve, representing the acrylic component in the blue sample that shows a linear trend due to the increase of the relative concentration of the binder, depending on the corresponding Area value. This arrangement of the points on the plane allows identifying with immediate effect any relationship existing between the two variables. Visually it is possible to identify the existence of a positive linear relationship between the two variables; linear because the points tend to align along a straight line.

Positive because when the values of a variable grow, also those of the other variable grow. The same trend is observed, both for the IR and Raman evaluation, and is also seen in the graphs in the appendix.

Name sample	Ratio P/BM	Relative concentration binder (w/w)	Relative concentration pigment (w/w)
C1	1:2	0.67	0.34
C2	1:3	0.75	0.25
BP1	1:5	0.83	0.167
C3	1:6	0.86	0.143
BP3	1:7	0.875	0.125

Tab. 19 – Summary table of blue acrylic samples used for the calibration curves
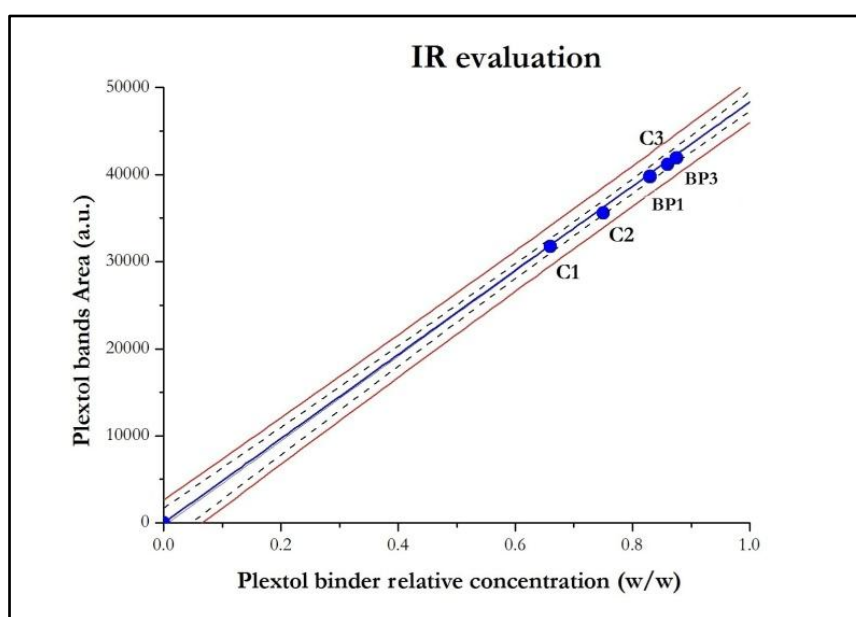
Graph 1 – Calibration curve of acrylic component in blue samples: the abscissa represents the relative concentration of binder, the ordinate the Area value of binder obtained by IR spectroscopy
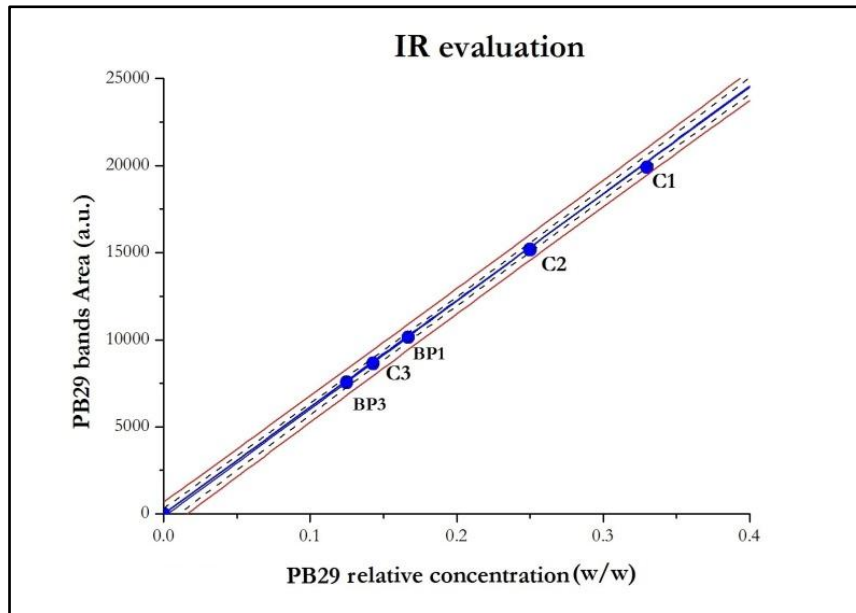
Graph 2 – Calibration curve of pigment component in blue acrylic samples: the abscissa represents the relative concentration of pigment PB29, the ordinate the Area value of pigment obtained by IR spectroscopy
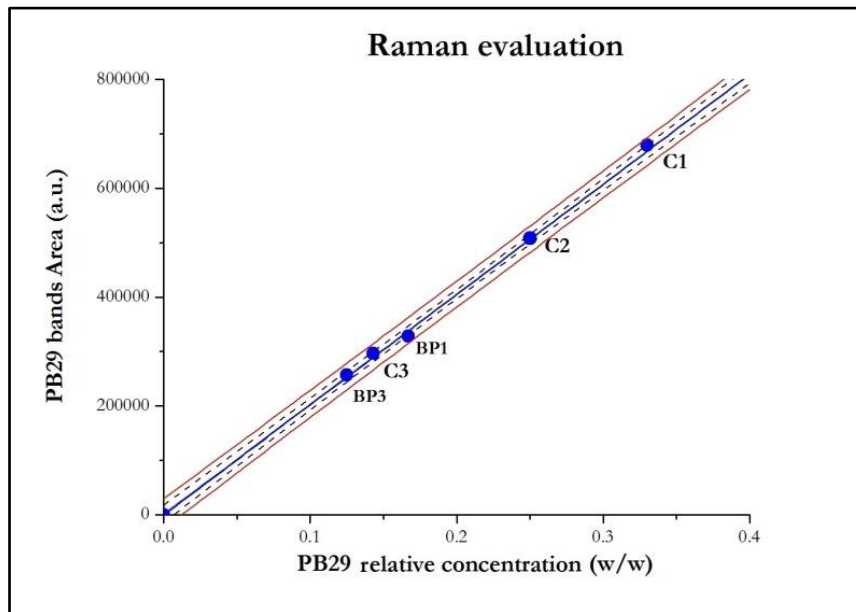
Graph 3 – Calibration curve of pigment component in blue acrylic samples: the abscissa represents the relative concentration of pigment PB29, the ordinate the Area value of pigment obtained by Raman spectroscopy

In all the graphs, previously illustrated (see also appendix, section I), a positive linear increasing trend is observed. In order to evaluate the quality of the interpolation points and the effectiveness of the straight line representing them, it is necessary to employ the correlation coefficient which, as

mentioned above, expresses the linearity relationship between the independent variable X (relative concentration) and the dependent variable Y (IR and Raman Area value).

Number graph	Composition samples	Technique used	Correlation coefficient value (R)
1	PB29 + Plextol binder	IR spectroscopy	0.99956
2	PB29 + Plextol binder	IR spectroscopy	0.99968
3	PB29 + Plextol binder	Raman spectroscopy	0.99972

Tab. 20 – Summary of the correlation coefficient values of each sample

As observed in table 20, all values are approaching 1. This indicates that the values of both variables are highly correlated to each other and the values of the dependent variable Y obtained (Area) best represent each pigment or binder component in the samples. Once the efficacy and accuracy of the calibration model for known samples is verified and validated, it is possible to determine the different pigment/binder relative concentration for unknown and commercial samples.

The samples used to test the calibration curves, previously developed, were prepared by a different operator, using the same materials but in different P/BM ratios. In this way, it was possible to test the reproducibility and stability of the quantitative model created. Below in table 21, the unknown samples used are listed (see also appendix, section II).

Unknown samples employed			
Name sample	Binder used	Pigment used	Unknown P/BM ratio
GP2	Plextol	Hydrate chromium oxide green	1:6
G1	Plextol	Hydrate chromium oxide green	1:1.2
GA2	Alkyd	Hydrate chromium oxide green	1:2
G2	Alkyd	Hydrate chromium oxide green	1:1.5

Tab. 21 – Summary of unknown samples used in the calibration curves

In each calibration curve, the values of the Area of unknown samples, obtained from spectroscopic analysis, are added. From the interpolation of these values to the calibration curve it is possible to determine the value of the variable x, i.e. the relative concentration.

In the graphs 4-5-6-7, a first example of quantification method of unknown samples is observed. From measured values on the Y axis, the calculated concentration values (X axis) are obtained.
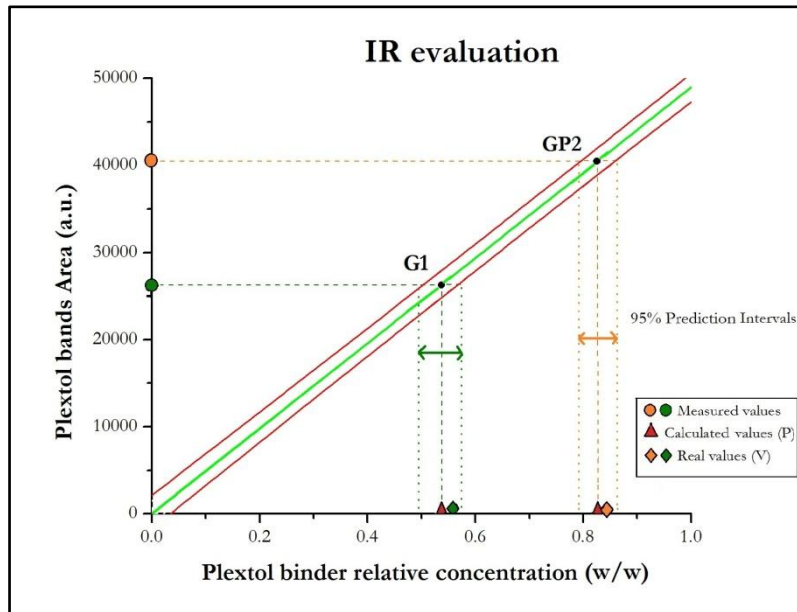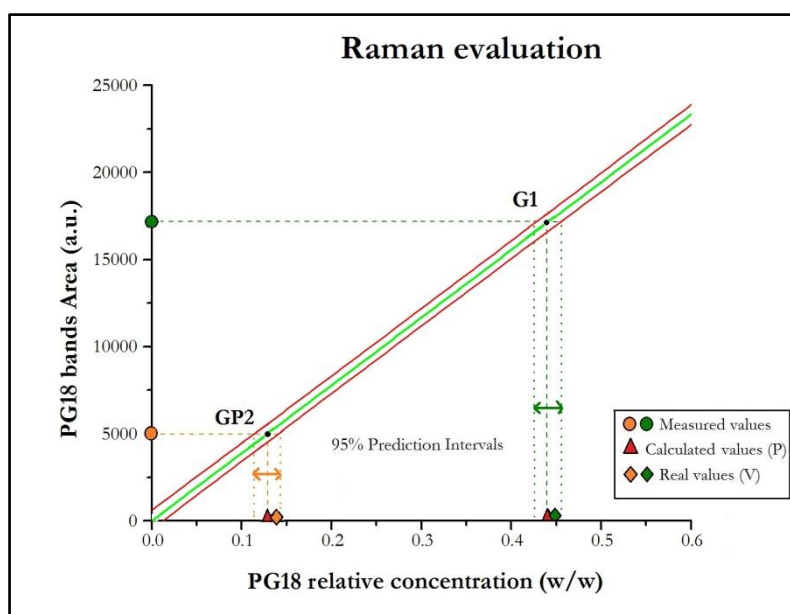
Graph 4 – Quantitative method of acrylic component in green unknown samples: the abscissa represents the relative concentration of binder, the ordinate the Area value of binder obtained by IR spectroscopy
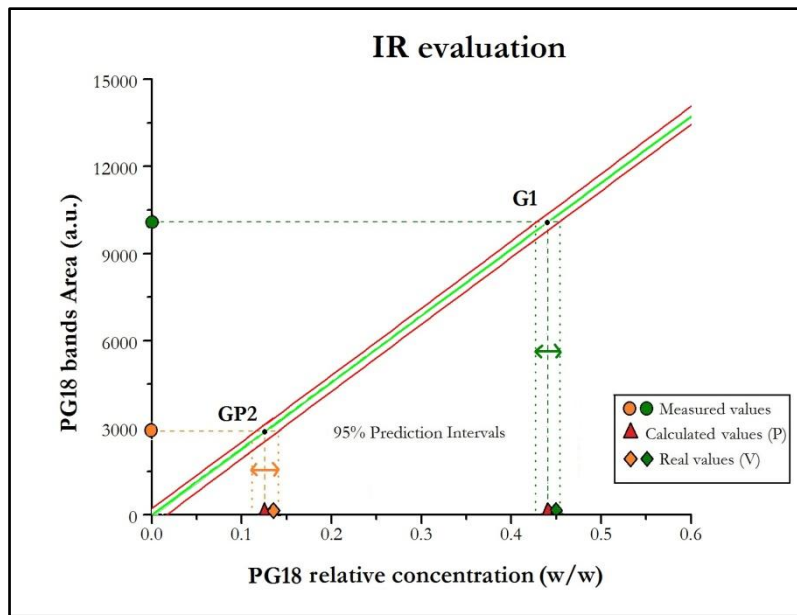
Graph 5 – Quantitative method of pigment component in green acrylic unknown samples: the abscissa represents the relative concentration of PG18, the ordinate the Area value of pigment obtained by IR spectroscopy
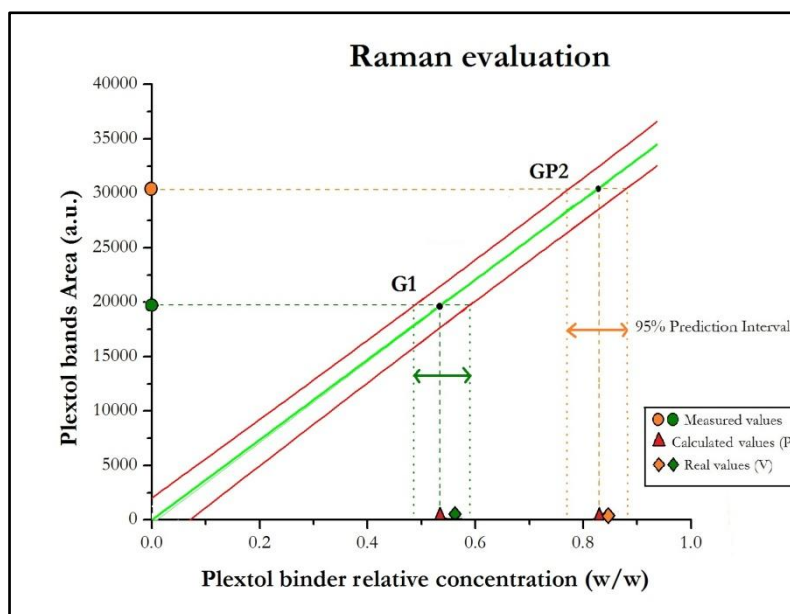
Graph 6 - Quantitative method of acrylic component in green unknown samples: the abscissa represents the relative concentration of binder, the ordinate the Area value of binder obtained by Raman spectroscopy

Graph 7 – Quantitative method of pigment component in green acrylic unknown samples: the abscissa represents the relative concentration of PG18, the ordinate the Area value of pigment obtained by Raman spectroscopy

They fall within the prediction interval with a probability of 95%. The same trend is shown in the graphs presented in appendix (section II). To estimate the error of the relative concentration obtained, the percentage standard deviation values for each sample analyzed are observed. It expresses the dispersion of data around a position index, such as the arithmetic mean or its

71

estimate. These values range from 1% to 3%. This indicates that the dispersion of the data obtained is contained and best depicts the samples.

The best parameter to evaluate the accuracy of the quantitative method and the changing between the calculated value and the real one is the percentage variation, or relative error (E_r). It expresses the difference between the measured final value (P) and the true value (V) of a magnitude in percentage terms, considering the true value as the reference value. The percentage variation is given by:

$$Percentage\ variation = \frac{(V - P)}{V} \cdot 100 \qquad \text{(Eq. 33)}$$

If the final value is greater than the real one, a positive percentage increase is observed; if instead the final value is less than the real one, a negative percentage decrease is observed. In this case, a positive percentage increase is always noticed. Percentage variation values of previous graphs are shown in tables 22-23 (see also the appendix, section II).

Samples	P/BM ratio	Real relative concentration values (w/w)		Calculated relative concentration values (w/w)		Percentage variation (%)	
		Binder	Pigment	Binder	Pigment	Binder	Pigment
G1	1:1.2	0.55	0.45	0.537	0.44	2.4	2.2
GP2	1:6	0.86	0.143	0.827	0.125	3.8	12.6

Tab. 22 – Summary of values of acrylic green samples, analyzed by IR spectroscopy: the real relative concentration of binder and pigment are compared to the calculated ones

Samples	P/BM ratio	Real relative concentration values (w/w)		Calculated relative concentration values (w/w)		Percentage variation (%)	
		Binder	Pigment	Binder	Pigment	Binder	Pigment
G1	1:1.2	0.55	0.45	0.534	0.44	2.9	2.2
GP2	1:6	0.86	0.143	0.829	0.129	3.6	9.8

Tab. 23 – Summary of values of acrylic green samples, analyzed by Raman spectroscopy: the real relative concentration of binder and pigment are compared to the calculated ones

Evaluating the different results obtained, high percentage variations are not observed and the values always fall within an acceptable range for the type of samples treated. In addition, all values measured and interpolated to the straight line fall within the prediction interval obtained from the calibration curves; it indicates that the quantitative model developed is valid, reproducible and reliable.

### 4.4.4 Evaluation of P/BM ratios of commercial paints

The quantitative analysis reveals that the statistical model developed is able to evaluate with good precision and accuracy the different pigment/binder relative concentrations within samples made in laboratory from different operators. The next aim is to be able to quantitatively determine and evaluate commercial painting samples out of tubes. In these samples, in addition to the binder and pigment other components are present such as additional elements (additives, charges, surfactants, etc.) that could compromise the final result of the study. The commercial paints chosen belong to three different manufactures, which normally do not give the pigment/binder ratio. Only the ratio of the sample, belonging to the Schmincke manufacturer, is known and considered. It is made up of acrylic binder in mixture with chromium hydrated oxide pigment PG18 (PRIMAcryl, Schmincke). The sample, from this moment on, will be called sample C. From the dust analysis of the company, the P/BM ratio is 1:2.7. The experimental procedures performed for the analysis are the same used for the analysis of unknown samples and the results obtained (Area value) are interpolated to the calibration curves previously developed. Observing the values obtained in table 24, it is possible to determine that even in this case the quantitative model is able to evaluate the relative concentrations of pigment and binder within the sample. The percentage variation values do not indicate a considerable change from the ones calculated to the real ones. In this case, compared to the ones shown above, it is observed that the analysis shows a negative percentage decrease in the pigment quantification, both by IR and Raman spectroscopy. However, the percentage variation remains low and not significant. The quantitative graphs, with the correspondent table, are shown below.

| Sample	P/BM ratio	Analytical technique used	Real relative concentration values (w/w)		Calculated relative concentration values (w/w)		Percentage variation (%)	
			Binder	Pigment	Binder	Pigment	Binder	Pigment
C	1:2.7	IR	0.73	0.27	0.708	0.287	3	-6.3
		Raman	0.73	0.27	0.714	0.286	2.2	-5.9

Tab. 24 – Summary of values of Schmincke sample, analyzed by IR and Raman spectroscopies: the real relative concentration of binder and pigment are compared to the calculated ones
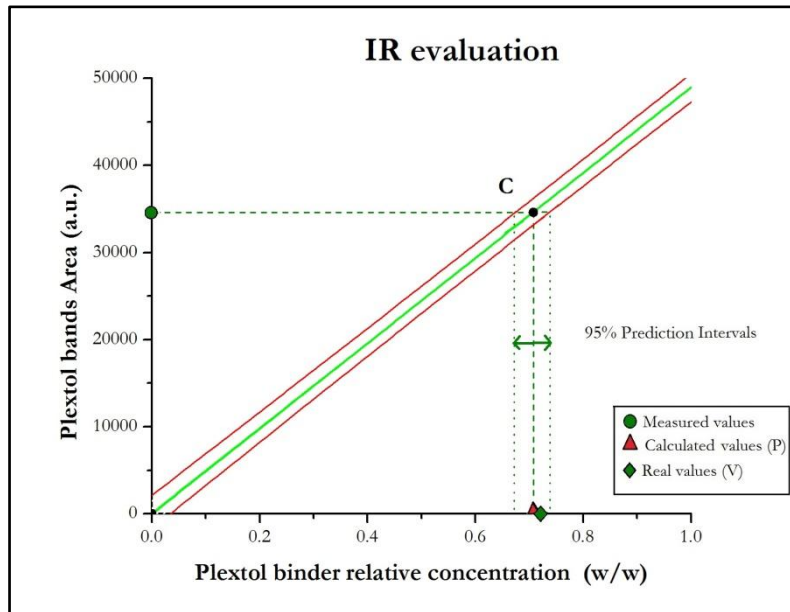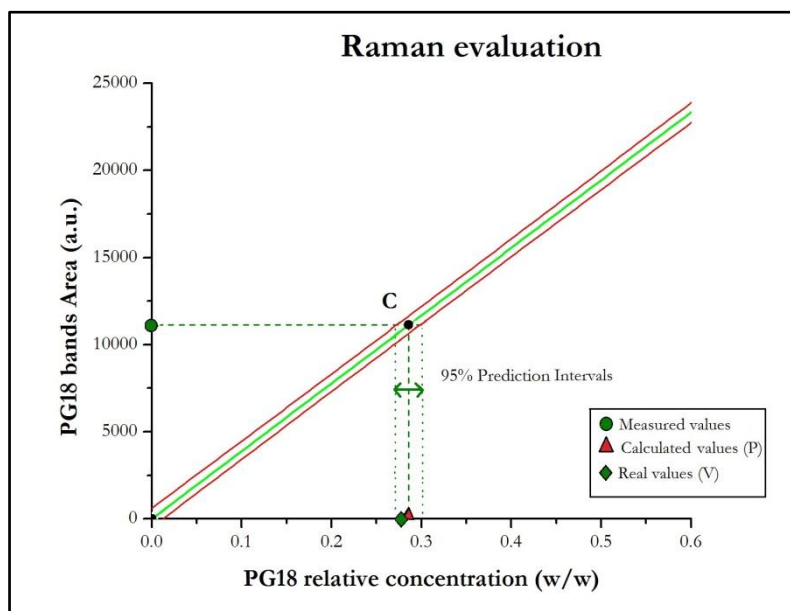
Graph 8 – Quantitative method of Schmincke sample: the abscissa represents the relative concentration of binder, the ordinate the Area value of binder obtained by IR spectroscopy
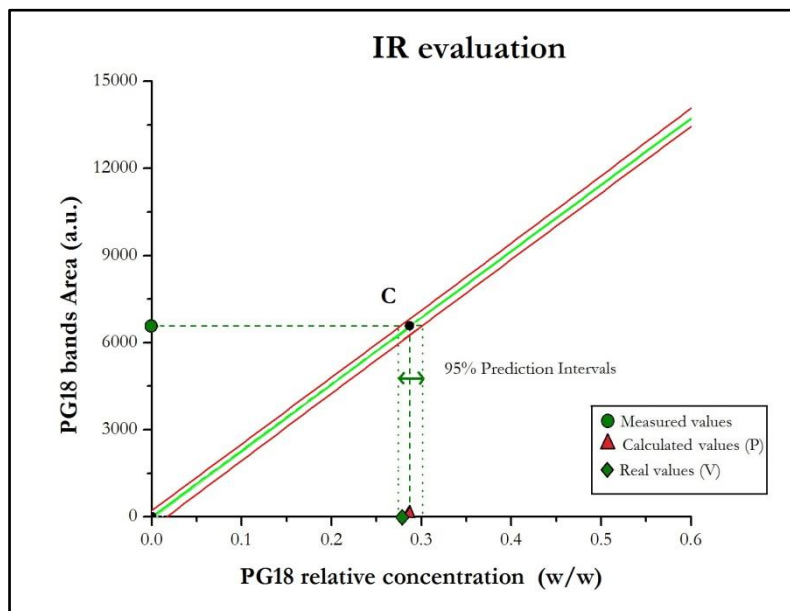
Graph 9 – Quantitative method of Schmincke sample: the abscissa represents the relative concentration of PG18, the ordinate the Area value of pigment obtained by IR spectroscopy
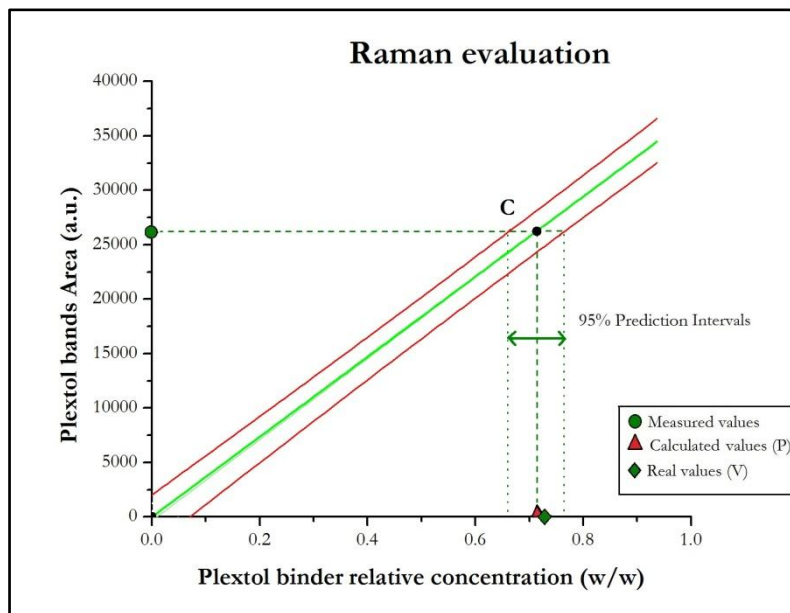
Graph 10 – Quantitative method of Schmincke sample: the abscissa represents the relative concentration of binder, the ordinate the Area value of binder obtained by Raman spectroscopy

Graph 11 – Quantitative method of Schmincke sample: the abscissa represents the relative concentration of PG18, the ordinate the Area value of pigment obtained by Raman spectroscopy

Chapter 5

Conclusion

This thesis project focused on the analytical study of modern painting materials, such as acrylic and alkyd binders in mixture with several inorganic pigments.

The first aim of the thesis was initially to carry out a qualitative analysis using optical microscopy and Vis-RS spectrophotometry, but also using the most advanced non-invasive spectroscopic techniques, such as IR and Raman. The results of this first evaluation allowed to identify and characterize the different binders and pigments used, and also to obtain important information on the paint layers, such as morphological observation of the surface layers and the identification of the main chemical functional groups. The latter allowed starting a study on the different drying processes of the two polymeric binders.

This research, mainly conducted with IR spectroscopy in reflection mode, observed significant spectral changes, shown by the increase and decrease of absorption bands of the two binders, both pure and in mixture with pigments. Both the two pure binders showed a decrease of methylene C-H absorptions (2930-2855 cm^{-1}), due to the oxidation of double bonds. An increase of the carbonyl stretching absorption (1730-1680 cm^{-1}) and a small increase of the stretching vibration of C=O groups (1635 cm^{-1}) is also observed. It represents the oxidation reactions that take place during natural ageing and that lead to the formation of alcohols and carbonyl species. For this reason it was possible to indicate these bands as the representative parameter of oxidation, useful to monitor the ageing process. A small difference is observed between the two binders: in the alkydic spectrum the negative band at 3600 cm^{-1} represents the gas phase water signal, while in the acrylic one, in the same region, the decrease of hydroxyl groups is observed, due to the evaporation of water.

Adding different pigments to binders some changes were noticed. With the artificial ultramarine blue, both in the acrylic and alkydic samples, only the increase of the bands at 987 cm^{-1} could be shown, representing the Si-O bond vibrations of the pigment, more visible after the physical drying of the binder. The cadmium yellow was not visible in IR spectroscopy, however a negative band at 3434 cm^{-1} was observed: probably due to the formation of aliphatic sulphide compound CH_3S. In the case of the hydrated chromium oxide green, an increase of the oxide bond vibrations at 567 cm^{-1} was verified and a spectral interference at 3600 cm^{-1} and at 1720-1490 cm^{-1} was present.

This spectral noise is due probably to the interaction between the hydrated components of the binders. The study of the drying processes of the various binders could not be investigated by Raman analysis, above all due to instrumental limitations. Principal problems were: the small measuring area employed, the loss of focus during the binder cross-linking, the presence of fluorescence for the identification of organic materials and the molecular damages due to the long-term laser exposure.

The second aim of the thesis was to carry out a quantitative analysis to evaluate different pigment/binder ratios within each mock-up sample. To develop a mathematical-statistical model, initially it was necessary to create a calibration curve with values of known concentration samples.

The graphs were constructed using 5 samples, depending on the different binder and pigment used in the samples, using their IR and Raman band Area value (Y axis) and the value of their relative concentration (X axis) and divided according to the technique used (IR and Raman). This first step was important to mathematically confirm the P/BM ratio in the samples, and to ensure that the quantification of unknown P/BM ratio samples was efficient. In order to evaluate the quality of the interpolation points, it was analyzed the correlation coefficient of each calibration curve. All values approach to 1, this indicated that the values of both variables are highly correlated each other and the values of the dependent variable Y obtained (Area) best represented each pigment or binder component in the samples. Once it was confirmed that the calibration curves were optimal, in each of them, the values of the Area of unknown samples were added. From the interpolation of these values it was possible to determine the value of the relative concentration, before unknown. To evaluate the efficacy of the quantitative method, the percentage variation values were observed. The values obtained were not shown a high percentage variations, moreover all values measured and interpolated to the straight line fell within the prediction interval; these parameters indicated that the quantitative model developed was valid, reproducible and reliable. At this point, using the same experimental procedures used for the previous samples, it was possible to quantitatively determine a commercial painting sample. It was observed that the results obtained and interpolated to the related calibration curve carried out to calculated values very close to the real ones. Also in this case the percentage variation values did not indicate a considerable change. For this reason it was possible to confirm that the quantitative analysis developed a statistical model able to evaluate with good precision and accuracy the different pigment/binder relative concentrations within of samples, both for those made in laboratory and the commercial ones.

Due to the importance of diagnostic-scientific analysis applied to cultural heritage have nowadays, this thesis allowed to characterize more in detail modern materials mainly used in art, by non-

invasive spectroscopic techniques. Moreover it allowed developing a mathematical-statistical model that could quantitatively determine the different components within a paint layer.

In this study, binder and pigment components were mainly investigated, but it is well known that in the composition of modern commercial paints are present also additional elements such as additives, fillers and surfactants. Therefore, this method could also quantify these components in the future. The method focused above all on the application of spectroscopic techniques such as IR and Raman, but it is supposed that in a future project this model could also be used on results obtained from other more sophisticated and precise analytical techniques. Knowledge on a quantitative level of modern materials is useful not only from an entirely instructive and academic point of view but it could develop more selective and precise methods of conservation and restoration. In fact, the theme of conservation of modern art is much discussed and it was treated especially in the famous book "Modern Art. Who cares?", promoted by Stichting Behoud Modern Kunst (SBMK) and the Institut Collectie Nederland (ICN), at an international conference held in Amsterdam in 1997, which for the expert community represented an interdisciplinary model of sharing and exchanging ideas and knowledge. Therefore, these new forms of art have stimulated the study of the chemical-physical nature of these modern contemporary materials, encouraging the development of new and special tools of analysis and evaluation, which in the future they will be increasingly innovative.

Appendix

- **<u>Section I</u>**

Number graph	Composition samples	Technique used	Correlation coefficient value (R)
4	PB29 + Alkydic binder	IR spectroscopy	0.99977
5	PB29 + Alkydic binder	IR spectroscopy	0.99976
6	PB29 + Alkydic binder	Raman spectroscopy	0.99962
7	PG18 + Plextol binder	IR spectroscopy	0.9998
8	PG18 + Plextol binder	IR spectroscopy	0.99981
9	PG18 + Plextol binder	Raman spectroscopy	0.99946
10	PG18 + Plextol binder	Raman spectroscopy	0.99983
11	PG18 + Alkydic binder	IR spectroscopy	0.99982
12	PG18 + Alkydic binder	IR spectroscopy	0.99954
13	PG18 + Alkydic binder	Raman spectroscopy	0.99968
14	PG18 + Alkydic binder	Raman spectroscopy	0.99966
15	PY37 + Plextol binder	IR spectroscopy	0.99967
16	PY37 + Plextol binder	Raman spectroscopy	0.99968
17	PY37 + Plextol binder	Raman spectroscopy	0.99933
18	PY37 + Alkydic binder	IR spectroscopy	0.99961
19	PY37 + Alkydic binder	Raman spectroscopy	0.99965

Tab. 25 – Summary of the correlation coefficient values of each sample
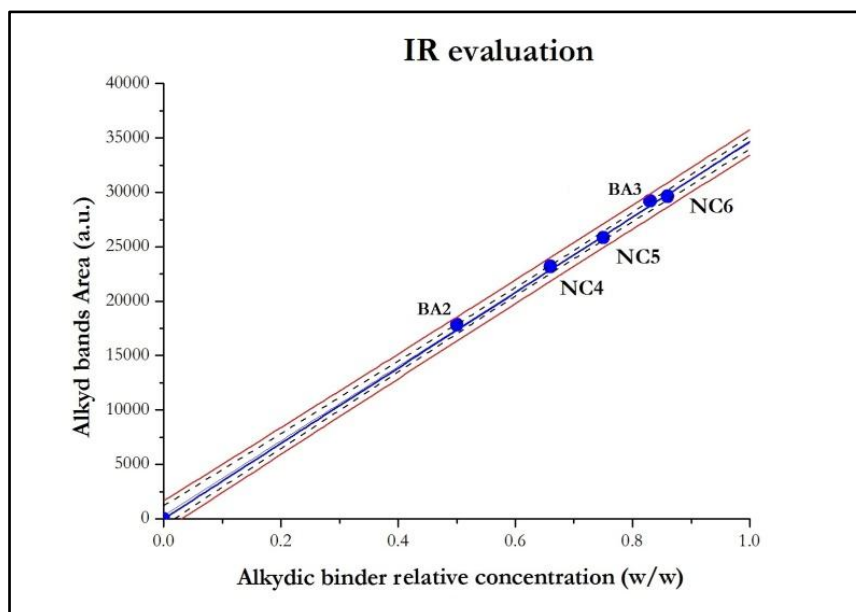
Graph 12 – Calibration curve of alkydic component in blue samples: the abscissa represents the relative concentration of binder, the ordinate the Area value of binder obtained by IR spectroscopy
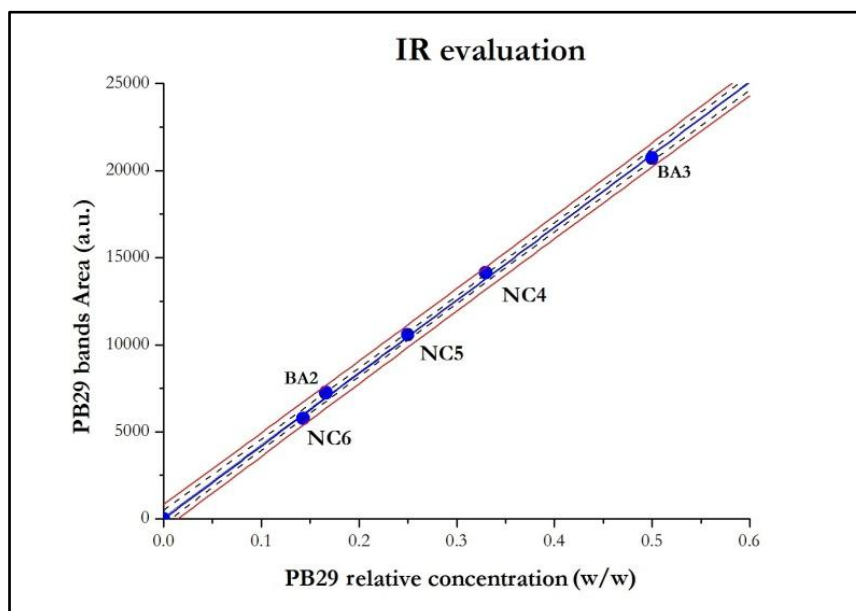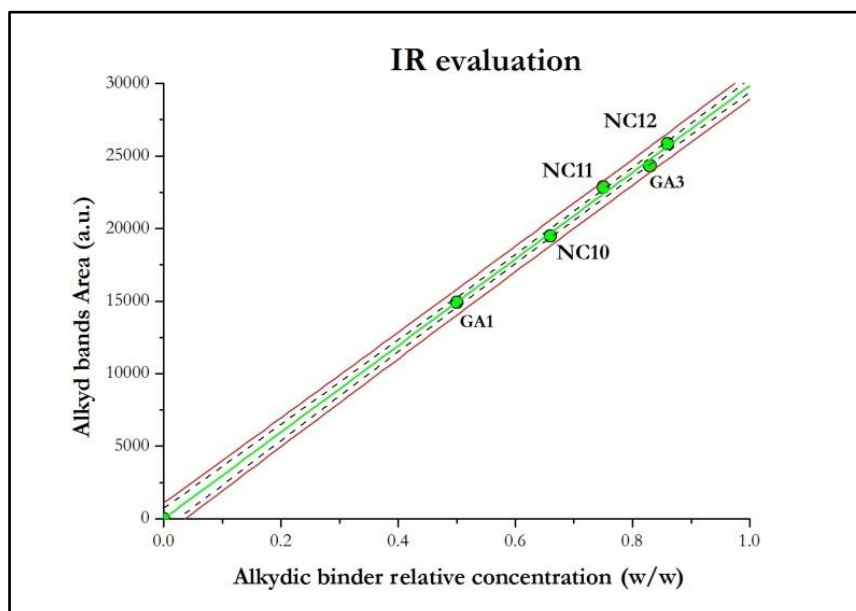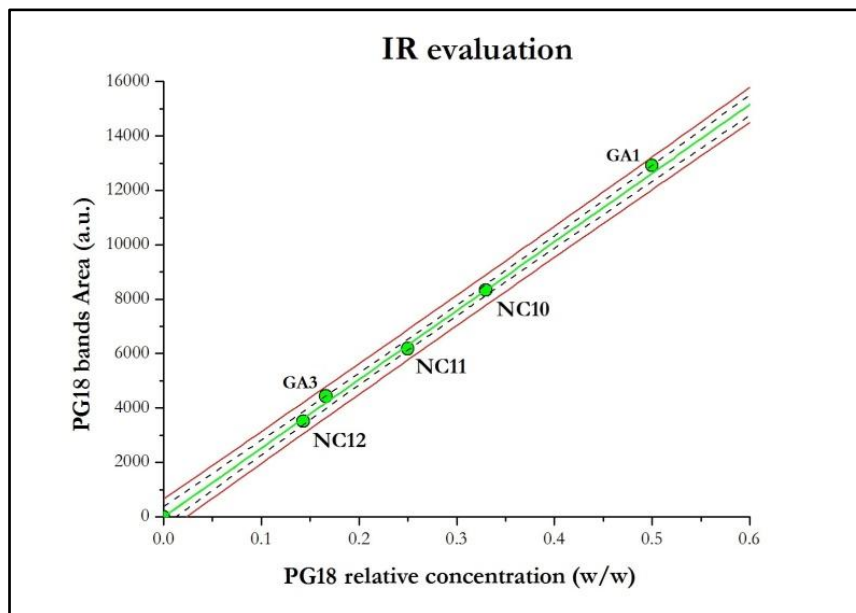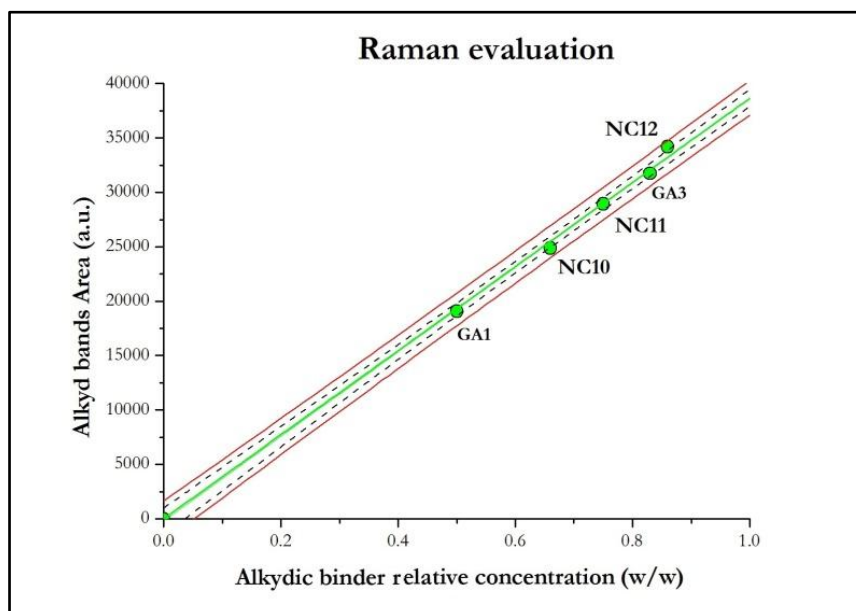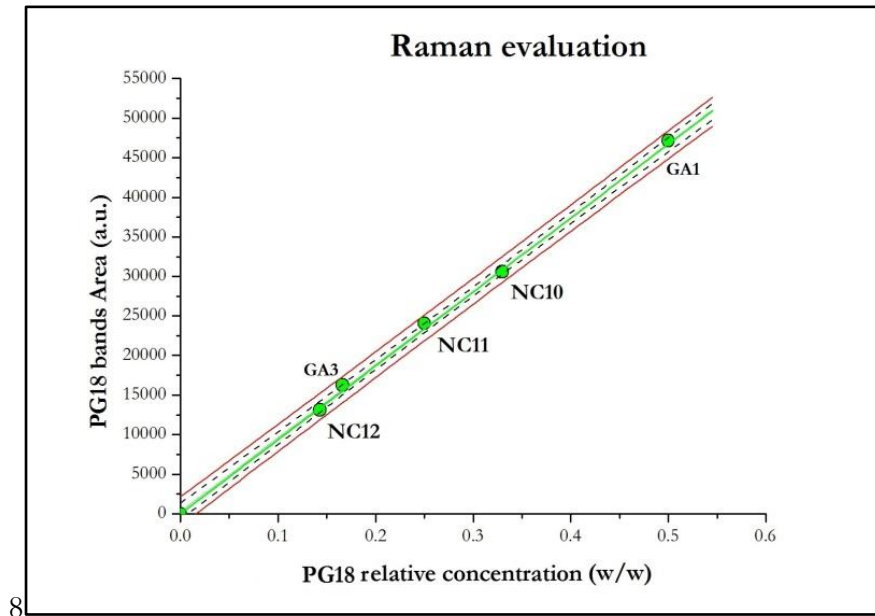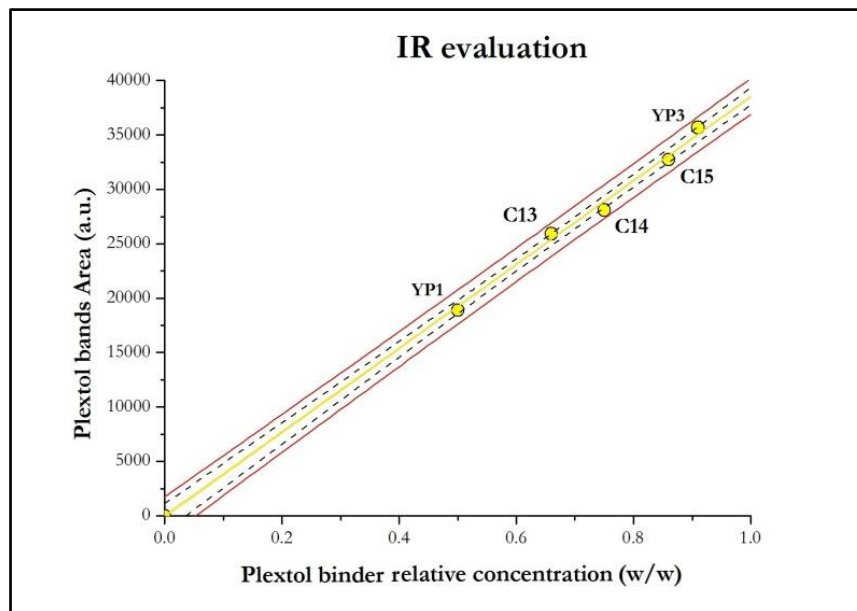

Graph 13 – Calibration curve of pigment component in blue alkydic samples: the abscissa represents the relative concentration of PB29, the ordinate the Area value of pigment obtained by IR spectroscopy
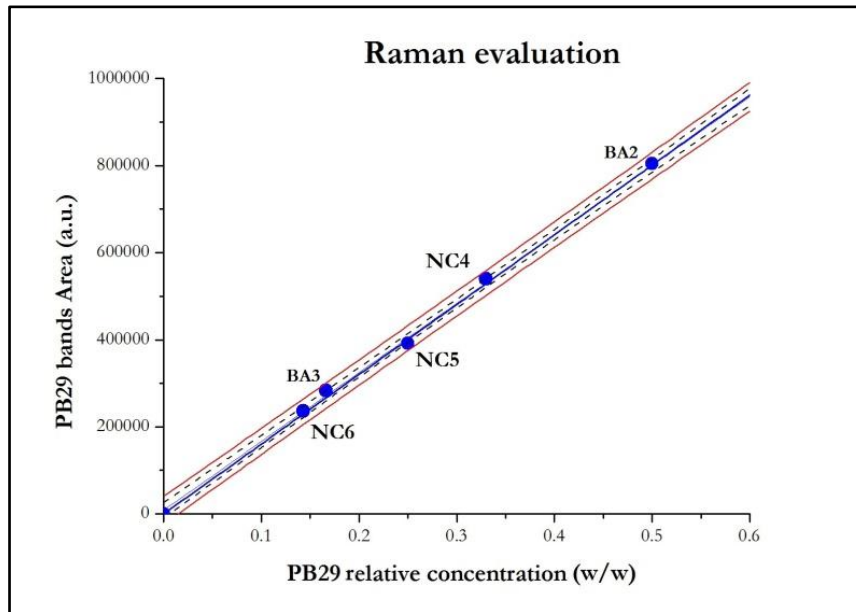
Graph 14 – Calibration curve of pigment component in blue alkydic samples: the abscissa represents the relative concentration of PB29, the ordinate the Area value of pigment obtained by Raman spectroscopy
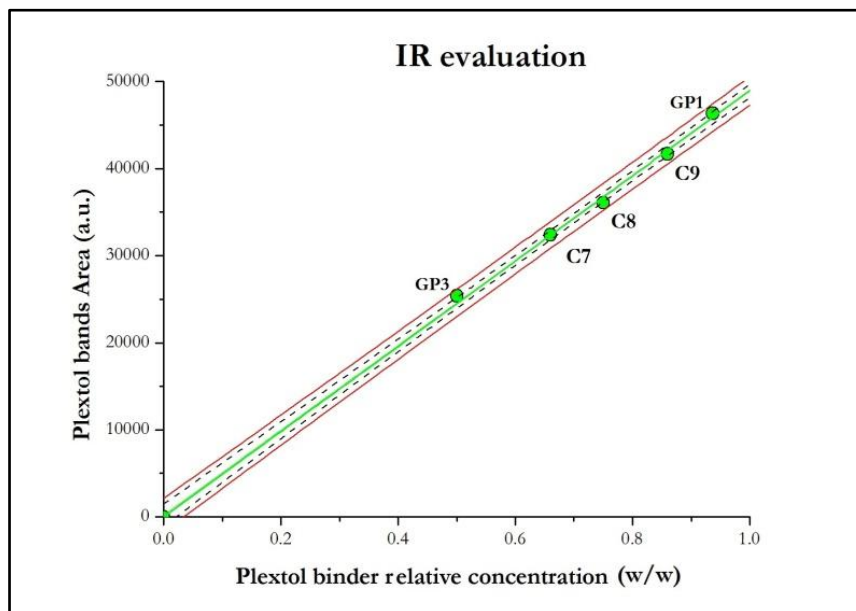
Graph 15 – Calibration curve of acrylic component in green samples: the abscissa represents the relative concentration of binder, the ordinate the Area value of binder obtained by IR spectroscopy
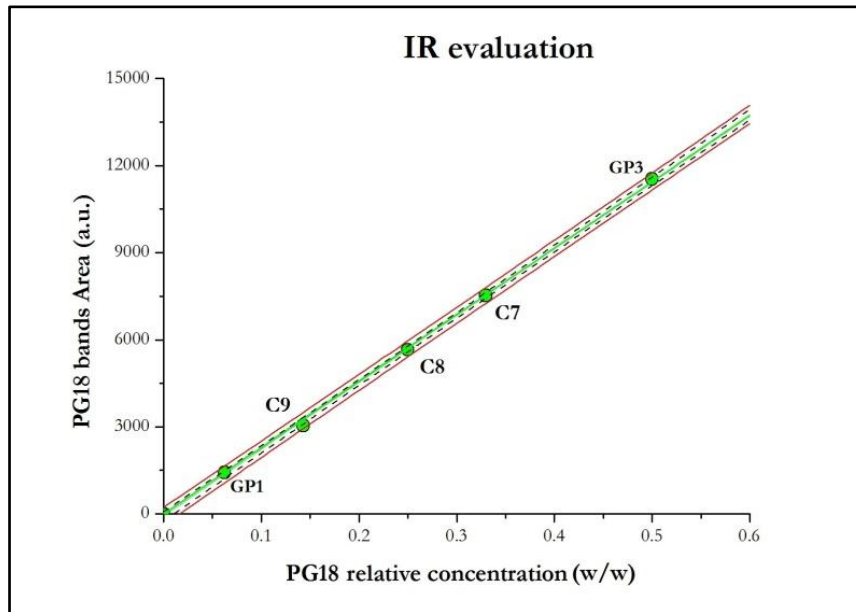
Graph 16 – Calibration curve of pigment component in green acrylic samples: the abscissa represents the relative concentration of PG18, the ordinate the Area value of pigment obtained by IR spectroscopy
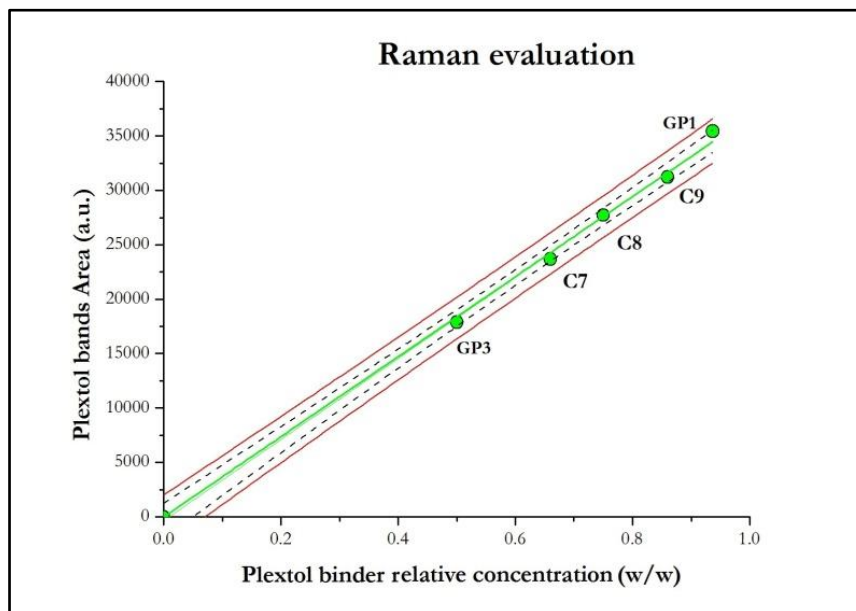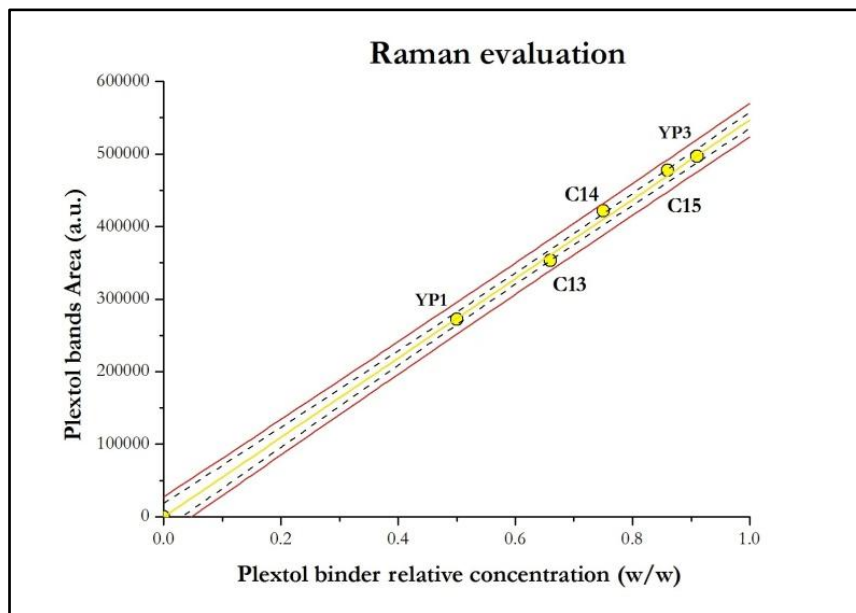

Graph 17 – Calibration curve of acrylic component in green samples: the abscissa represents the relative concentration of binder, the ordinate the Area value of binder obtained by Raman spectroscopy
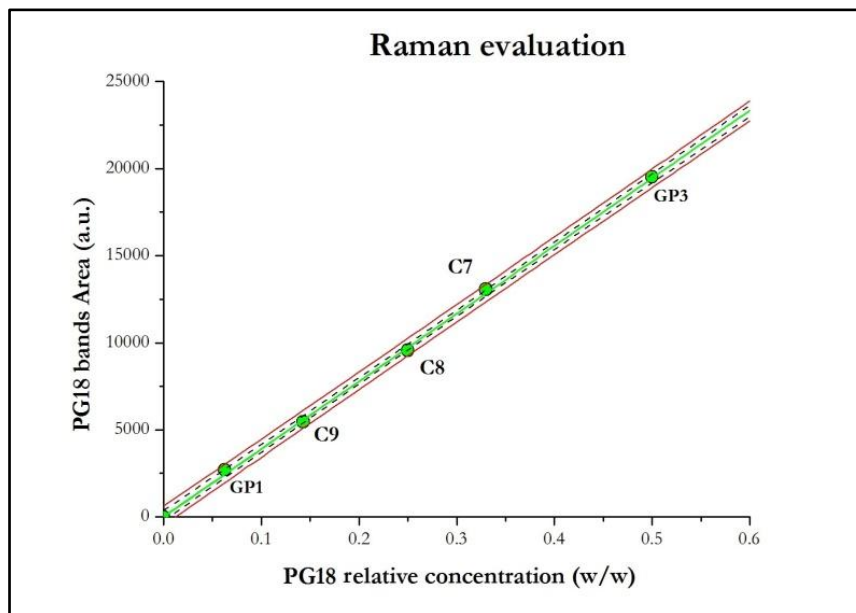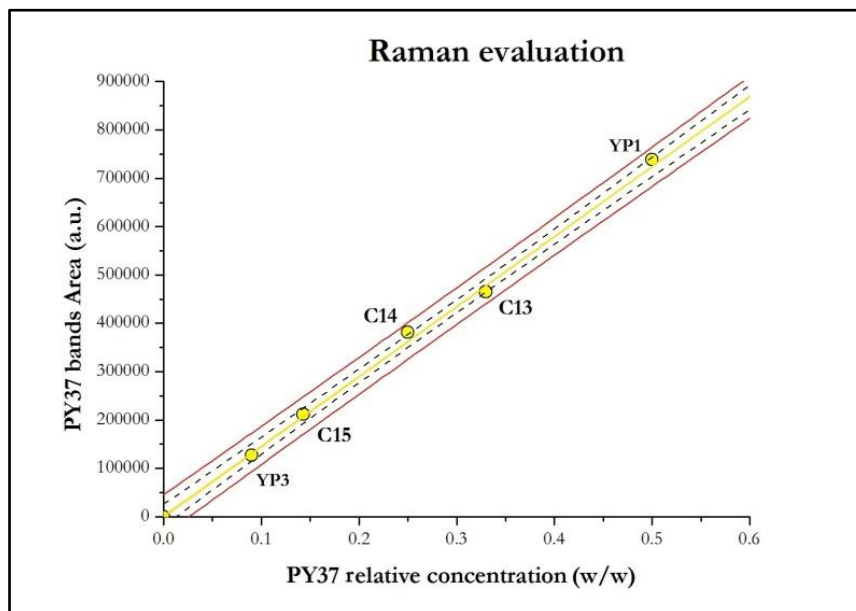
Graph 18 – Calibration curve of pigment component in green acrylic samples: the abscissa represents the relative concentration of PG18, the ordinate the Area value of pigment obtained by Raman spectroscopy
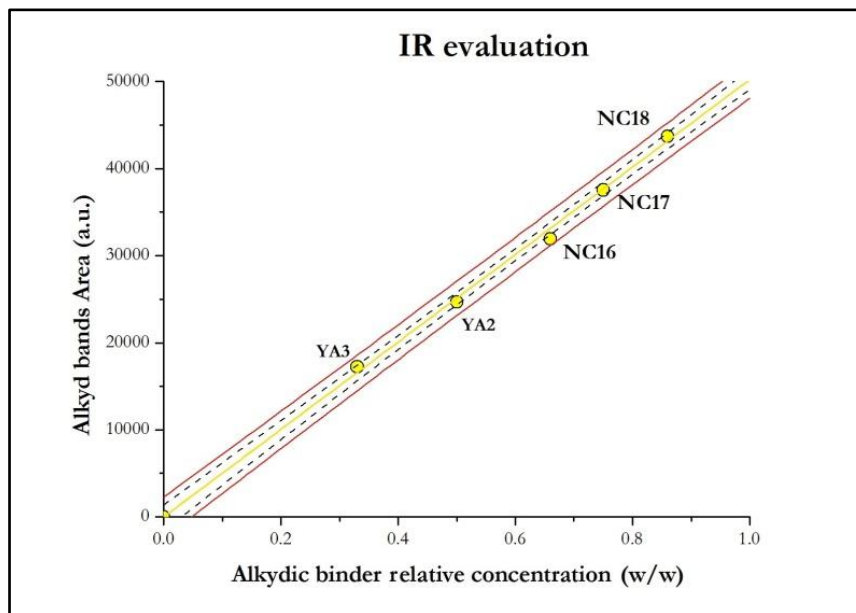

Graph 19 – Calibration curve of alkydic component in green samples: the abscissa represents the relative concentration of binder, the ordinate the Area value of binder obtained by IR spectroscopy

Graph 20 – Calibration curve of pigment component in green alkydic samples: the abscissa represents the relative concentration of PG18, the ordinate the Area value of pigment obtained by IR spectroscopy

Graph 21 – Calibration curve of alkydic component in green samples: the abscissa represents the relative concentration of binder, the ordinate the Area value of binder obtained by Raman spectroscopy

Graph 22 – Calibration curve of pigment component in green alkydic samples: the abscissa represents the relative concentration of PG18, the ordinate the Area value of pigment obtained by Raman spectroscopy
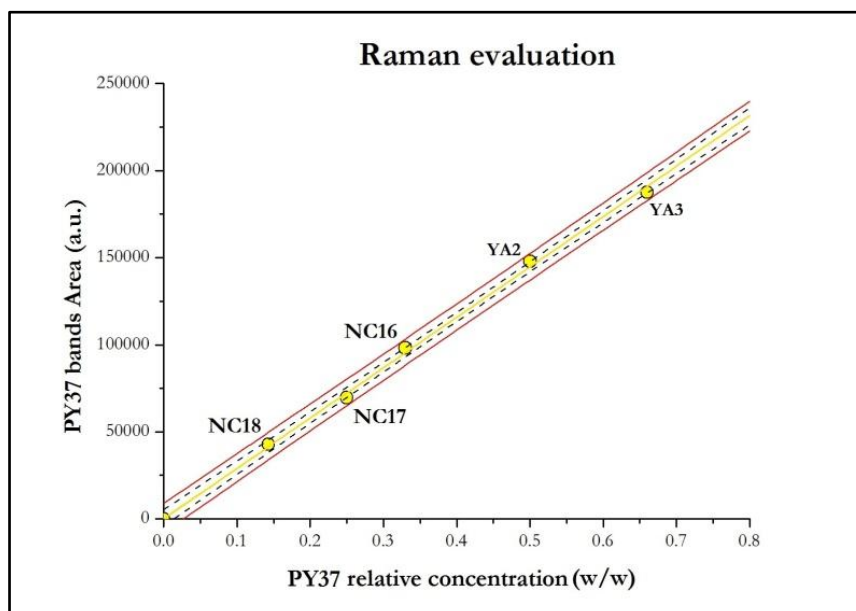

Graph 23 – Calibration curve of acrylic component in yellow samples: the abscissa represents the relative concentration of binder, the ordinate the Area value of binder obtained by IR spectroscopy

Graph 24 – Calibration curve of acrylic component in yellow samples: the abscissa represents the relative concentration of binder, the ordinate the Area value of binder obtained by Raman spectroscopy

Graph 25 – Calibration curve of pigment component in yellow acrylic samples: the abscissa represents the relative concentration of PY37, the ordinate the Area value of pigment obtained by Raman spectroscopy

Graph 26 – Calibration curve of alkydic component in yellow samples: the abscissa represents the relative concentration of binder, the ordinate the Area value of binder obtained by IR spectroscopy

Graph 27 – Calibration curve of pigment component in yellow alkydic samples: the abscissa represents the relative concentration of PY37, the ordinate the Area value of pigment obtained by Raman spectroscopy

- **Section II**

Unknown samples employed			
Name sample	Binder used	Pigment used	Unknown P/BM ratio
BP2	Plextol	Artificial ultramarine blue	1:2
B1	Plextol	Artificial ultramarine blue	1:3
BA1	Alkyd	Artificial ultramarine blue	1:2
B2	Alkyd	Artificial ultramarine blue	1:0.7
YP2	Plextol	Cadmium yellow	1:0.5
Y1	Plextol	Cadmium yellow	1:0.4
YA1	Alkyd	Cadmium yellow	1:2
Y2	Alkyd	Cadmium yellow	1:0.7

Tab. 26 - Summary of unknown samples used in the calibration curves

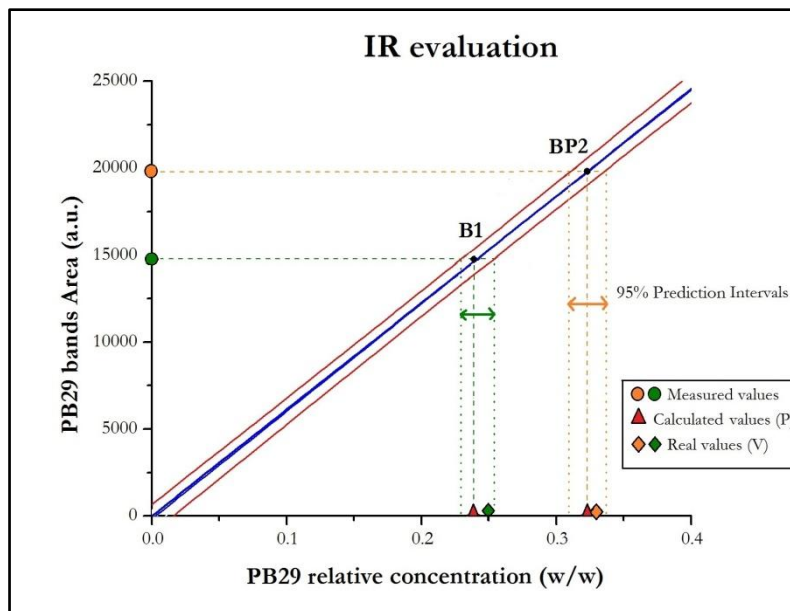| Samples	P/BM ratio	Real relative concentration values (w/w)		Calculated relative concentration values (w/w)		Percentage variation (%)	
		Binder	Pigment	Binder	Pigment	Binder	Pigment
BP2	1:2	0.66	0.33	0.63	0.323	4.5	2.1
B1	1:3	0.75	0.25	0.727	0.239	3.1	4.4
B2	1:0.7	0.42	0.58	0.403	0.568	4.0	2.1
BA1	1:2	0.66	0.33	0.636	0.317	3.6	3.9
G2	1:1.5	0.6	0.4	0.587	0.389	2.2	2.75
GA2	1:2	0.66	0.33	0.631	0.316	4.4	4.2
Y1	1:0.4	0.28	0.71	0.262	/	6.4	/
YP2	1:0.5	0.33	0.66	0.321	/	2.7	/
Y2	1:0.7	0.41	0.58	0.391	/	4.6	/
YA1	1:2	0.66	0.33	0.628	/	4.8	/

Tab. 27 – Summary of values of all samples, analyzed by IR spectroscopy: the real relative concentration of

binder and pigment are compared to the calculated ones

Samples	P/BM ratio	Real relative concentration values (w/w)		Calculated relative concentration values (w/w)		Percentage variation (%)	
		Binder	Pigment	Binder	Pigment	Binder	Pigment
BP2	1:2	0.66	0.33	/	0.321	/	2.73
B1	1:3	0.75	0.25	/	0.24	/	4
B2	1:0.7	0.42	0.58	/	0.568	/	2.1
BA1	1:2	0.66	0.33	/	0.319	/	3.3
G2	1:1.5	0.6	0.4	0.582	0.391	3	2.25
GA2	1:2	0.66	0.33	0.63	0.315	4.5	4.5
Y1	1:0.4	0.28	0.71	0.269	0.703	3.9	0.9
YP2	1:0.5	0.33	0.66	0.319	0.649	3.3	1.6
Y2	1:0.7	0.41	0.58	/	0.573	/	1.2
YA1	1:2	0.66	0.33	/	0.314	/	4.8

Tab. 28 – Summary of values of all samples, analyzed by Raman spectroscopy: the real relative concentration

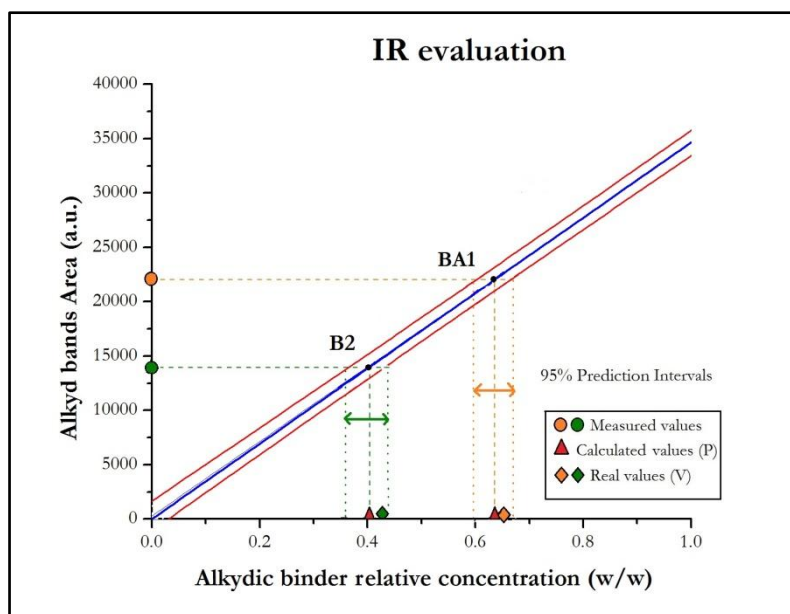of binder and pigment are compared to the calculated ones
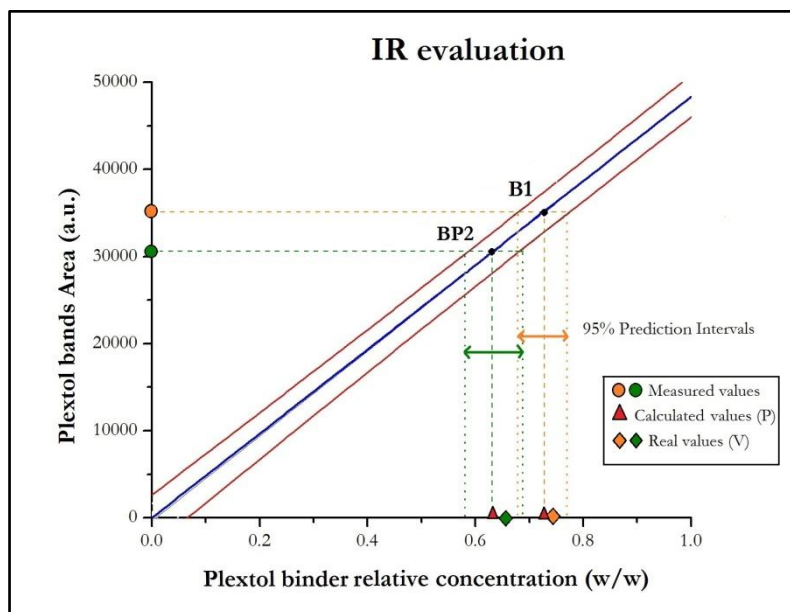
Graph 28 – Quantitative method of acrylic component in blue unknown samples: the abscissa represents the relative concentration of binder, the ordinate the Area value of binder obtained by IR spectroscopy
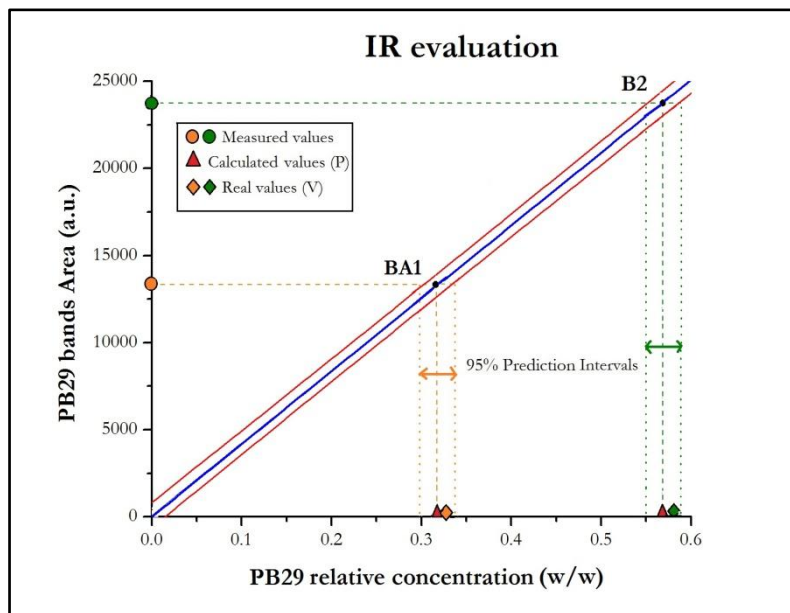

Graph 29 – Quantitative method of pigment component in blue acrylic unknown samples: the abscissa represents the relative concentration of PB29, the ordinate the Area value of pigment obtained by IR spectroscopy
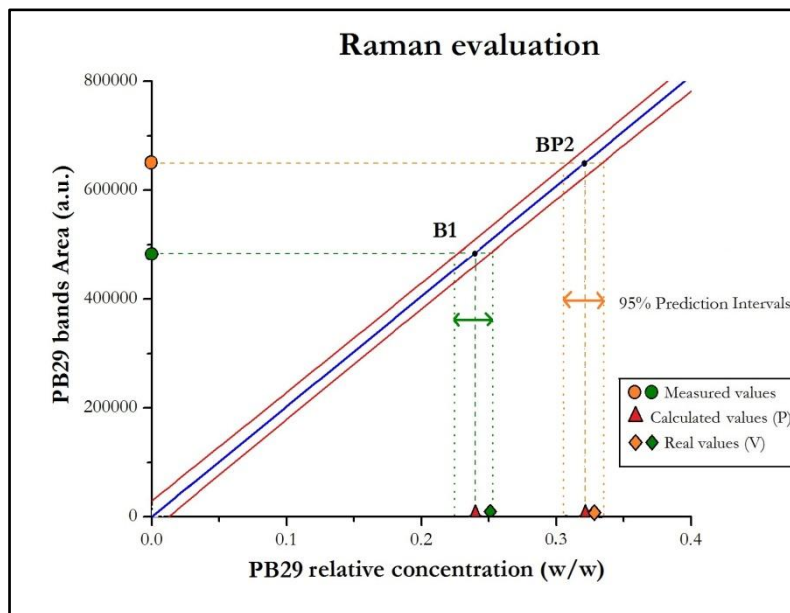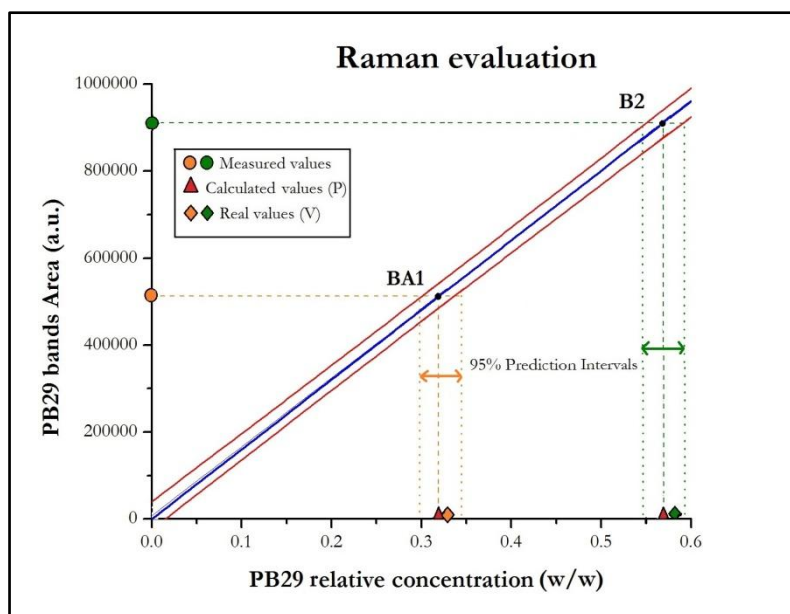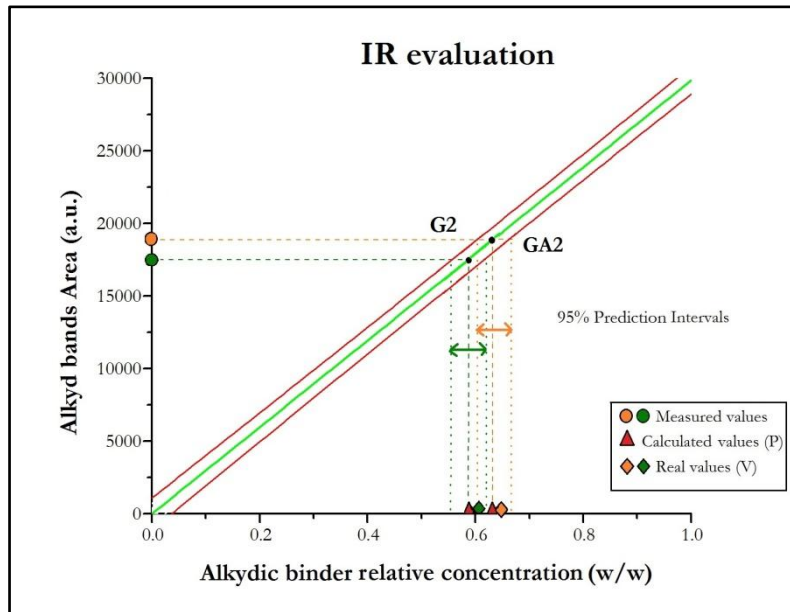
Graph 30 - Quantitative method of pigment component in blue acrylic unknown samples: the abscissa represents the relative concentration of PB29, the ordinate the Area value of pigment obtained by Raman spectroscopy

Graph 31 - Quantitative method of alkydic component in blue unknown samples: the abscissa represents the relative concentration of binder, the ordinate the Area value of binder obtained by IR spectroscopy
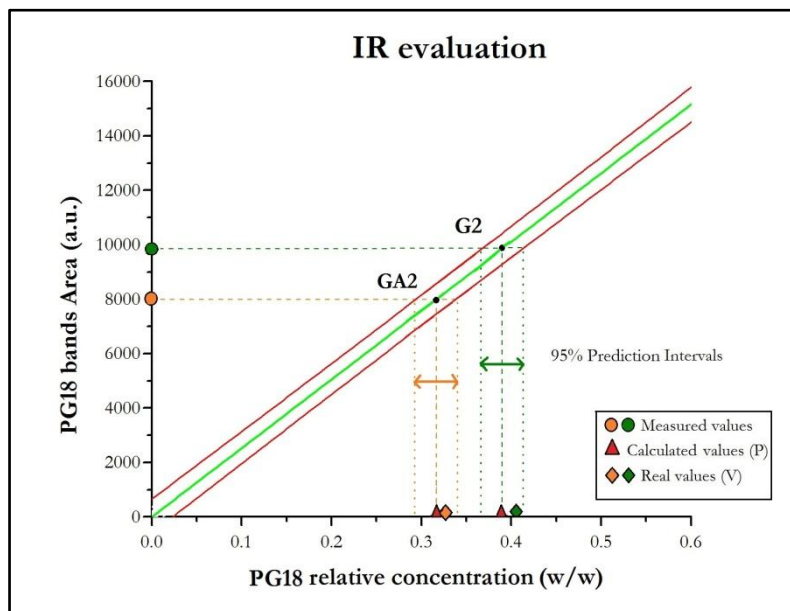
Graph 32 - Quantitative method of pigment component in blue alkydic unknown samples: the abscissa represents the relative concentration of PB29, the ordinate the Area value of pigment obtained by IR spectroscopy
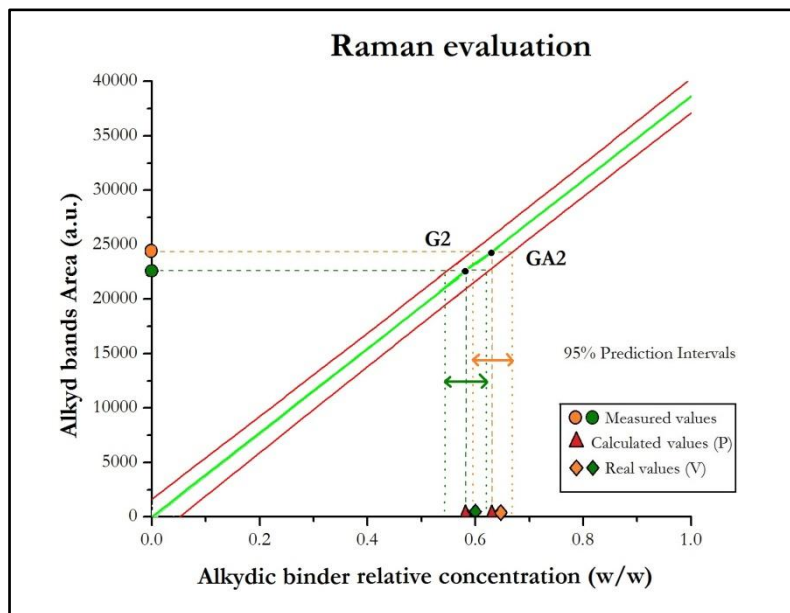

Graph 33 - Quantitative method of pigment component in blue alkydic unknown samples: the abscissa represents the relative concentration of PB29, the ordinate the Area value of pigment obtained by Raman spectroscopy
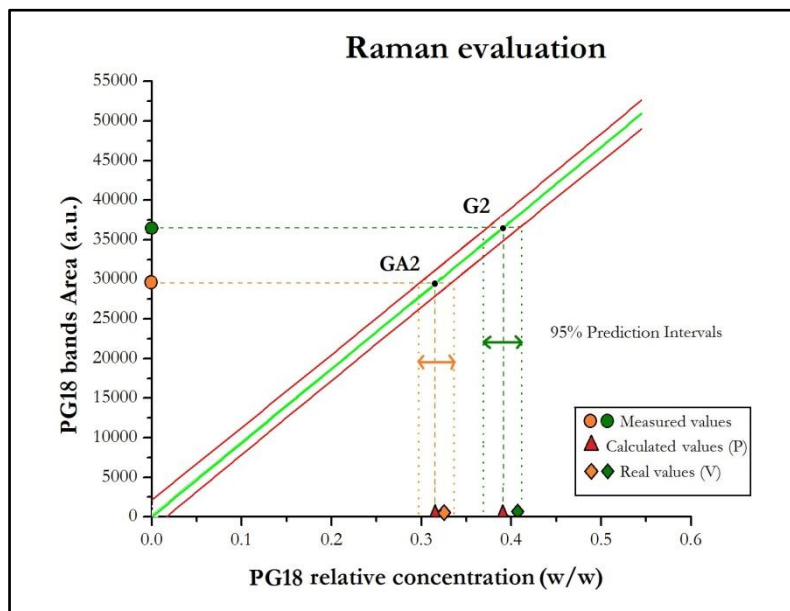
Graph 34 - Quantitative method of alkydic component in green unknown samples: the abscissa represents the relative concentration of binder, the ordinate the Area value of binder obtained by IR spectroscopy
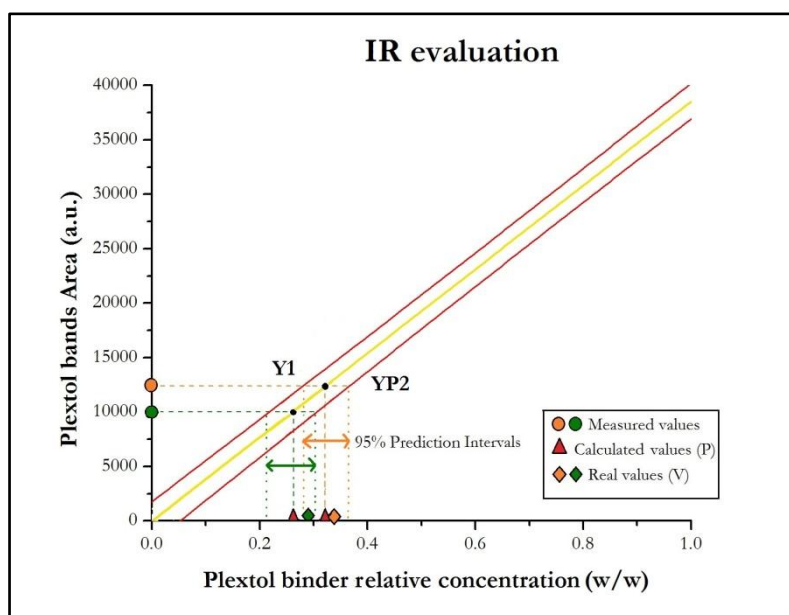

Graph 35 – Quantitative method of pigment component in green alkydic unknown samples: the abscissa represents the relative concentration of PG18, the ordinate the Area value of pigment obtained by IR spectroscopy
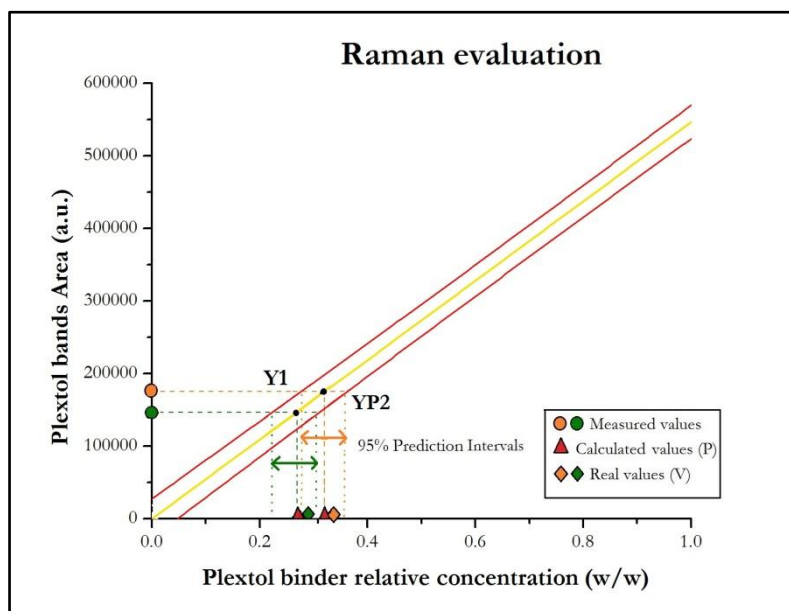
Graph 36 - Quantitative method of alkydic component in green unknown samples: the abscissa represents the relative concentration of binder, the ordinate the Area value of binder obtained by Raman spectroscopy
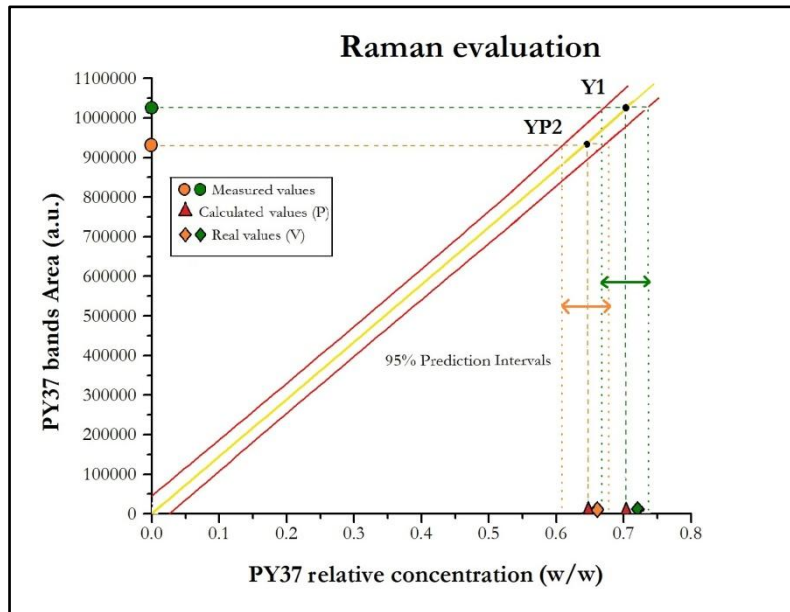

Graph 37 – Quantitative method of pigment component in green alkydic unknown samples: the abscissa represents the relative concentration of PG18, the ordinate the Area value of pigment obtained by Raman spectroscopy

Graph 38 – Quantitative method of acrylic component in yellow unknown samples: the abscissa represents
the relative concentration of binder, the ordinate the Area value of binder obtained by IR spectroscopy

Graph 39 – Quantitative method of acrylic component in yellow unknown samples: the abscissa represents
the relative concentration of binder, the ordinate the Area value of binder obtained by Raman spectroscopy

Graph 40 – Quantitative method of pigment component in yellow acrylic unknown samples: the abscissa represents the relative concentration of PY37, the ordinate the Area value of pigment obtained by Raman spectroscopy
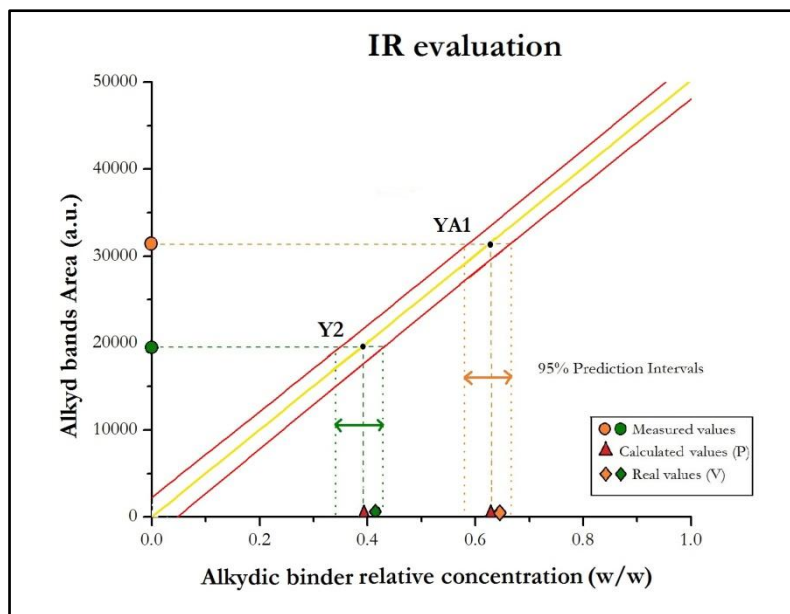

Graph 41 - Quantitative method of alkydic component in yellow unknown samples: the abscissa represents the relative concentration of binder, the ordinate the Area value of binder obtained by IR spectroscopy
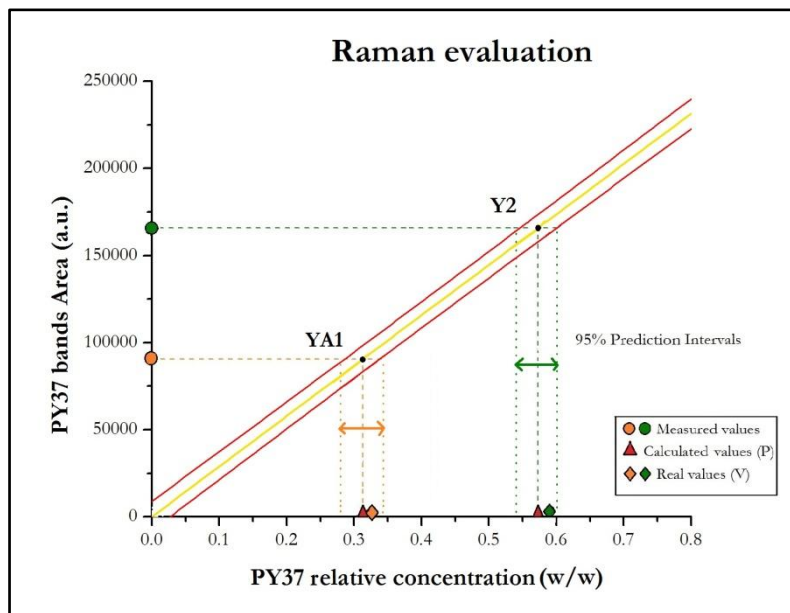
Graph 42 – Quantitative method of pigment component in yellow alkydic unknown samples: the abscissa represents the relative concentration of PY37, the ordinate the Area value of pigment obtained by Raman spectroscopy

References

[1] Chiantore O., Rava A., "Conserving contemporary art. Issues, methods, materials, and research", the Getty Conservation Institute, Los Angeles (2005)

[2] Lodge R., "A history of synthetic painting media with special reference to commercial materials", American Institute for Conservation, Washington, (1988)

[3] Van Grieken R., Janssens K., "Cultural heritage conservation and environmental impact assessment by non-destructive testing and micro-analysis", A.A. Balkema Publishers, London (2005)

[4] Artioli G., "Scientific methods and cultural heritage", Oxford University (2010)

[5] Learner T, "Modern paints uncovered: proceedings from the modern paints uncovered symposium by Getty museum (2007)

[6] Pintus V., Wei S., Schreiner M., "UV ageing studies: evaluation of lightfastness declarations of commercial acrylic paints", Anal. Bioanal. Chem. (2012)

[7] Learner T., "Analysis of Modern paints", The Getty Conservation Institute (2004)

[8] Pintus V., Schreiner M., "Characterization and identification of acrylic binding media: influence of UV light on the ageing process", Anal. Bioanal. Chem. (2011)

[9] Jablonski E., Learner T., Hayes J., Golden M., "The conservation of Acrylic Emulsion Paintings: A Literature Review"

[10] Study course "Contemporary materials for modern art", Ca' Foscari University of Venice

[11] Gorkum R., Bouwman E., "The oxidative drying of alkyd paint catalysed by metal complexes", Coordination Chemistry Reviews, Elsevier (2005)

[12] Chiantore O., Lazzari M., "Drying and oxidative degradation of linseed oil", Polymer Degradation and stability, Elsevier (1999)

[13] Fitzhugh E. W., "Artists' pigments, a handbook of their history and characteristics", National Gallery of Art, (1997)

[14] Zambuehl S., Scherrer N. C., Berger A., Eggenberger I., "Early Viridian Pigment Composition characterization of a (hydrated) chromium oxide borate pigment", Studies in Conservation, (2009)

[15] Roy A. "Artists' pigments, a handbook of their history and characteristics", National Gallery of Art (2007)

[16] Favaro M., Guastoni A., Marini F., Bianchin S., Gambirasi A., "Characterization of lapis lazuli and corresponding purified pigments for a provenance study of ultramarine pigments used in works of art", Anal. Bioanal. Chem., Springer-Verlag (2011)

[17] Osticioli I., Mendes N.F.C., Nevin A., Gil Francisco P.S.C., Becucci M., Castellucci E., "Analysis of natural and artificial ultramarine blue pigments using laser induced breakdown and pulsed Raman spectroscopy, statistical analysis and light microscopy", Spectrochim. Acta A Mol. Biomol. Spectrosc., Elsevier, (2009)

[19] Feller R. L., "Artists' pigments, a handbook of their history and characteristics", National Gallery of Art, (2007)

[19] Pouyet E., Cotte M., Fayard B., Salome M., Meirer F., Mehta A., "2D X-ray and FTIR micro-analysis of the degradation of cadmium yellow pigment in paintings of Henri Matisse", Appl. Phys. A (2015)

[20] Van der Snickt G., Dik J., Cott M., Janssens K., Jaroszewicz J., De Nolf W., Groenewegen J., Van der Loeff L., "Characterization of a Degraded Cadmium Yellow (CdS) Pigment in an Oil Painting by Means of Synchrotron Radiation Based X-ray Techniques", Analytical Chemistry, (2009)

[21] Berge B., "The ecology of building materials", second edition, Elsevier, United States (2009)

[22] Hesse M., Meier H., Zeeh B., "Metodi spettroscopici in chimica organica", seconda edizione EdiSES, Napoli (2014)

[23] Prati S., Sciutto G., Bonacini I., Mazzeo R. "New frontiers in application of FTIR Microscopy for characterization of cultural heritage materials", Top. Curr. Chem., Springer, (2016)

[24] Chalmers J., Griffiths P., "Handbook of vibrational spectroscopy", volume 1, Wiley

[25] Schrader B., "Infrared and Raman spectroscopy", VCH, Germany, (1995)

[26] Neil J. Everall, John M., Chalmers J., and Peter R. Griffiths, "Vibrational spectroscopy of polymers: principles and practice", Wiley, England (2007)

[27] Reffner J., Martoglio P., "Practical guide to infrared microspectroscopy", Huecki HJ editor, New York (1995)

[28] Wiesinger R., Dissertation "Development and application of surface sensitive methods for the in-situ investigation of atmospheric corrosion processes on non-transparent materials", Institut für Chemische Technnische und Analytik, Wien (2009)

[29] Socrates G., "Infrared and Raman characteristic group frequencies", Wiley, England (2001)

[30] Edwards H. G. M., Chalmers J. M., Hargreaves M. D., Infrared and Raman Spectroscopy in Forensic Science, Wiley, New York (2011)

[31] Smith E., Dent G., "Modern Raman Spectroscopy, a practical approach", Wiley, England (2005)

[32] Creagh D. C., Bradley D.A., "Radiation in Art and Archeometry", Elsevier, United Kingdom, (2000)

[33] Nakamoto K., "Infrared and Raman Spectra of Inorganic and Coordination Compounds" Part A, sixth edition, Wiley, United States (2009)

[34] "LabRAM Aramis User manual", Horiba Scientific

[35] Feller R. J., "Color science in the examination of museum objects, nondestructive procedures", the Getty Conservation Institute, Los Angeles (2001)

[36] Palazzi S., Colorimetria: la scienza del colore nell'arte e nella tecnica, Nardini editore, Fiesole (1995)

[37] Ball P., Colore, una biografia tra arte storia e chimica, la bellezza e i misteri del mondo del colore, Rizzoli, edizione Milano (2010)

[38] Orsega E. F., lecture notes for the course of "Colorimetry", University of Ca' Foscari, Venice (2015)

[39] Aceto M., Agostino A., Fenoglio G., Picollo M., "Non-invasive differentiation between natural and synthetic ultramarine blue pigments by means of 250–900 nm FORS analysis", Analytical methods, (2013)

[40] Ellis G., Claybourn M., Richards S. E., "the application of Fourier Transform Raman spectroscopy to the study of paint system", Spectrochim. Acta A Mol. Biomol. Spectrosc., (1990)

[41] Hayes P. A., Vahur S., Leito I., "ATR-FTIR spectroscopy and quantitative multivariate analysis of paints and coating materials", Spectrochim. Acta A Mol. Biomol. Spectrosc., (2014)

[42] Rosi F., Miliani C., Clementi C., Kahrim K., Presciutti F., Vagnini M., Manuali V., Daveri A., Cartechini L., Brunetti B.G., Sgamellotti A., "An integrated spectroscopic approach for the non-invasive study of modern art materials and techniques", Applied Physics A, Springer, (2010)

[43] Vahur S., Teearu A., Leito I., "ATR-FT-IR spectroscopy in the region of 550–230cm−1 for identification of inorganic pigments", Spectrochimica Acta Part A 75, (2010)

[44] Vahur S., Teearu A., Leito I., "ATR-FT-IR spectroscopy in the region of 500–230cm−1 for identification of inorganic red pigments", Spectrochimica Acta Part A 73, (2009)

[45] Burgio L., Clark Robin J.H., "Library of FT-Raman spectra of pigments, minerals, pigment media and varnishes, and supplement to existing library of Raman spectra of pigments with visible excitation", Spectrochimica Acta Part A 57, Elsevier, (2001)

[46] Vandenabeele P., Wehling B., Moens L., Edwards H., De Reu M., Van Hooydonk G., "Analysis with micro-Raman spectroscopy of natural organic binding media and varnishes used in art", Analytica Chimica Acta 407, Elsevier, (2000)

[47] Coccato A., Bersani D., Coudray A., Sanyova J., Moens L., Vandenabeele P., "Raman spectroscopy of green minerals and reaction products with an application in Cultural Heritage research", J. Raman Spectrosc. (2016)

[48] Maslar J.E., Hurst W.S., Bowers W.J., Hendricks J.H., Aquino M.I., Levin I., "In situ Raman spectroscopic investigation of chromium surfaces under hydrothermal conditions", Applied Surface Science 180, Elsevier, (2011)

[49] Franquelo M.L., Duran A., Herrera L.K., Jimenez de Haro M.C., Perez-Rodriguez J.L., "Comparison between micro-Raman and micro-FTIR spectroscopy techniques for the characterization of pigments from Southern Spain Cultural Heritage", Journal of Molecular Structure, Elsevier, (2009)

[50] Daher C., Paris C., Le Hô A.S., Bellot-Gurlet L., Échard J., "A joint use of Raman and infrared spectroscopes for the identification of natural organic media used in ancient varnishes", J. Raman Spectrosc., Wiley, (2010)

[51] Roselli G., "Spettroscopia Infrarossa in scienza della conservazione"

[52] Duce C., Della Porta V., Tiné M. R., Spesi A., Ghezzi L., Colombini M. P., Bramanti E., " FTIR study of ageing of fast drying oil colour (FDOC) alkyd paint replicas", Spectrochimica Acta Part A, Elsevier (2014)

[53] Bartolozzi G., Marchiafava V., Mirabello V., Peruzzini M., Picollo M., "Chemical curing in alkyd paints: An evaluation via FT-IR and NMR spectroscopies", Spectrochimica Acta Part A, Elsevier (2014)

[54] Ye G., Courtecuisse F., Allonas X., Ley C., Croutxe-Barghorn C., Raja P., Taylor Phil, Bescond G., "Photoassisted oxypolymerization of alkyd resins: Kinetic and mechanisms", Progress in Organic Coating 73, Elsevier (2012)

[55] Van der Weerd J., Van Loon A., Boon J. J., "FTIR Studies of the Effects of Pigments on the Aging of Oil", Studies in conservation, Taylor & Francis, (2005)

[56] Chiantore O. Trossarelli L., Lazzari M., "Photooxidative degradation of acrylic and methacrylic polymers", Polymer 41, Elsevier, (2000)

[57] Doménech-Carbó M. T., Silva M. F., Aura-Castro E., Fuster-López L., Kröner S., Martínez-Bazán M. L., Más-Barberá X., Mecklenburg M. F., Osete-Cortina L., Doménech A., Gimeno-Adelantado J. V., Yusá-Marco D. J., "Study of behavior on simulated daylight ageing of artists' acrylic and poly(vinyl acetate) paint films", Analytical and Bioanalytical Chemistry, Springer, (2011)

[58] Rubinson K. A., Rubinson J. F. "Chimica Analitica strumentale", Zanichelli, Bologna (2002)

[59] Skoog D., West D., Holler F., Crouch S., "Fondamenti di Chimica analitica", EdiSES, Napoli (2009)

[60] Boella M., "Probabilità e statistica per ingegneria e scienze", Pearson, Milano (2010)

[61] Harris D., "Chimica analitica quantitativa", Zanichelli, Milano (2005)

[62] Hage D., Carr J., "Chimica analitica e analisi quantitativa", Piccin, Padova (2012)